

Detection of 107 glitches in 36 southern pulsars

M. Yu,^{1,2*} R. N. Manchester,² G. Hobbs,² S. Johnston,² V. M. Kaspi,³
M. Keith,² A. G. Lyne,⁴ G. J. Qiao,⁵ V. Ravi,^{6,2} J. M. Sarkissian,² R. Shannon,²
and R. X. Xu¹

¹ School of Physics and State Key Laboratory of Nuclear Physics and Technology, Peking University, Beijing 100871, P. R. China

² CSIRO Astronomy and Space Science, Australia Telescope National Facility, PO Box 76, Epping, NSW 1710, Australia

³ Department of Physics, Rutherford Physics Building, McGill University, 3600 University Street, Montreal, Quebec H3A 2T8, Canada

⁴ Jodrell Bank Centre for Astrophysics, The University of Manchester, Alan Turing Building, Manchester M13 9PL, UK

⁵ Department of Astronomy, School of Physics, Peking University, Beijing 100871, P. R. China

⁶ School of Physics, University of Melbourne, Parkville, VIC 3010, Australia

12 November 2012

ABSTRACT

Timing observations from the Parkes 64-m radio telescope for 165 pulsars between 1990 and 2011 have been searched for period glitches. Data spans for each pulsar ranged between 5.3 years and 20.8 years. From the total of 1911 years of pulsar rotational history, 107 glitches were identified in 36 pulsars. Out of these glitches, 61 have previously been reported whereas 46 are new discoveries. Glitch parameters, both for the previously known and the new glitch detections, were measured by fitting the timing residual data. Observed relative glitch sizes $\Delta\nu_g/\nu$ range between 10^{-10} and 10^{-5} , where $\nu = 1/P$ is the pulse frequency. We confirm that the distribution of $\Delta\nu_g/\nu$ is bimodal with peaks at approximately 10^{-9} and 10^{-6} . Glitches are mostly observed in pulsars with characteristic ages between 10^3 and 10^5 years, with large glitches mostly occurring in the younger pulsars. Exponential post-glitch recoveries were observed for 27 large glitches in 18 pulsars. The fraction Q of the glitch that recovers exponentially also has a bimodal distribution. Large glitches generally have low Q , typically just a few per cent, but large Q values are observed in both large and small glitches. Observed time constants for exponential recoveries ranged between 10 and 300 days with some tendency for longer timescales in older pulsars. Shorter timescale recoveries may exist but were not revealed by our data which typically have observation intervals of 2–4 weeks. For most of the 36 pulsars with observed glitches, there is a persistent linear increase in $\dot{\nu}$ (i.e., decrease in the slow-down rate $|\dot{\nu}|$) in the inter-glitch interval. Where an exponential recovery is also observed, the effects of this are superimposed on the linear increase in $\dot{\nu}$. In some but not all cases, the slope of the linear recovery changes at the time of a glitch. The $\dot{\nu}$ values characterising the linear changes in $\dot{\nu}$ are almost always positive and, after subtracting the magnetospheric component of the braking, are approximately proportional to the ratio of $|\dot{\nu}|$ and the inter-glitch interval, as predicted by vortex-creep models.

Key words: stars: neutron - pulsars: general

1 INTRODUCTION

Pulsars are thought to be highly-magnetised, rapidly-rotating neutron stars. They are remarkably stable rotators, which has enabled tests of general relativity (Kramer et al. 2006), searches for gravitational waves (e.g., Yardley et al. 2011) and the establishment of a pulsar timescale (Hobbs et al. 2011). These results have been be-

ing obtained by the technique known as “pulsar timing”. The pulsar timing technique allows observed pulse times-of-arrival (ToAs) to be compared with predicted arrival times. The predicted arrival times are determined using a model of the pulsar’s rotation, position, orbit etc. The differences between the actual and predicted pulse arrival times are known as “timing residuals”. Timing residuals can be induced by an inaccuracy or omission in the parameters in the timing model or by the timing model not including all phenomena affecting the propagation of a pulse from the pulsar to

* E-mail: vela.yumeng@gmail.com

the observer. The timing residuals for some pulsars are very small. For instance, PSR J0437–4715 has an rms residual of 75 ns over several years (Manchester et al. 2012). However, most pulsars are not so stable. Hobbs et al. (2010) analysed the timing residuals of 366 normal and recycled pulsars on timescales longer than 10 yr. They found that in most cases the residuals comprise low-frequency structures. For young pulsars, the timing residuals were further found to be dominated by recovery processes from glitch events.

A glitch is an abrupt increase in the pulse frequency $\nu = 1/P$ of a pulsar, often followed by an exponential recovery toward the extrapolation of the pre-glitch pulse frequency (Baym et al. 1969). Post-glitch behaviours generally exhibit another recovery process which is characterised by a linear increase in $\dot{\nu}$ or decrease in slow-down rate $|\dot{\nu}|$. This often extends from the end of the initial exponential recovery until the next glitch event. Such “linear-decay” processes were first observed in the Vela pulsar (Downs 1981; Lyne et al. 1996), and were subsequently seen in other sources (Yuan et al. 2010a). The first known glitch was detected in the Vela pulsar (Radhakrishnan & Manchester 1969; Reichley & Downs 1969). Since then more than 350 glitch events have been observed in about 120 pulsars. Glitch databases are now available: the ATNF Pulsar Catalogue glitch table (Manchester et al. 2005)¹ and the Jodrell Bank Glitch Catalogue (Espinoza et al. 2011a).² Since the original glitch discovery, the Vela pulsar has been observed to undergo 15 further glitch events, most of which have $\Delta\nu_g/\nu \sim 10^{-6}$. In contrast, the Crab pulsar has been observed to have $\Delta\nu_g/\nu \sim 10^{-7} - 10^{-9}$ for most of its glitch events. Most glitches have been observed in relatively young radio pulsars but they have also been observed in magnetars (Woods et al. 2004; Dib et al. 2007) and even in a millisecond pulsar (Cognard & Backer 2004). Observed fractional glitch sizes range from $\sim 10^{-10}$ to $\sim 10^{-5}$, but it is important to note that the low end of this distribution is strongly limited by observational selection.

The increase of the pulse frequency during a glitch is usually unresolvable and exponential recoveries typically have timescales of ten to a few hundred days (Wang et al. 2000; Yuan et al. 2010a). However, intensive observations of glitch events in the Crab and Vela pulsars have shown that 1) the rising edge of the pulse frequency can sometimes be resolved into multiple components (Lyne et al. 1992) and 2) very short exponential decays can occur (Dodson et al. 2002). For two pulsars, sinusoidal oscillations have been observed in timing residuals after glitch events (McCulloch et al. 1990; Yuan et al. 2010b).

“Slow glitch” events have been observed in PSR B1822–09 and other pulsars (Zou et al. 2004; Shabanova 2005, 2007; Yuan et al. 2010a). Unlike normal glitches, a slow glitch builds up over several hundred days, and the increased pulse frequency is usually maintained until the next event. This corresponds to a fluctuation in $|\dot{\nu}|$, characterised by an impulsive decrease followed by a gradual increase. Hobbs et al. (2010) and Lyne et al. (2010) suggested that slow glitches are a manifestation of the “ $\dot{\nu}$ switching” observed in some pulsars.

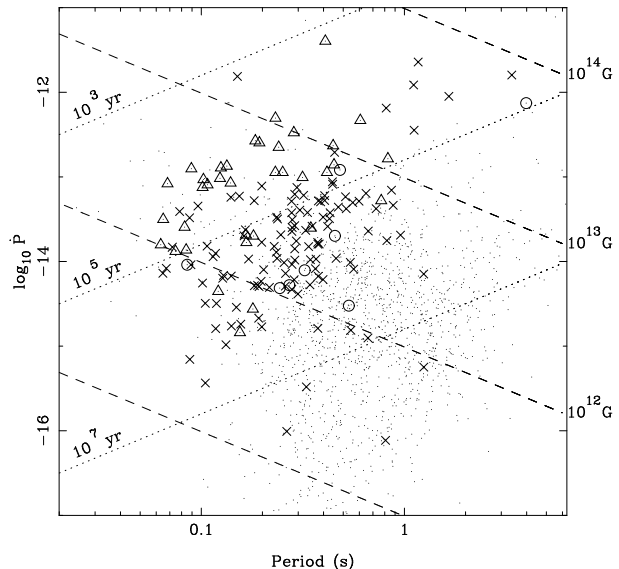


Figure 1. Period–period-derivative ($P - \dot{P}$) diagram showing the pulsars in our sample where no glitch is detected (\times), a glitch is detected (Δ) and a glitch was detected prior to our observations (\circ). Other pulsars are marked with a dot. Data are from the ATNF Pulsar Catalogue.

Glitches are thought to be triggered either by the neutron-star crustquakes (e.g., Ruderman 1991; Ruderman et al. 1998) or by the sudden transfer of angular momentum from the faster-rotating crustal neutron superfluid to the rest of the star (e.g., Anderson & Itoh 1975; Ruderman 1976; Alpar et al. 1981). The post-event exponential recoveries have been explained as the re-establishment of an equilibrium between pinning and unpinning in a vortex-creep region interior to a neutron star (Alpar et al. 1993; Lyne et al. 2000). Fractional glitch sizes $\Delta\nu_g/\nu$ show a bimodal distribution with peaks at $\sim 10^{-9}$ and $\sim 10^{-6}$ (Lyne et al. 2000; Wang et al. 2000; Yuan et al. 2010a). Using a sample containing 315 glitches, Espinoza et al. (2011a) confirmed this bimodal distribution and also found that the rate of glitch occurrence peaks for pulsars with a characteristic age ($\tau_c \equiv P/(2\dot{P})$) of about 10 kyr. They also showed that, on average, nearly one per cent of the spin-down is reversed by glitches for those pulsars with a slow-down rate $|\dot{\nu}|$ between 10^{-14} to 10^{-11} s^{-2} .

Even though glitch events and their subsequent recoveries have been extensively studied, theoretical predictions have been unable to model fully the timing residuals induced by a glitch event. Theoretical models also cannot yet explain why some pulsars exhibit a large number of glitch events, whereas other pulsars with similar characteristics have never been observed to glitch. Melatos et al. (2008) showed that the waiting-time sequences of the glitches in seven pulsars followed a constant-rate Poisson process, which suggests that a neutron star could be a system fluctuating around a self-organised critical state.

For this paper, we searched a total of 1911 yr of pulsar rotational history for glitch events. In §2, we describe our observations. In §3, we present our method for determining glitch parameters. Our results are shown in §4, and discussed in §5. We conclude the paper in §6.

¹ <http://www.atnf.csiro.au/research/pulsar/psrcat/glitchTbl.html>

² <http://www.jb.man.ac.uk/pulsar/glitches.html>

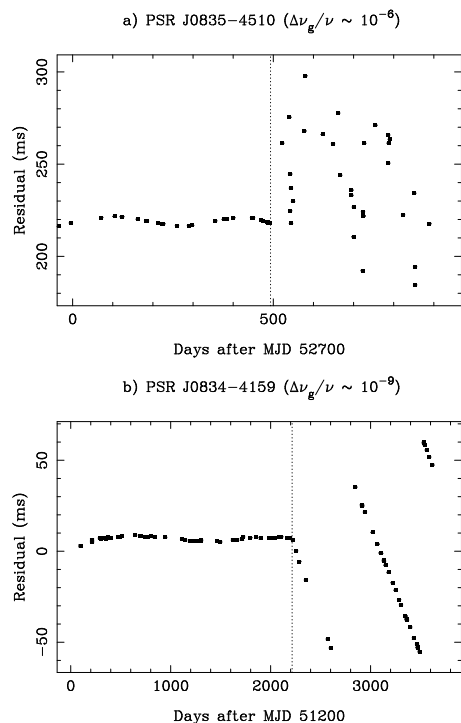


Figure 2. Illustration of the identification of glitch events with two typical sizes 10^{-6} and 10^{-9} . Sub-plot a) shows the effect on the timing residuals of the large glitch that occurred in the Vela pulsar around MJD 53193. The pre-glitch solution contains ν , $\dot{\nu}$ and phase-coherency is broken by the glitch. Sub-plot b) shows timing residuals relative to a pre-glitch solution containing ν and $\dot{\nu}$ for a small glitch in PSR J0834–4159 that occurred at MJD ~ 53415 . In this case, phase coherency is maintained after the glitch although there are several phase wraps. In each plot the vertical dashed line indicates the glitch epoch (from Dodson et al. 2004 for the Vela glitch).

2 OBSERVATIONS

The observations of 165 pulsars analysed in this paper were obtained using the Parkes 64-m radio telescope between 1990 January and 2011 January. Almost all observations were at radio frequencies near 1400 MHz, in the 20-cm band. For 1990 – 1994 the “H-OH” receiver was used with an analogue filterbank having 64×5 MHz channels for each polarisation (Johnston et al. 1992). The data were summed and high-pass filtered before one-bit digitisation. From 1994 – 2001 most data were obtained using the “FPTM” digital filterbank (Sandhu et al. 1997) with one (later two) 128 MHz bands for each polarisation. Up until 1997 the H-OH receiver was used. From 1997 on, most observations used the centre beam of the 20-cm Multibeam receiver (Staveley-Smith et al. 1996) although a few were at higher frequencies between 1700 and 2200 MHz using other receivers. Between 1997 and 2007 observations were usually made with the analogue filterbank system used for the Parkes Multibeam Pulsar Survey (Manchester et al. 2001) which has 96×3 MHz channels for each polarisation. Intervals between observing sessions were typically 2 – 4 weeks and a ToA was obtained for most of the pulsars each session. Some pulsars with lower priority were observed less fre-

quently. Observation times per ToA were normally between one and ten minutes.

From 1991 to 2000 these observations were in part used to support the Energetic Gamma-Ray Experiment Telescope (EGRET) aboard the *Compton Gamma-Ray Observatory* (Thompson 2008). Between 2007 and 2011, observations were obtained with the primary goal of supporting the *Fermi Gamma-ray Space Telescope* mission (Smith et al. 2008; Weltevrede et al. 2010). Observing sessions are separated by approximately four weeks, each lasts for 24 h, allowing ~ 170 pulsars to be observed. The centre beam of the Multibeam receiver is used at 1369 MHz with a bandwidth of 256 MHz. Digital filterbank systems (Manchester et al. 2012) were used to record the data, with integration times of 2 to 20 min for each pulsar to ensure a signal-to-noise ratio larger than five. A few observations were taken as part of the PULSE@Parkes project (Hobbs et al. 2009). These data are available for download from the Parkes pulsar data archive³ (Hobbs et al. 2011).

In Table 1, we summarise the properties of the 165 pulsars. The pulsar name, pulse period P , period derivative \dot{P} , dispersion measure (DM), data span in Modified Julian Day (MJD) and years, and number of observations are presented. The final column in this table indicates whether the pulsar has never been observed to glitch (N), has been detected to glitch during our observations (Y) or has been reported to glitch prior to our observations (P). Figure 1 shows the pulsars in our sample on the period–period-derivative ($P - \dot{P}$) diagram. The P and \dot{P} data are from the ATNF Pulsar Catalogue⁴ (Manchester et al. 2005). The identification and modelling of glitch events will be introduced in detail in the following section.

3 DATA ANALYSIS

Off-line data reduction used the PSRCHIVE pulsar data analysis system (Hotan et al. 2004). Each observation was summed in time, frequency and polarisation to form a total intensity pulse profile. In order to determine the pulse time-of-arrival (ToA), each of the total intensity profiles was cross-correlated with a high signal-to-noise ratio “standard” profile. Timing residuals were formed using the pulsar timing software package TEMPO2 (Hobbs et al. 2006; Edwards et al. 2006), with the Jet Propulsion Laboratories (JPL) planetary ephemeris DE405 (Standish 1998) to correct the local ToAs to the solar-system barycentre. Each observed ToA was first referred to terrestrial time as realised by International Atomic Time and subsequently to Barycentric Coordinate Time. For each pulsar, TEMPO2 was used to find a set of parameters that provided a phase-connected timing solution. The solution contains the pulse frequency ν and its first derivative $\dot{\nu}$. The pulse frequency second derivative was only fitted when a cubic structure in timing residuals could be seen after fitting for ν and $\dot{\nu}$. In some cases, particularly for pulsars that had glitched or have large amounts of timing noise, it was not possible to obtain a phase-connected

³ <http://data.csiro.au>

⁴ <http://www.atnf.csiro.au/research/pulsar/psrcat/>; catalogue version 1.43

Table 1. Pulsars in our sample observed at the Parkes Observatory with a data span larger than 5 yr.

PSR J	PSR B	P (s)	\dot{P} (10^{-15})	DM (cm^{-3} pc)	Data range (MJD)	Data span (yr)	No. of ToAs	Glitched? (Y/N/P) ¹
J0108–1431	-	0.807565	0.08	2.38	49373 — 55144	15.8	135	N
J0401–7608	B0403–76	0.545253	1.54	21.60	53033 — 55144	5.8	58	N
J0536–7543	B0538–75	1.245856	0.56	17.50	48957 — 55144	16.9	103	N
J0630–2834	B0628–28	1.244419	7.12	34.47	51524 — 55144	9.9	62	N
J0729–1448	-	0.251659	113.29	92.30	51896 — 55429	9.7	89	Y
J0738–4042	B0736–40	0.374920	1.62	160.80	52995 — 55144	5.9	73	N
J0742–2822	B0740–28	0.166762	16.82	73.78	49364 — 55579	17.0	481	Y
J0834–4159	-	0.121116	4.44	240.50	51299 — 55145	10.5	120	Y
J0835–3707	-	0.541404	9.78	112.30	50940 — 53948	8.2	62	N
J0835–4510	B0833–45	0.089328	125.01	67.99	49608 — 55172	15.2	667	Y
J0855–4644	-	0.064686	7.26	238.20	51158 — 55144	10.9	225	N
J0857–4424	-	0.326774	23.34	184.43	51899 — 55144	8.9	94	N
J0901–4624	-	0.441995	87.49	198.80	50849 — 55144	11.7	127	N
J0905–5127	-	0.346287	24.90	196.43	49363 — 55145	15.8	101	Y
J0908–4913	B0906–49	0.106755	15.15	180.37	48957 — 55182	17.0	271	N
J0940–5428	-	0.087545	32.87	134.50	50941 — 55144	11.5	163	N
J0942–5552	B0940–55	0.664367	22.85	180.20	48928 — 53948	13.7	181	N
J0954–5430	-	0.472834	43.91	200.30	50940 — 55182	11.6	106	N
J1012–5857	B1011–58	0.819911	17.69	383.90	50536 — 53948	9.3	64	N
J1015–5719	-	0.139882	57.37	278.70	51215 — 55182	10.9	166	N
J1016–5819	-	0.087834	0.70	252.10	50940 — 55144	11.5	77	N
J1016–5857	-	0.107386	80.83	394.20	51299 — 55429	11.3	250	Y
J1019–5749	-	0.162499	20.08	1039.40	51158 — 55182	11.0	85	N
J1020–6026	-	0.140480	6.74	445.00	52854 — 55182	6.4	67	N
J1038–5831	B1036–58	0.661992	1.25	72.74	50536 — 53948	9.3	61	N
J1043–6116	-	0.288602	10.40	449.20	51158 — 55182	11.0	75	N
J1047–6709	-	0.198451	1.69	116.16	50538 — 53948	9.3	62	N
J1048–5832	B1046–58	0.123671	96.32	129.10	47910 — 55183	19.9	353	Y
J1052–5954	-	0.180592	19.98	491.00	51411 — 55460	11.1	92	Y
J1057–5226	B1055–52	0.197108	5.83	30.10	49363 — 55182	15.9	291	N
J1105–6107	-	0.063193	15.83	271.01	49589 — 55461	16.1	297	Y
J1112–6103	-	0.064962	31.46	599.10	50850 — 55207	11.9	178	Y
J1114–6100	B1112–60	0.880820	46.09	677.00	50538 — 53948	9.3	54	N
J1115–6052	-	0.259777	7.23	228.20	50849 — 55205	11.9	97	N
J1119–6127	-	0.407963	4020.22	707.40	50852 — 55576	12.9	348	Y
J1123–6259	-	0.271434	5.25	223.26	50400 — 55205	13.1	182	P
J1136–5525	B1133–55	0.364706	8.22	85.50	51844 — 53948	5.8	33	N
J1138–6207	-	0.117564	12.48	519.80	50849 — 55205	11.9	129	N
J1152–6012	-	0.376570	6.68	74.00	51216 — 53948	7.5	54	N
J1156–5707	-	0.288409	26.45	243.50	51944 — 55205	8.9	67	N
J1216–6223	-	0.374047	16.82	786.60	50851 — 55205	11.9	61	N
J1224–6407	B1221–63	0.216476	4.95	97.47	48330 — 55205	18.8	661	N
J1248–6344	-	0.198335	16.92	433.30	51260 — 55205	10.8	78	N
J1301–6305	-	0.184528	266.75	374.00	50941 — 55104	11.4	177	Y
J1305–6203	-	0.427762	32.14	470.00	50940 — 55205	11.7	58	N
J1316–6232	-	0.342825	5.30	983.30	49589 — 53948	11.9	163	N
J1320–5359	B1317–53	0.279729	9.25	97.60	50536 — 55205	12.8	178	N
J1327–6400	-	0.280678	31.18	680.90	50940 — 55205	11.7	63	N
J1328–4357	B1325–43	0.532699	3.01	42.00	50738 — 53948	8.8	88	P
J1341–6220	B1338–62	0.193340	253.11	717.30	49540 — 55461	16.2	265	Y
J1349–6130	-	0.259363	5.12	284.60	50940 — 55205	11.7	71	N
J1359–6038	B1356–60	0.127501	6.34	293.71	48330 — 55205	18.8	661	N
J1412–6145	-	0.315225	98.66	514.70	50850 — 55461	12.6	159	Y
J1413–6141	-	0.285625	333.44	677.00	50850 — 55461	12.6	198	Y
J1420–6048	-	0.068180	83.17	358.80	51100 — 55461	11.9	272	Y
J1452–5851	-	0.386625	50.71	262.40	51088 — 55205	11.3	120	N
J1452–6036	-	0.154991	1.45	349.70	51302 — 55461	11.4	93	Y
J1453–6413	B1449–64	0.179485	2.75	71.07	50669 — 55205	12.4	143	Y
J1456–6843	B1451–68	0.263377	0.10	8.60	48330 — 55205	18.8	222	N
J1509–5850	-	0.088922	9.17	140.60	51214 — 55205	10.9	155	N
J1512–5759	B1508–57	0.128694	6.85	628.70	51527 — 55205	10.1	85	N
J1513–5908	B1509–58	0.150658	1536.53	252.50	47913 — 55205	20.0	384	N
J1514–5925	-	0.148796	2.88	194.10	51220 — 55205	10.9	66	N
J1515–5720	-	0.286646	6.10	482.00	51391 — 55205	10.4	54	N
J1524–5625	-	0.078219	38.95	152.70	51214 — 55205	10.9	122	N
J1524–5706	-	1.116049	356.47	833.00	51101 — 55205	11.2	110	N
J1530–5327	-	0.278957	4.68	49.60	51013 — 55205	11.5	113	N
J1531–5610	-	0.084202	13.74	110.90	51215 — 55461	11.6	161	Y
J1538–5551	-	0.104675	3.21	603.00	51300 — 55205	10.7	81	N
J1539–5626	B1535–56	0.243392	4.85	175.88	49358 — 55205	16.0	261	P
J1541–5535	-	0.295838	75.02	428.00	51300 — 55205	10.7	69	N
J1543–5459	-	0.377119	52.02	345.70	50941 — 55205	11.7	113	N
J1548–5607	-	0.170934	10.74	315.50	50941 — 55205	11.7	127	N
J1549–4848	-	0.288347	14.11	55.98	49358 — 55205	16.0	239	N
J1551–5310	-	0.453394	195.13	493.00	51099 — 55205	11.2	152	N
J1557–4258	-	0.329187	0.33	144.50	50538 — 53948	9.3	54	N
J1559–5545	B1555–55	0.957242	20.48	212.90	49359 — 53948	12.6	117	N
J1600–5044	B1557–50	0.192601	5.06	260.56	50618 — 55205	12.6	128	N
J1601–5335	-	0.288457	62.37	194.60	50941 — 55205	11.7	118	N
J1602–5100	B1558–50	0.864227	69.58	170.93	47913 — 55205	20.0	246	N
J1611–5209	B1607–52	0.182492	5.17	127.57	51526 — 55205	10.1	80	N
J1614–5048	B1610–50	0.231694	494.94	582.80	47910 — 55461	20.7	413	Y
J1623–4949	-	0.725732	42.09	183.30	50851 — 53975	8.5	57	N
J1626–4807	-	0.293928	17.48	817.00	50941 — 55205	11.7	71	N
J1627–4706	-	0.140746	1.73	456.10	52807 — 55205	6.6	84	N

Table 1. — *continued*

PSR J	PSR B	P (s)	\dot{P} (10^{-15})	DM (cm^{-3} pc)	Data range (MJD)	Data span (yr)	No. of ToAs	Glitched? (Y/N/P)
J1632–4757	-	0.228564	15.07	578.00	51216 — 55205	10.9	92	N
J1632–4818	-	0.813453	650.42	758.00	50852 — 55182	11.9	135	N
J1637–4553	B1634–45	0.118771	3.19	193.23	50669 — 55205	12.4	132	N
J1637–4642	-	0.154027	59.20	417.00	51393 — 55205	10.4	86	N
J1638–4417	-	0.117802	1.61	436.00	51633 — 55205	9.8	82	N
J1638–4608	-	0.278137	51.50	424.30	51089 — 55205	11.3	75	N
J1640–4715	B1636–47	0.517405	42.03	591.70	51528 — 55205	10.1	39	N
J1643–4505	-	0.237383	31.83	484.00	52738 — 55205	6.8	44	N
J1644–4559	B1641–45	0.455060	20.09	478.80	47913 — 55101	19.7	298	P
J1646–4346	B1643–43	0.231603	112.75	490.40	47913 — 55273	20.2	305	Y
J1648–4611	-	0.164950	23.75	392.90	51216 — 55205	10.9	73	N
J1649–4653	-	0.557019	49.74	332.00	51089 — 55205	11.3	93	N
J1650–4502	-	0.380870	16.06	319.70	50941 — 55205	11.7	82	N
J1650–4921	-	0.156399	1.82	229.90	52983 — 55205	6.1	69	N
J1702–4128	-	0.182136	52.34	367.10	51089 — 55205	11.3	87	N
J1702–4310	-	0.240524	223.78	377.00	51223 — 55461	11.6	125	Y
J1705–1906	B1702–19	0.298987	4.14	22.91	51901 — 55206	9.0	75	N
J1705–3950	-	0.318941	60.60	207.10	51217 — 55205	10.9	63	N
J1709–4429	B1706–44	0.102459	92.98	75.69	47910 — 55507	20.8	395	Y
J1713–3949	-	0.392451	-	342.00	51557 — 54504	8.1	84	N
J1715–3903	-	0.278481	37.69	313.10	51217 — 55205	10.9	111	N
J1718–3718	-	3.378574	1613.59	371.10	51244 — 54859	9.9	100	N
J1718–3825	-	0.074670	13.22	247.40	50878 — 55507	12.7	164	Y
J1721–3532	B1718–35	0.280424	25.19	496.00	51879 — 55205	9.1	96	N
J1722–3712	B1719–37	0.236173	10.85	99.50	49363 — 55205	16.0	197	N
J1723–3659	-	0.202722	8.01	254.20	50851 — 55205	11.9	102	N
J1726–3530	-	1.110132	1216.75	727.00	50681 — 55205	12.4	147	N
J1730–3350	B1727–33	0.139460	84.83	259.00	50539 — 55507	13.6	182	Y
J1731–4744	B1727–47	0.829829	163.63	123.33	48184 — 55507	20.0	228	Y
J1733–3716	B1730–37	0.337586	15.05	153.50	51893 — 55205	9.1	80	N
J1734–3333	-	1.169008	2278.98	578.00	50686 — 55205	12.4	136	N
J1735–3258	-	0.350963	26.08	754.00	51393 — 55205	10.4	64	N
J1737–3137	-	0.450432	138.76	488.20	51157 — 55507	11.9	83	Y
J1737–3555	B1734–35	0.397585	6.12	89.41	52003 — 53948	5.3	21	N
J1738–2955	-	0.443398	81.86	223.40	51158 — 55205	11.1	63	N
J1739–2903	B1736–29	0.322882	7.88	138.56	50739 — 55205	12.2	156	P
J1739–3023	-	0.114368	11.40	170.00	51879 — 55205	9.1	98	N
J1740–3015	B1737–30	0.606887	466.12	152.15	50669 — 55507	13.2	190	Y
J1745–3040	B1742–30	0.367429	10.67	88.37	51901 — 55205	9.0	121	N
J1752–2806	B1749–28	0.562558	8.13	50.37	47911 — 55083	19.6	177	N
J1756–2225	-	0.404980	52.69	326.00	51217 — 54564	9.2	47	N
J1757–2421	B1754–24	0.234101	12.92	179.45	51529 — 55205	10.1	96	N
J1759–2205	B1756–22	0.460974	10.87	177.16	51529 — 53975	6.7	28	N
J1801–2154	-	0.375297	16.00	387.90	51218 — 55205	10.9	61	N
J1801–2304	B1758–23	0.415827	112.93	1073.90	47911 — 55507	20.8	411	Y
J1801–2451	B1757–24	0.124924	127.91	289.00	48957 — 55507	17.9	331	Y
J1803–2137	B1800–21	0.133667	134.36	233.99	50669 — 55530	13.3	182	Y
J1806–2125	-	0.481789	121.40	750.40	51155 — 55206	11.1	74	P
J1809–1917	-	0.082747	25.54	197.10	50782 — 55530	13.0	134	Y
J1812–1910	-	0.430991	37.74	892.00	51804 — 55206	9.3	41	N
J1814–1744	-	3.975905	744.70	792.00	51212 — 54505	9.0	50	P
J1815–1738	-	0.198436	77.85	728.00	51157 — 55205	11.1	96	N
J1820–1529	-	0.333243	37.91	772.00	51244 — 55206	10.8	41	N
J1821–1419	-	1.656010	894.50	1123.00	51410 — 54505	8.5	53	N
J1824–1945	B1821–19	0.189335	5.23	224.65	51844 — 55206	9.2	99	N
J1825–0935	B1822–09	0.769006	52.50	19.38	51844 — 55073	8.8	85	Y
J1825–1446	B1822–14	0.279187	22.68	357.00	51844 — 55205	9.2	96	N
J1826–1334	B1823–13	0.101487	75.25	231.00	50749 — 55530	13.1	174	Y
J1828–1057	-	0.246328	20.70	245.00	51805 — 55206	9.3	70	N
J1828–1101	-	0.072052	14.81	607.40	51214 — 55206	10.9	42	N
J1830–1059	B1828–11	0.405043	60.03	161.50	51133 — 55206	11.1	212	N
J1831–0952	-	0.067267	8.32	247.00	51301 — 55206	10.7	77	N
J1832–0827	B1829–08	0.647293	63.88	300.87	51844 — 55206	9.2	80	N
J1833–0827	B1830–08	0.085284	9.17	411.00	50748 — 55206	12.2	132	P
J1834–0731	-	0.512980	58.20	295.00	51632 — 55206	9.8	63	N
J1835–0643	B1832–06	0.305830	40.46	472.90	51529 — 55206	10.1	91	N
J1835–1106	-	0.165907	20.61	132.68	51945 — 55530	9.8	105	Y
J1837–0604	-	0.096294	45.17	462.00	51089 — 55206	11.3	91	N
J1838–0549	-	0.235303	33.43	274.00	51691 — 55206	9.6	49	N
J1839–0905	-	0.418969	26.03	348.00	51410 — 55206	10.4	60	N
J1841–0524	-	0.445749	233.72	289.00	52150 — 55507	9.2	134	Y
J1842–0905	-	0.344643	10.49	343.30	51460 — 55206	10.3	48	N
J1843–0355	-	0.132314	1.04	797.60	51159 — 55206	11.1	42	N
J1843–0702	-	0.191614	2.14	228.10	51692 — 55206	9.6	61	N
J1844–0256	-	0.272963	-	820.20	51559 — 55206	10.0	109	N
J1844–0538	B1841–05	0.255699	9.71	412.80	51844 — 55206	9.2	75	N
J1845–0743	-	0.104695	0.37	281.00	51633 — 55206	9.8	50	N
J1847–0402	B1844–04	0.597769	51.71	141.98	51844 — 55206	9.2	75	N
J1853–0004	-	0.101436	5.57	438.20	51411 — 55206	10.4	37	N
J1853+0011	-	0.397882	33.54	568.80	51148 — 55183	11.0	26	N

¹ Y: Glitch detected in this work; N: No glitch detection; P: Previously known glitch before data span.

timing solution across the entire data span. In such cases, multiple timing solutions were required.

In order to obtain precise and accurate timing solutions (including glitch parameters), it is essential to have well-determined pulsar positions. For some pulsars, positions from the ATNF Pulsar Catalogue were insufficiently accurate and we therefore determined positions from our data. Initially, we obtained timing residuals using the positions (and proper motions) provided by the Catalogue. We fitted for these parameters using the “Cholesky” method that accounts for the effects of correlated noise (Coles et al. 2011). For each fit, we used the longest data span in which no glitch event was observed. The resulting positions were held fixed in subsequent processing.

Glitch events are recognised by a sudden discontinuity in the timing residuals relative to a solution based on earlier data. For glitches with a fractional size $\Delta\nu_g/\nu$ larger than $\sim 10^{-6}$, the residuals change by a large fraction of the pulse period in a few days and phase connection is normally lost as illustrated in sub-plot a) of Figure 2. By analysing short sections of post-glitch data, phase coherence can normally be recovered and an approximate value for the frequency glitch $\Delta\nu_g$ determined. As shown in sub-plot b) of Figure 2, glitches with smaller fractional sizes, typically $\sim 10^{-9}$, have no loss of phase coherence over several hundred days and the post-glitch pulse frequency is easy to determine. Even smaller glitches, with $\Delta\nu_g/\nu \sim 10^{-10}$, are often hard to distinguish from irregular timing noise and so the observed sample of these is incomplete. For each pulsar data set exhibiting a possible glitch, we used the GLITCH plug-in of TEMPO2 to determine the variations of the pulse frequency and its first time derivative as a function of time. The GLITCH plug-in realises this by carrying out a sequence of local fits for these two parameters to the timing residuals. Typically, we included five or six observations in each fit (spanning from about two to six months). After completing the sequence of local fits, a list of dates, pulse frequencies and pulse frequency derivatives are obtained for each glitching pulsar.

In TEMPO2, the additional pulse phase induced by a glitch is described by Equation (121) in Edwards et al. (2006)⁵:

$$\begin{aligned} \phi_g = & \Delta\phi + \Delta\nu_p(t - t_g) + \frac{1}{2}\Delta\dot{\nu}_p(t - t_g)^2 + \\ & [1 - e^{-(t-t_g)/\tau_d}]\Delta\nu_d\tau_d \end{aligned} \quad (1)$$

where the glitch event is modelled by an offset in pulse phase $\Delta\phi$ and the permanent increments in the pulse frequency $\Delta\nu_p$ and first frequency derivative $\Delta\dot{\nu}_p$, in addition to a transient frequency increment $\Delta\nu_d$ which decays exponentially to zero with a timescale τ_d . The phase offset $\Delta\phi$ is needed to allow for uncertainty in the glitch epoch t_g . An initial estimate of t_g was taken to be halfway between the last pre-glitch observation and the first post-glitch observation. Initial estimates of $\Delta\nu_p$ and $\Delta\dot{\nu}_p$ were given by the GLITCH plug-in. Improved values were obtained by including the glitch model in the timing model and subsequently

using TEMPO2 to fit for the glitch parameters. For our work, we extended the Taylor series in equation (1) to include $\Delta\ddot{\nu}_p$ to characterise the long-term variations in $\dot{\nu}$. These parameters and their corresponding uncertainties were obtained from a TEMPO2 least-squares-fit to a segment of data typically spanning ~ 200 d to ~ 3000 d across the glitch event, with the glitch epoch around the centre of the data range. The long-term variations in pulse frequency were described by a truncated Taylor series, $\phi(t) = \phi_0 + \nu t + \frac{1}{2}\dot{\nu}t^2 + \frac{1}{6}\ddot{\nu}t^3$. Fits including τ_d are more complicated. As TEMPO2 implements only a linear fitting algorithm, it is necessary to have a good initial estimate for τ_d . The estimate can be realised by two steps. In the first step, an estimate for τ_d was obtained by eye by inspecting the post-glitch $\dot{\nu}$ variations. In the second step, the first-step value was introduced into the fitting. By increasing or decreasing τ_d , one can eventually find a τ_d which minimises the post-fit χ^2 . This τ_d was determined as the estimate and subsequently included as part of the TEMPO2 fit. We note that, when a fit included an exponential recovery, the post-glitch data range was selected to be larger than the recovery timescale, τ_d . The changes in the pulse frequency and its first derivative at the glitch are then described as

$$\Delta\nu_g = \Delta\nu_p + \Delta\nu_d \quad (2)$$

and

$$\Delta\dot{\nu}_g = \Delta\dot{\nu}_p - \frac{\Delta\nu_d}{\tau_d}, \quad (3)$$

with their uncertainties obtained using standard error propagation equations. In addition, a factor $Q \equiv \Delta\nu_d/\Delta\nu_g$ can be defined, describing the fraction of glitch recovery. In a few cases, after following this procedure the timing residuals revealed a shorter-timescale exponential recovery. In these cases, the second exponential was fitted, initially holding the parameters of the first recovery fixed, and then finally fitting for all parameters of both recoveries.

For some glitches, the glitch epoch could be determined by requiring that the pulse phase was continuous over the glitch, i.e., that $\Delta\phi = 0$. However, a unique solution is only possible when both the amplitude of the glitch and the interval between the last pre-glitch observation and the first post-glitch observation are small, such that $\Delta\phi$ is less than one period between the bounding observations. For situations in which this was not possible, we checked the literature to determine whether a precise glitch epoch had already been published. If so, then we used the published epoch for the rest of the analysis. If not, the glitch epoch t_g was kept at halfway between the last pre-glitch observation and the first post-glitch observation, with an uncertainty of half the observation gap. To take account of this uncertainty for the glitch parameters, we assume a linear dependence on the epoch for each of the glitch parameters. The fitting routine was carried out again with t_g close to the epoch of the first post-glitch observation. A difference between the original and the new values for each parameter could then be obtained. The final uncertainty was then the quadrature sum of the parameter difference and its original uncertainty. For glitches that have a large epoch uncertainty and/or large exponential recoveries, the epoch uncertainty term generally dominates the final parameter uncertainties.

Slow glitches are difficult to recognise from timing resid-

⁵ Corrigendum for Equation (121) in Edwards et al. (2006): the fourth term of the right hand side of the equation should be $[1 - e^{-(t_g^{\text{post}} - t_g)/\tau}]\Delta\nu_t \tau$, rather than $[1 - e^{-(t_g^{\text{post}} - t_g)/\tau}]\Delta\nu_t(t_g^{\text{post}} - t_g)$.

uals alone and are best identified in plots of $\dot{\nu}$ versus time. Their identification is somewhat subjective and they cannot be fitted with standard glitch analyses. In this paper (in §5.3) we describe slow glitches detected in one pulsar, PSR J1539–5626.

4 RESULTS

The data sets for the 165 pulsars in the sample were processed, and 36 pulsars were observed to have glitched (indicated with a “Y” in the last column in Table 1). A total of 107 glitches were detected, among which 46 are new detections. We identified exponential recoveries for 27 glitches. A total of 22 previously published glitches are within our data span, but we were unable to identify these events. This is mainly because the sampling of our observations is often insufficient, such that glitches with a small fractional size ($\Delta\nu_g/\nu < 10^{-9}$) are hard to detect. For the same reason, only those exponential recoveries with a timescale between a few tens to a few hundred days are detectable; any exponential recoveries with a timescale shorter than a few tens of days are likely to have been missed.

Table 2 gives the positions and proper motions in J2000 coordinate for each glitching pulsar. The positions for 28 pulsars are from the ATNF Pulsar Catalogue. As described in §3, we fit for the positions for a further eight pulsars. All of the proper motions are from the ATNF Pulsar Catalogue.

Table A1 lists the pre-, inter- and post-glitch timing solutions for the glitching pulsars. For each pulsar, the table contains the pulsar name, the interval relative to glitch number, ν , $\dot{\nu}$, $\ddot{\nu}$, reference epoch, fitted data span, number of ToAs, post-fit rms residuals, reduced χ^2 and the number of degrees of freedom for the least-squares fit. For pulsars with exponential post-glitch recoveries, to avoid contaminating the long-term post-glitch parameters, the start of post-glitch data span is at least two decay timescales from the glitch. These solutions include long-term timing noise and so are only valid within the fitted data range; they cannot be used for extrapolation.

Table A2 contains the parameters for each observed glitch. The second column gives a reference number for each glitch and the glitch epochs are given in the third column. The fourth column indicates whether the glitch is new (N) or has been previously published (P). References for previously published glitches may be found in the web databases. For each glitch parameter, we give two uncertainties. The TEMPO2 1σ uncertainties are given in the first pair of parentheses. If inclusion of effect of the glitch epoch uncertainty made a significant difference, the final uncertainty is given in the second pair of parentheses. Note that errors refer to the last digit quoted. The number of observations, the fitted data span, the post-fit rms residuals and the reduced χ^2 and degrees of freedom are listed in columns 11, 12, 13 and 14, respectively.

In each of the sub-sections below, we describe the observed glitch events for each pulsar in more detail. In Figures 3 to 11, for the 36 glitching pulsars, we show the evolution of pulse frequency and its first time derivative within our data span. For convenience, observed glitches are numbered as in Table A2.

4.1 PSR J0729–1448

A data gap lasting for ~ 6 yr exists in the data set of this pulsar. During our data span of the recent three years, this pulsar exhibited four glitches (see Figure 3). The first three glitches were small ($\Delta\nu_g/\nu \sim 10^{-8}$). The fourth glitch was significantly larger ($\Delta\nu_g/\nu \sim 6 \times 10^{-6}$). These glitch events have been reported by Weltevrede et al. (2010) and Espinoza et al. (2011a). The Parkes data are unfortunately not well sampled. The three small glitches were identified with prior knowledge from Espinoza et al. (2011a). For the same reason, it is impossible to evaluate the permanent change in $\dot{\nu}$ and other long-term parameters. Weltevrede et al. (2010) reported the large glitch that occurred at MJD 54711(21). Our analysis provides a more precise epoch of MJD 54681(9) which is consistent with Espinoza et al. (2011a) result of MJD 54687(3).

4.2 PSR J0742–2822 (PSR B0740–28)

In total, seven glitch events have been reported for this pulsar (D’Alessandro et al. 1993; Janssen & Stappers 2006; Espinoza et al. 2011a). In Figure 3, we present our 17-yr data span. No new glitches were detected. A glitch at MJD ~ 55020 can clearly be seen. However, we were unable to detect the four small previously reported glitches covered by the data set. For the observed glitch, Espinoza et al. (2011a) gave $\Delta\dot{\nu}/\dot{\nu} = -0.372(96)$, corresponding to $\Delta\dot{\nu} = 225(58) \times 10^{-15} \text{ s}^{-2}$. Our measurement of $\dot{\nu}$ presented in Figure 3 and Table A2 shows $\Delta\dot{\nu} = -1.3(3) \times 10^{-15} \text{ s}^{-2}$, despite the evident noise.

4.3 PSR J0834–4159

This pulsar was not previously known to glitch, but we identify a small glitch at MJD ~ 53415 . Figure 3 shows the 10-yr evolution of pulse frequency and pulse-frequency derivative of this source observed at Parkes. Both of the measured $\Delta\nu$ and $\dot{\nu}$ exhibit noise. $\dot{\nu}$ shows a small permanent change at the glitch event (Table A2). Our observations do not reveal any post-glitch relaxation process.

4.4 PSR J0835–4510 (PSR B0833–45)

The Vela pulsar has undergone 16 known glitch events over a period of ~ 38 yr (for a complete list of these glitches, see the ATNF Pulsar Catalogue glitch table or the Jodrell Bank Glitch Catalogue). Thirteen have a fractional glitch size larger than 10^{-6} . In Figure 3, we present the variations of pulse frequency and its first derivative spanning the last ~ 15 yr. Four glitches were detected. These events have been reported and analysed by Flanagan (1996); Wang et al. (2000); De Luca et al. (1999); Dodson et al. (2002, 2004) and Flanagan & Buchner (2006).

As Figure 3 shows, these glitches are large, with $\Delta\nu_g/\nu > 2 \times 10^{-6}$. Each of the post-glitch behaviours exhibits both exponential and linear recoveries. We attempted to model each of the glitches including both of the exponential and linear recoveries. Each of the glitches is discussed in more detail as below.

For glitch 1, Wang et al. (2000) reported an exponential

Table 2. Position and proper motion parameters for 36 glitching pulsars.

PSR J	R. A. (h:m:s)	Dec. (° ' ")	Position epoch (MJD)	μ_α (mas yr ⁻¹)	μ_δ (mas yr ⁻¹)	References
J0729–1448	07:29:16.45(2)	–14:48:36.8(8)	51367	-	-	1
J0742–2822	07:42:49.058(2)	–28:22:43.76(4)	49326	–29(2)	4(2)	2,3
J0834–4159	08:34:17.815(8)	–41:59:36.01(9)	52347	-	-	This work
J0835–4510	08:35:20.61149(2)	–45:10:34.8751(3)	51544	–49.68(6)	29.9(1)	4
J0905–5127	09:05:51.94(5)	–51:27:54.0(4)	54072	-	-	This work
J1016–5857	10:16:21.16(1)	–58:57:12.1(1)	52717	-	-	5
J1048–5832	10:48:12.2(1)	–58:32:05.8(8)	50889	-	-	6
J1052–5954	10:52:38.11(7)	–59:54:44.1(5)	51683	-	-	7
J1105–6107	11:05:26.17(4)	–61:07:51.4(3)	50794	-	-	6
J1112–6103	11:12:14.81(4)	–61:03:31.1(6)	51055	-	-	8
J1119–6127	11:19:14.30(2)	–61:27:49.5(2)	51485	-	-	9
J1301–6305	13:01:45.76(14)	–63:05:33.9(12)	51206	-	-	8
J1341–6220	13:41:42.63(8)	–62:20:20.7(5)	50859	-	-	6
J1412–6145	14:12:07.69(5)	–61:45:28.8(6)	51186	-	-	8
J1413–6141	14:13:09.87(9)	–61:41:13(1)	51500	-	-	7
J1420–6048	14:20:08.237(16)	–60:48:16.43(15)	51600	-	-	10
J1452–6036	14:52:51.898(8)	–60:36:31.35(6)	51630	-	-	7
J1453–6413	14:53:32.684(8)	–64:13:15.81(7)	52608	–16(1)	–21.3(8)	This work
J1531–5610	15:31:27.91(1)	–56:10:55.0(1)	51448	-	-	7
J1614–5048	16:14:11.29(3)	–50:48:03.5(5)	50853	-	-	6
J1646–4346	16:46:50.8(3)	–43:45:48(8)	52792	-	-	This work
J1702–4310	17:02:26.94(5)	–43:10:40(2)	51597	-	-	7
J1709–4429	17:09:42.728(2)	–44:29:08.24(6)	50042	-	-	6
J1718–3825	17:18:13.565(4)	–38:25:18.06(15)	51184	-	-	8
J1730–3350	17:30:32.28(6)	–33:50:28(4)	53826	-	-	This work
J1731–4744	17:31:42.17(7)	–47:44:37(2)	54548	-	-	This work
J1737–3137	17:37:04.29(4)	–31:37:21(3)	51234	-	-	1
J1740–3015	17:40:33.82(1)	–30:15:43.5(2)	52200	-	-	3
J1801–2304	18:01:19.829(9)	–23:04:44.2(2)	50809	-	-	11
J1801–2451	18:01:00.016(8)	–24:51:27.5(2)	53348	–11(9)	–1(15)	12
J1803–2137	18:03:51.4105(10)	–21:37:07.351(10)	51544	11.6(18)	14.8(23)	13
J1809–1917	18:09:43.132(6)	–19:17:40(1)	54632	-	-	This work
J1825–0935	18:25:30.629(6)	–09:35:22.3(3)	53300	–13(11)	–9(5)	14,3
J1826–1334	18:26:13.175(3)	–13:34:46.8(1)	52400	23.0(25)	–3.9(31)	14,15
J1835–1106	18:35:18.41(7)	–11:06:15(4)	53882	-	-	This work
J1841–0524	18:41:49.32(5)	–05:24:29.5(12)	52360	-	-	5

References for positions and proper motions: 1 – Morris et al. (2002); 2 – Hobbs et al. (2004); 3 – Fomalont et al. (1997); 4 – Dodson et al. (2003); 5 – Hobbs et al. (2004); 6 – Wang et al. (2000); 7 – Kramer et al. (2003); 8 – Manchester et al. (2001); 9 – Camilo et al. (2000); 10 – D’Amico et al. (2001); 11 – Frail et al. (1993); 12 – Zeiger et al. (2008); 13 – Briskin et al. (2006); 14 – Yuan et al. (2010a); 15 – Pavlov et al. (2008).

recovery with a time constant 916(48) d. However, the post-event $\dot{\nu}$ variations shown in Figure 3 indicate that the exponential recovery completes within ~ 200 d and the long-term evolution exhibits a linear recovery. Fitting the timing phase residuals showed that the exponential timescale is 186(12) d, with $Q = 0.030(4)$ (Table A2). Glitch 2 was captured with high time resolution by Dodson et al. (2002). Four short-term exponential decays were identified with the smallest timescale just ~ 1.2 min. Parkes data, however, are not sufficient to resolve these short-term recoveries. However an ex-

ponential recovery that completes in ~ 100 d can be seen in our data. Fitting gave $Q \sim 0.02$ and $\tau_d \sim 125$ d. For glitch 3, the exponential recovery is characterised by $Q \sim 0.009$ and $\tau_d \sim 37$ d. The most recent glitch 4 also exhibits an exponential recovery. Our fitting showed $Q \sim 0.0119$ and $\tau_d \sim 73$ d.

At least in the long term, the post-glitch behaviour is dominated by the linear recovery of $\dot{\nu}$. This is superimposed on the shorter-term exponential decays and persists until the next glitch. As Table A1 shows, the observed values of

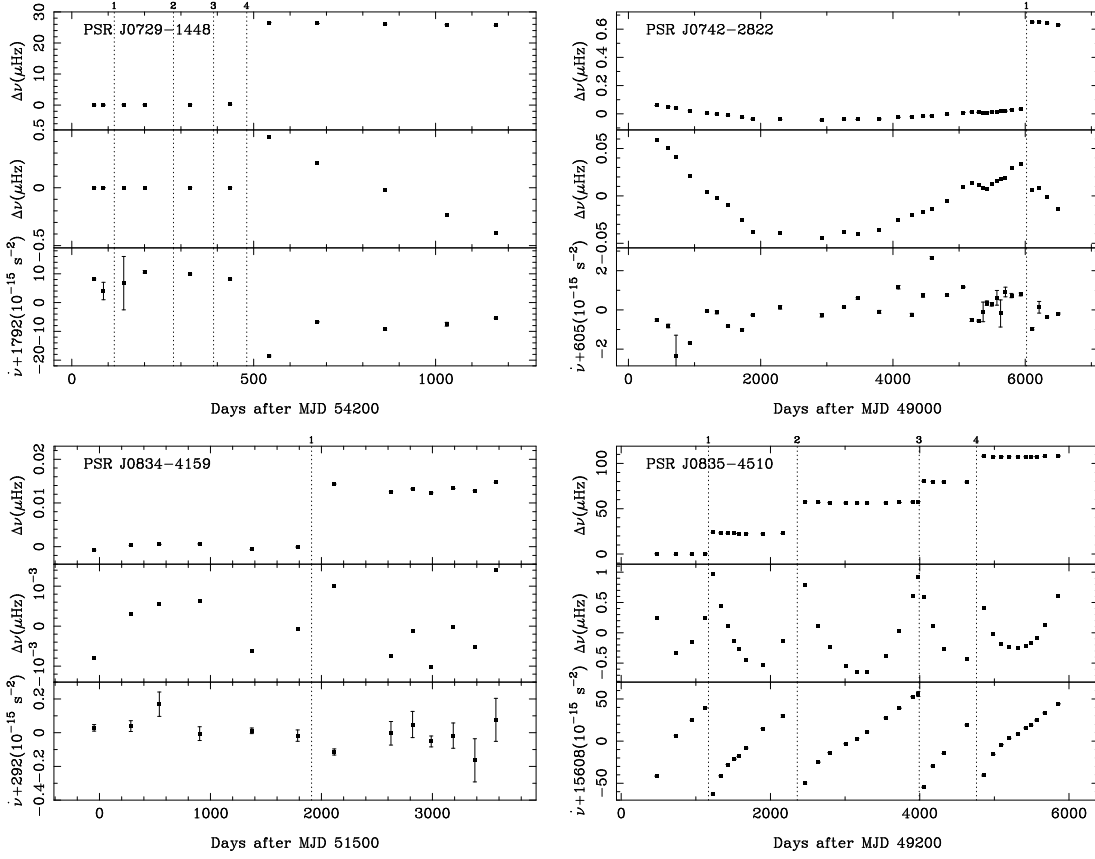


Figure 3. Glitches in PSRs J0729–1448, J0742–2822, J0834–4159 and J0835–4510. The top panel shows the pulse-frequency residuals $\Delta\nu$, obtained by subtracting the (extrapolated) pulse frequency derived from the ν and $\dot{\nu}$ values of the first pre-glitch solution; the middle panel is an expanded plot of $\Delta\nu$ where the mean of each inter-glitch (or post-glitch) solution is subtracted; the bottom panel shows the variations of the pulse-frequency first time derivative $\dot{\nu}$. The glitch epochs are indicated by vertical dashed lines, and the numbers at the top of each dashed line denote the sequence of glitches detected within our data span.

$\ddot{\nu}$ representing the slope of this long-term linear recovery are relatively large for the Vela pulsar and also that they change significantly after each glitch. Fitting for $\Delta\ddot{\nu}_p$ along with the other glitch parameters was generally difficult. The superimposed timing noise and the shorter data spans used for the glitch fitting often led to values somewhat different to those obtained by differencing the long-term fits for $\ddot{\nu}$ given in Table A1 or to an insignificant value. For example, glitch 3 has a fitted value of $304(23) \times 10^{-24} \text{ s}^{-3}$ but the difference between the post- and pre-glitch values of $\ddot{\nu}$ in Table A1 is $491(7) \times 10^{-24} \text{ s}^{-3}$.

4.5 PSR J0905–5127

No glitch events have previously been reported for this pulsar. Figure 4 presents the evolution of ν and $\dot{\nu}$ observed at Parkes. The entire data span is ~ 16 yr, but there exists a data gap lasting for ~ 4 yr. Two glitch events were detected. Both are small, with a fractional glitch size $\sim 10^{-8}$. The available observations are not sufficient to study the post-glitch behaviour for glitch 1. For glitch 2, no significant post-glitch recovery was observed.

4.6 PSR J1016–5857

In Figure 4, the variations of ν and $\dot{\nu}$ of this pulsar for ~ 11 yr are shown. Two glitches were detected. They are similar with $\Delta\nu_g/\nu \sim 2 \times 10^{-6}$ and $\Delta\dot{\nu}_g/\dot{\nu} \sim 4 \times 10^{-3}$. The different slopes of $\dot{\nu}$ before and after glitch 1 imply a permanent change in $\ddot{\nu}$; fitting showed that $\Delta\ddot{\nu}_p = 69(7) \times 10^{-24} \text{ s}^{-3}$, approximately consistent with the $\ddot{\nu}$ values in Table A1. For glitch 2, the available data are not sufficient to characterise the long-term post-glitch relaxations.

4.7 PSR J1048–5832 (PSR B1046–58)

For PSR J1048–5832, the evolution of ν and $\dot{\nu}$ spanning 20 yr is shown in Figure 4. Wang et al. (2000) and Urama (2002) have published details for glitches 1, 2 and 3. Weltevrede et al. (2010) discovered glitch 6. We report here glitches 4 and 5 as new discoveries. Glitch 4 is large with $\Delta\nu_g/\nu \sim 1.8 \times 10^{-6}$, whereas glitch 5 is much smaller with a fractional size $\sim 2.5 \times 10^{-8}$. As shown in Figure 4, for these two glitches there is little evidence for exponential recoveries.

For glitches 2 and 3, Wang et al. (2000) included exponential terms to model the post-glitch behaviour; the time constants were assumed to be 100 d and 400 d, respectively.

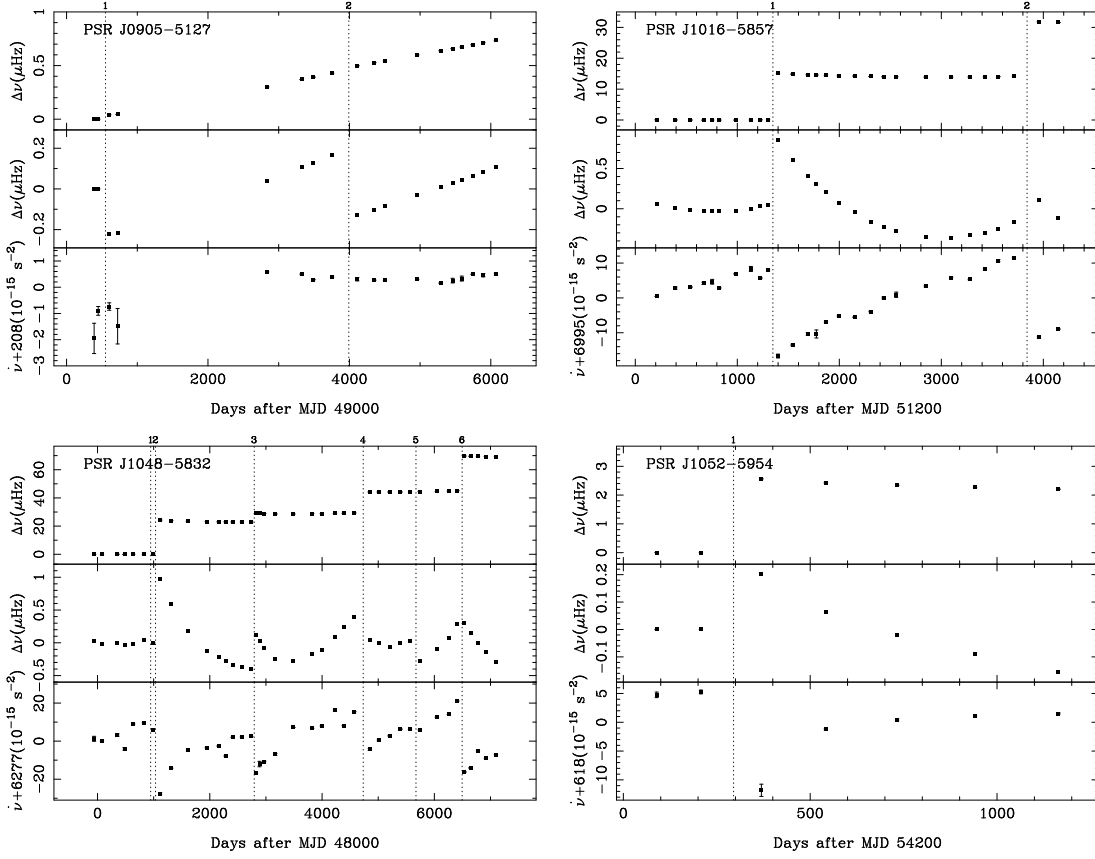


Figure 4. Glitches in PSRs J0905–5127, J1016–5857, J1048–5832 and J1052–5954. See Figure 3 for a description of each sub-plot.

Urama (2002) observed glitch 3 with high observing cadence. Two exponential recoveries were detected; the timescales are 32(9) d and 130(40) d, respectively. As shown in Figure 4, for both of the glitches 2 and 3, the post-glitch $\dot{\nu}$ variations exhibit significant noise. For glitch 2, our fitting for the exponential recovery showed $Q = 0.026(6)$ and $\tau_d = 160(43)$ d. We note that, for this glitch, because there is only one pre-glitch measurement of $\dot{\nu}$, so we are unable to measure the permanent change in $\dot{\nu}$. For glitch 3, our fitting showed $Q = 0.008(3)$ and $\tau_d = 60(20)$ d. Table A1 shows significant values of $\ddot{\nu}$ for all except glitch 2, with significant variations from glitch to glitch. On average, the values are about an order of magnitude smaller than those for the Vela pulsar.

4.8 PSR J1052–5954

The available data set for this pulsar contains a data gap of ~ 6 yr. Figure 4 shows the evolution of ν and $\dot{\nu}$ after the data gap. The detected glitch at MJD ~ 54495 was reported by Weltevrede et al. (2010). An exponential relaxation and a significant permanent increase in spin-down rate $|\dot{\nu}|$ can be identified in the post-glitch data. Fitting to the timing residuals indicated that ~ 0.067 of the glitch recovered in ~ 46 d.

4.9 PSR J1105–6107

Three glitch events have previously been identified for this source (Wang et al. 2000; Weltevrede et al. 2010). In Fig-

ure 5, we present the evolution of ν and $\dot{\nu}$ for ~ 16 yr of this pulsar. We confirm the previously detected glitches 1 and 3 (Wang et al. 2000; Weltevrede et al. 2010). Wang et al. (2000) reported a small glitch occurred at MJD ~ 50610 . However, we found that the timing behaviour of this source around this epoch is more likely to be dominated by timing noise. We report new glitch events as glitches 2 and 4. As shown in Figure 5, the post-glitch behaviour is noisy and no exponential recoveries were observed. There appears to be a persistent increase in $|\dot{\nu}|$ at the time of each of glitches 1, 2 and 3. For glitch 4, the available data span is not adequate to study the post-glitch behaviour.

4.10 PSR J1112–6103

As shown in Figure 5, two large glitch events were detected in this pulsar, with $\Delta\nu_g/\nu \sim 10^{-6}$. For glitch 1, the observed variations of $\dot{\nu}$ indicate a large change in $\ddot{\nu}$; fitting gave $\Delta\ddot{\nu}_p \sim 240 \times 10^{-24} \text{ s}^{-3}$. No exponential recovery was observed for this glitch. For glitch 2, a long-term exponential relaxation was observed, which is characterised by $Q \sim 0.022$ and $\tau_d \sim 300$ d.

4.11 PSR J1119–6127

For PSR J1119–6127, Figure 5 shows the evolution of the observed pulse frequency and its first derivative spanning ~ 13 yr. Three glitches were observed. The first is small

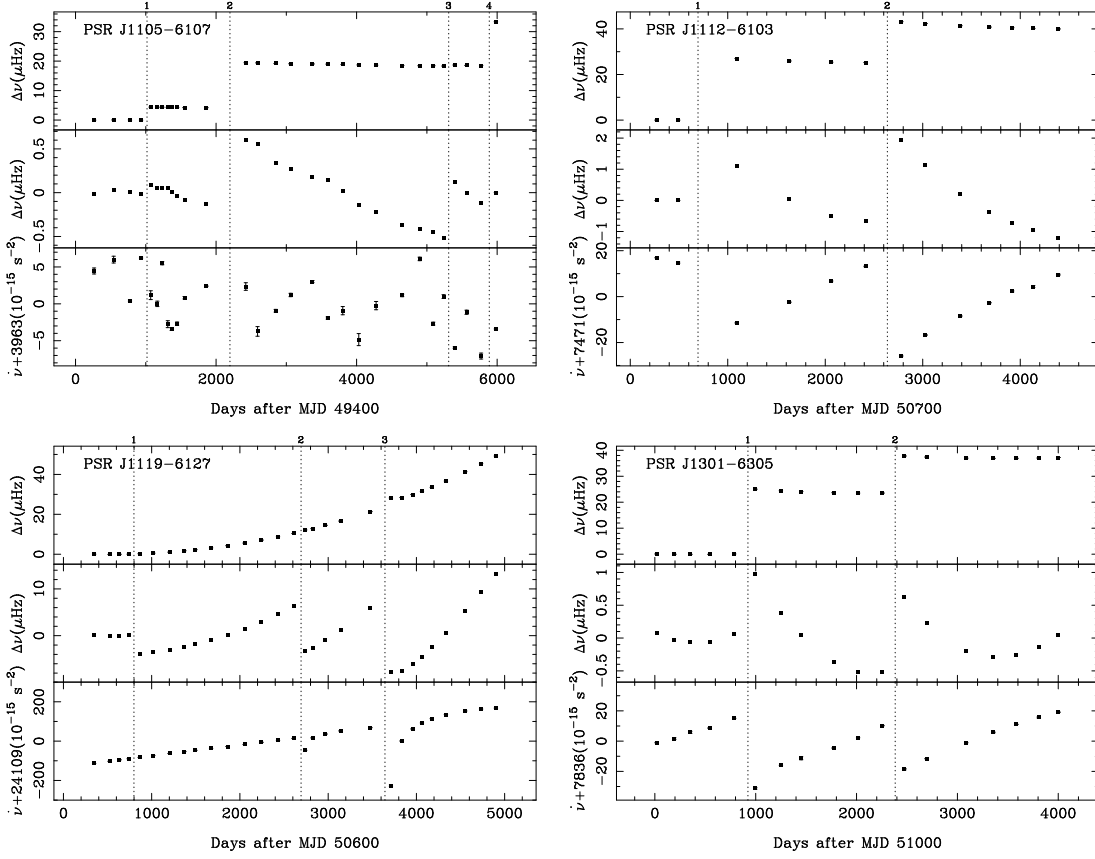


Figure 5. Glitches in PSRs J1105–6107, J1112–6103, J1119–6127 and J1301–6305. See Figure 3 for a description of each sub-plot.

with $\Delta\nu_g/\nu \sim 4 \times 10^{-9}$ as was reported by Camilo et al. (2000). The second and third glitches are much larger and were studied in detail by Weltevrede et al. (2011). Our results are generally consistent with theirs.

4.12 PSR J1301–6305

Figure 5 shows the evolution of ν and $\dot{\nu}$ for PSR J1301–6305 over ~ 11 yr. We detected two large glitch events. Glitch 1 has $\Delta\nu_g/\nu \sim 4.6 \times 10^{-6}$ and for glitch 2 the fractional frequency change is about half this. For glitch 1, an exponential recovery was identified; fitting gave $Q \sim 0.0049$ and $\tau_d \sim 58$ d. As shown in Figure 5, the pre- and post-glitch intervals show clear linear recoveries. As Table A1 indicates, the $\ddot{\nu}$ values are all $\sim 250 \times 10^{-24} \text{ s}^{-3}$. Because of timing noise, we were unable to fit for the $\Delta\ddot{\nu}_p$ changes at the glitches.

4.13 PSR J1341–6220 (PSR B1338–62)

This pulsar is well known to have frequent glitches — Wang et al. (2000) and Weltevrede et al. (2010) have reported 14 glitches. Figure 6 shows the evolution of ν and $\dot{\nu}$ for ~ 16 yr, where a total of 17 glitches are presented. We report here the new detections of nine glitch events. For glitch 6, an exponential decay with $Q \sim 0.0112$ and $\tau_d \sim 24$ d was detected. Unfortunately, for the other glitches the observations are insufficient to study the post-glitch behaviour.

4.14 PSR J1412–6145

PSR J1412–6145 has not previously been known to glitch. Here, we report the discovery of a large glitch with $\Delta\nu_g/\nu \sim 7.2 \times 10^{-6}$ that occurred at MJD ~ 51868 . As shown in Figure 6, there was a clear exponential recovery with timescale ~ 60 d, a significant increase in $|\dot{\nu}|$ at the time of the glitch and a slow linear recovery of part of this increase.

4.15 PSR J1413–6141

Figure 6 presents seven new glitch events detected in this pulsar over a 12.6-yr data span. Among these events, three are small ($\Delta\nu_g/\nu \sim 10^{-8}$), while the other four are larger, with a fractional size $\gtrsim 10^{-6}$. Exponential post-glitch recoveries are not observed for these glitches. Significant values of $\ddot{\nu}$ are seen after each of the latest four glitches (cf. Table A1). We were able to fit for $\Delta\ddot{\nu}_p$ for glitch 4, giving a value of $491(42) \times 10^{-24} \text{ s}^{-3}$; this is consistent with the difference between the post- and pre-glitch solutions for $\ddot{\nu}$, which is $457(40) \times 10^{-24} \text{ s}^{-3}$.

4.16 PSR J1420–6048

Figure 6 shows that five glitch events were observed in this pulsar. Glitch 4 was first reported by Weltevrede et al. (2010). All of these glitches are large, with $\Delta\nu_g/\nu \sim 10^{-6}$. The post-glitch slow-down rates exhibit linear decays, and changes in $\ddot{\nu}$ are observed (Tables A1 and A2). For glitch

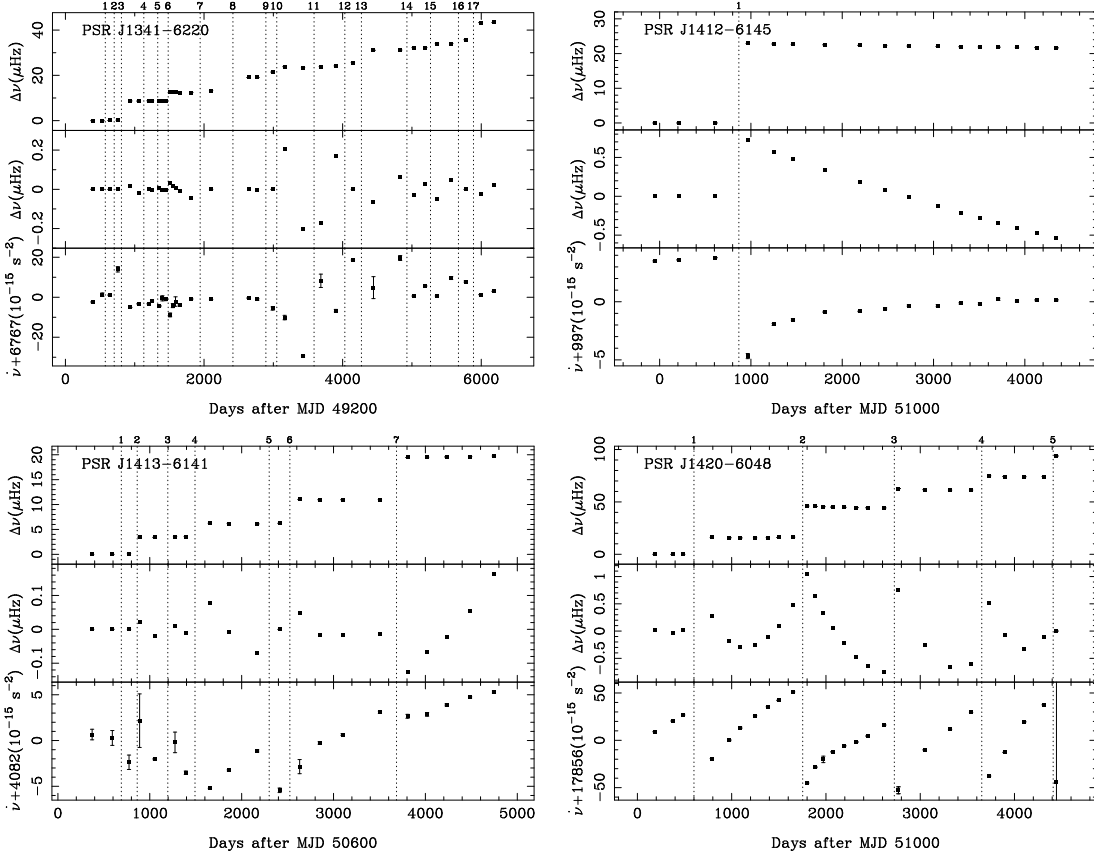


Figure 6. Glitches in PSRs J1341–6220, J1412–6145, J1413–6141 and J1420–6048. See Figure 3 for a description of each sub-plot.

2, an exponential recovery was measured, with obtaining $Q \sim 0.008$ and $\tau_d \sim 99$ d. For glitch 5, the available data are not sufficient to study the post-glitch behaviour.

4.17 PSR J1452–6036

This pulsar was not previously known to glitch. Since the end of the Multibeam Survey timing (Kramer et al. 2003), no observations were made until the start of the *Fermi* project. Hence, a data gap lasting for ~ 5 yr exists. Figure 7 shows the evolution of ν and $\dot{\nu}$. A small glitch event with $\Delta\nu_g/\nu \sim 3 \times 10^{-8}$ was detected at MJD ~ 55055 . The available data are not adequate to study the post-glitch behaviour.

4.18 PSR J1453–6413 (PSR B1449–64)

No glitch event has previously been reported for this pulsar. Figure 7 shows the evolution of ν and $\dot{\nu}$ for ~ 12 yr. We detected a very small glitch with $\Delta\nu_g/\nu \sim 3 \times 10^{-10}$. We cannot comment on the post-glitch behaviour since the data are insufficient.

4.19 PSR J1531–5610

PSR J1531–5610 was not previously known to glitch. Figure 7 shows a large glitch event at MJD ~ 51730 , detected by Parkes timing. As in PSR J1412–6145, this glitch has an

exponential recovery, an offset in $\dot{\nu}$ at the time of the glitch and a slow linear recovery. Our fitting of the exponential term showed that ~ 0.007 of the glitch recovered within a timescale of ~ 76 d and the long-term $\ddot{\nu}$ is $\sim 20 \times 10^{-24} \text{ s}^{-3}$ (Table A1).

4.20 PSR J1614–5048 (PSR B1610–50)

PSR J1614–5048 has been observed at Parkes for ~ 20 yr. As shown in Figure 7, two glitches were detected. Both of the events are large, with $\Delta\nu_g/\nu > 6 \times 10^{-6}$. This pulsar exhibits remarkable timing noise; the large-scale fluctuations in $\dot{\nu}$ reflect this. As a result, phase-connected timing residuals cannot be obtained for the entire data range between the two glitch events. We thus report the timing solutions for this data span in two sections (see Table A1). Glitch 1 has previously been reported by Wang et al. (2000); our results for $\Delta\nu_g/\nu$ and $\Delta\dot{\nu}_g/\dot{\nu}$ are consistent with theirs. Glitch 2 is a new detection. Values of $\ddot{\nu}$ given in Table A1 show significant variations, but these are likely to be contaminated by the timing noise. Despite the noise, there does appear to be a significant linear recovery after glitch 1 with $\ddot{\nu} \sim 200 \times 10^{-24} \text{ s}^{-3}$.

4.21 PSR J1646–4346 (PSR B1643–43)

Figure 8 presents the evolution of ν and $\dot{\nu}$ for this pulsar for ~ 16 yr. A glitch event was detected at MJD ~ 53875 .

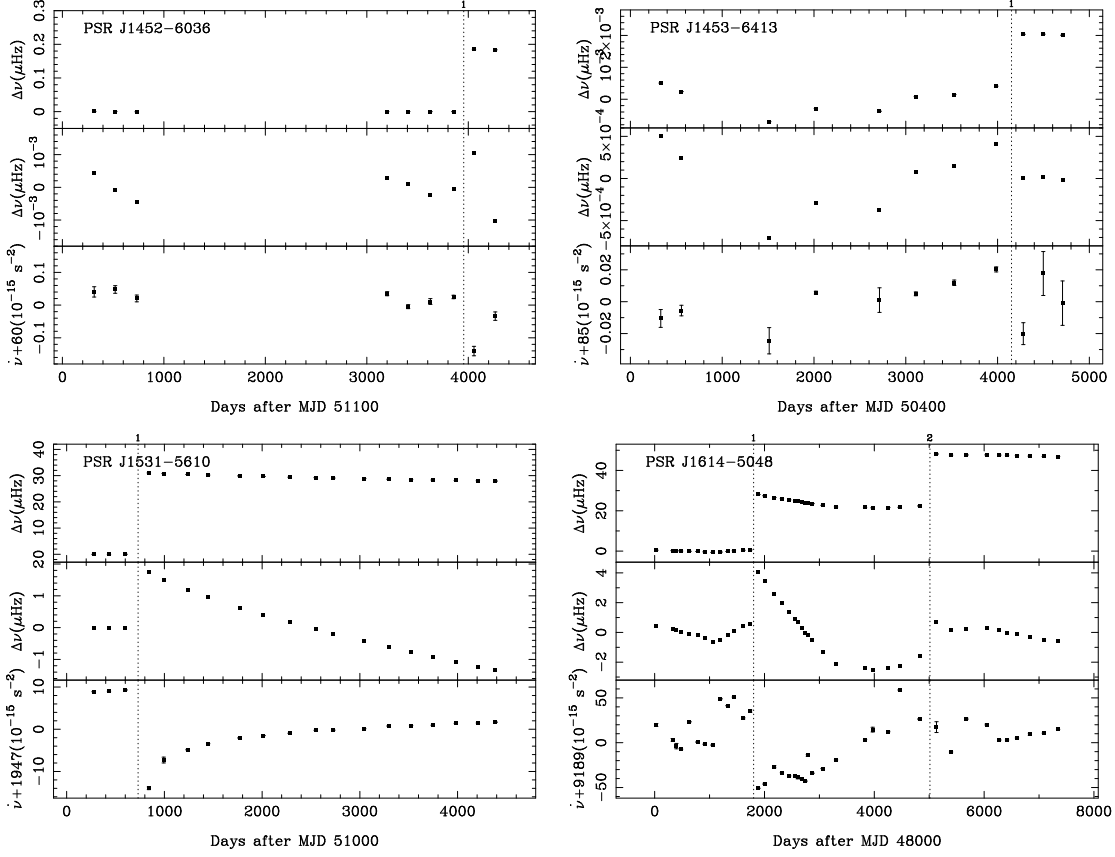


Figure 7. Glitches in PSRs J1452–6036, J1453–6413, J1531–5610 and J1614–5048. See Figure 3 for a description of each sub-plot.

This is the first reported glitch for this pulsar and it has a fractional size $\sim 8.8 \times 10^{-7}$. There is a clear linear recovery from a presumed earlier glitch before the observed glitch.

4.22 PSR J1702–4310

This pulsar was not previously known to glitch. Here, as shown in Figure 8, we report our discovery of a glitch event. Our observations suggest both exponential and linear decays following the glitch and a linear decay with almost the same slope preceding the glitch. Fitting for the exponential decay gave $Q \sim 0.023$ and $\tau_d \sim 96$ d. A data gap of ~ 3 yr exists in the pre-glitch data span. However, there is little period noise and no phase ambiguity across this gap.

4.23 PSR J1709–4429 (PSR B1706–44)

In Figure 8, we present the evolution of ν and $\dot{\nu}$ of this pulsar for ~ 20 yr. Four glitches were detected. These glitches are large, with $\Delta\nu_g/\nu > 1 \times 10^{-6}$. Johnston et al. (1995) and Weltevrede et al. (2010) have reported glitches 1 and 4, but no post-glitch recoveries were reported. As Figure 8 shows, all four glitches show significant post-glitch recoveries, most with both exponential and linear components. Dramatic slope changes in the linear recoveries are seen after each glitch (Table A1). Just a small fraction of each glitch recovers exponentially, with time constants ~ 100 d (Table A2).

4.24 PSR J1718–3825

This pulsar was not previously reported to glitch. Figure 8 shows the evolution of ν and $\dot{\nu}$ for ~ 13 yr. A glitch was detected at MJD ~ 54910 . This event is small with $\Delta\nu_g/\nu \sim 2 \times 10^{-9}$.

4.25 PSR J1730–3350 (PSR B1727–33)

Two glitch events that occurred at MJDs ~ 48000 and ~ 52107 were previously detected for this pulsar (Johnston et al. 1995; Espinoza et al. 2011a). Both are large, with $\Delta\nu_g/\nu > 3 \times 10^{-6}$. Figure 9 shows the MJD ~ 52017 glitch. There is a clear linear recovery following the glitch and a small exponential recovery with $Q \sim 0.01$ and timescale of ~ 100 d.

4.26 PSR J1731–4744 (PSR B1727–47)

Three glitches have been reported for this pulsar (D’Alessandro & McCulloch 1997; Wang et al. 2000; Espinoza et al. 2011a). Figure 9 shows these numbered 1, 2 and 3 and a newly detected glitch 4. Glitches 1 and 3 have $\Delta\nu_g/\nu \sim 1 \times 10^{-7}$, whereas glitches 2 and 4 have $\Delta\nu_g/\nu \sim 3 \times 10^{-9}$. For glitch 3, we measured an exponential recovery, with obtaining $Q \sim 0.073$ and $\tau_d \sim 210$ d. There is some evidence for linear recoveries following each glitch (cf., Wang et al. 2000). The measured values of $\ddot{\nu}$ are small, ranging from $1 \times 10^{-24} \text{ s}^{-3}$ to $20 \times 10^{-24} \text{ s}^{-3}$. For

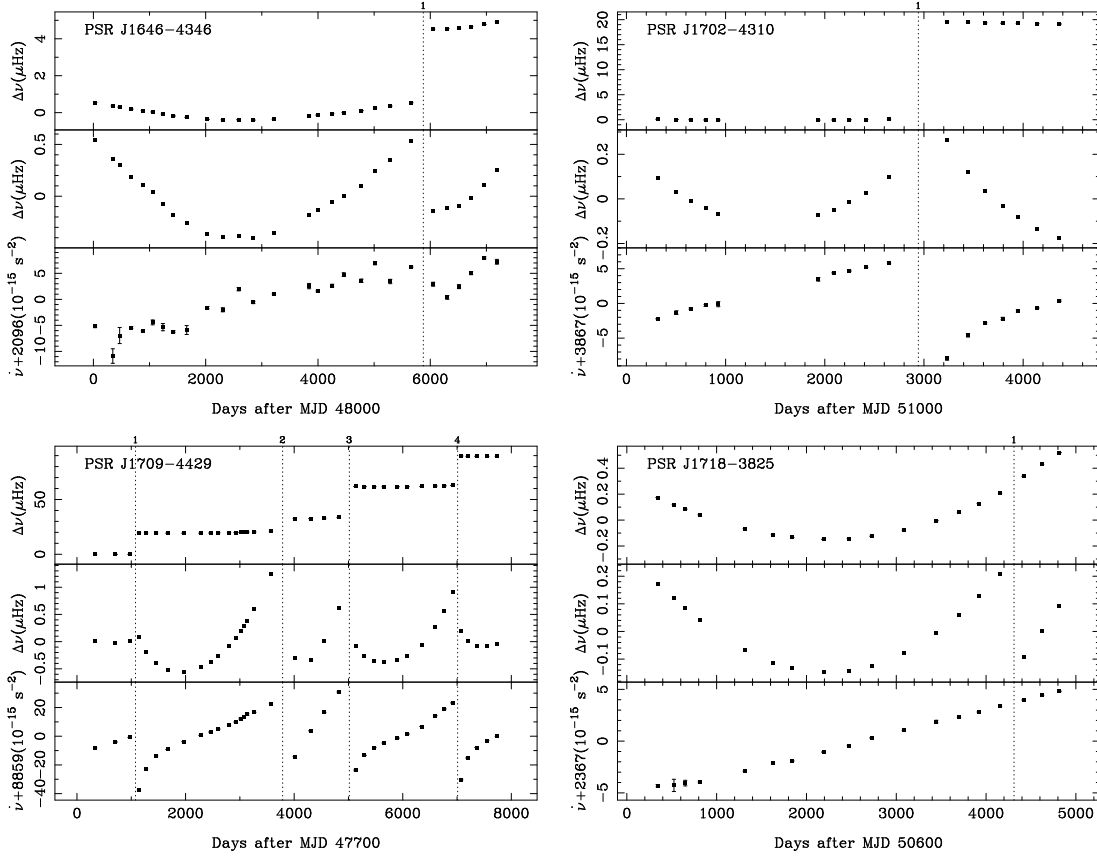


Figure 8. Glitches in PSRs J1646–4346, J1702–4310, J1709–4429 and J1718–3825. See Figure 3 for a description of each sub-plot.

glitch 2, Wang et al. (2000) reported the glitch epoch as MJD 50703(5). We obtained a more accurate epoch MJD 50715.9(8) by solving for phase continuity across the glitch.

4.27 PSR J1737–3137

Since the end of the Multibeam Pulsar Survey timing (Morris et al. 2002), this source was not observed until the commencement of the *Fermi* project, leaving a data gap of ~ 7 yr. Three glitches have been reported for this pulsar (Weltevrede et al. 2010; Espinoza et al. 2011a). We detected the most recent glitch (Figure 9). This glitch is large, with $\Delta\nu_g/\nu \sim 10^{-6}$. There is evidence for a significant change in $\dot{\nu}$ at the time of the glitch, and maybe exponential and linear recoveries, but the available data are insufficient to be sure.

4.28 PSR J1740–3015 (PSR B1737–30)

PSR J1740–3015 is one of the most frequently glitching pulsars known. Previously, a total of 31 glitches were detected over a 25-yr data span. Figure 9 presents the evolution of ν and $\dot{\nu}$ for ~ 13 yr from Parkes timing. During this period, this pulsar was found to have undergone 17 glitches (Urama 2002; Krawczyk et al. 2003; Janssen & Stappers 2006; Zou et al. 2008; Yuan et al. 2010a; Weltevrede et al. 2010; Espinoza et al. 2011a). However, because of the frequent glitching and the relatively poor sampling of our observations, only five major glitches can be detected. The first

four have been published. Glitch 5 is a new detection; it has a fractional size of $\sim 2.7 \times 10^{-6}$, which is the largest ever seen in this pulsar. Linear recoveries are seen after most of the large glitches, including glitch 5, but we have no evidence for exponential recoveries. If such recoveries exist, they must have timescales of less than a few tens of days.

4.29 PSR J1801–2304 (PSR B1758–23)

PSR J1801–2304 has been found to have suffered nine glitches in ~ 24 yr (Kaspi et al. 1993; Shemar & Lyne 1996; Wang et al. 2000; Krawczyk et al. 2003; Yuan et al. 2010a; Espinoza et al. 2011a). Figure 10 presents the variations of ν and $\dot{\nu}$ for ~ 20 yr, where eight glitches are shown, the last being a new discovery. This is a small glitch, with a fractional size $\sim 4 \times 10^{-9}$. For glitch 4, Wang et al. (2000) fit it with an exponential recovery, assuming the timescale to be 100 d. However, as shown in Figure 10, our observations suggest that a linear recovery with $\ddot{\nu} \sim 40 \times 10^{-24} \text{ s}^{-3}$ (Table A1) dominates the post-glitch behaviour.

4.30 PSR J1801–2451 (PSR B1757–24)

Figure 10 shows the evolution of ν and $\dot{\nu}$ of this pulsar for ~ 18 yr, where five glitches are shown. These glitches have been reported previously (Lyne et al. 1996; Wang et al. 2000; Weltevrede et al. 2010; Espinoza et al. 2011a). Figure 10 suggests that the post-glitch recoveries are dominated by

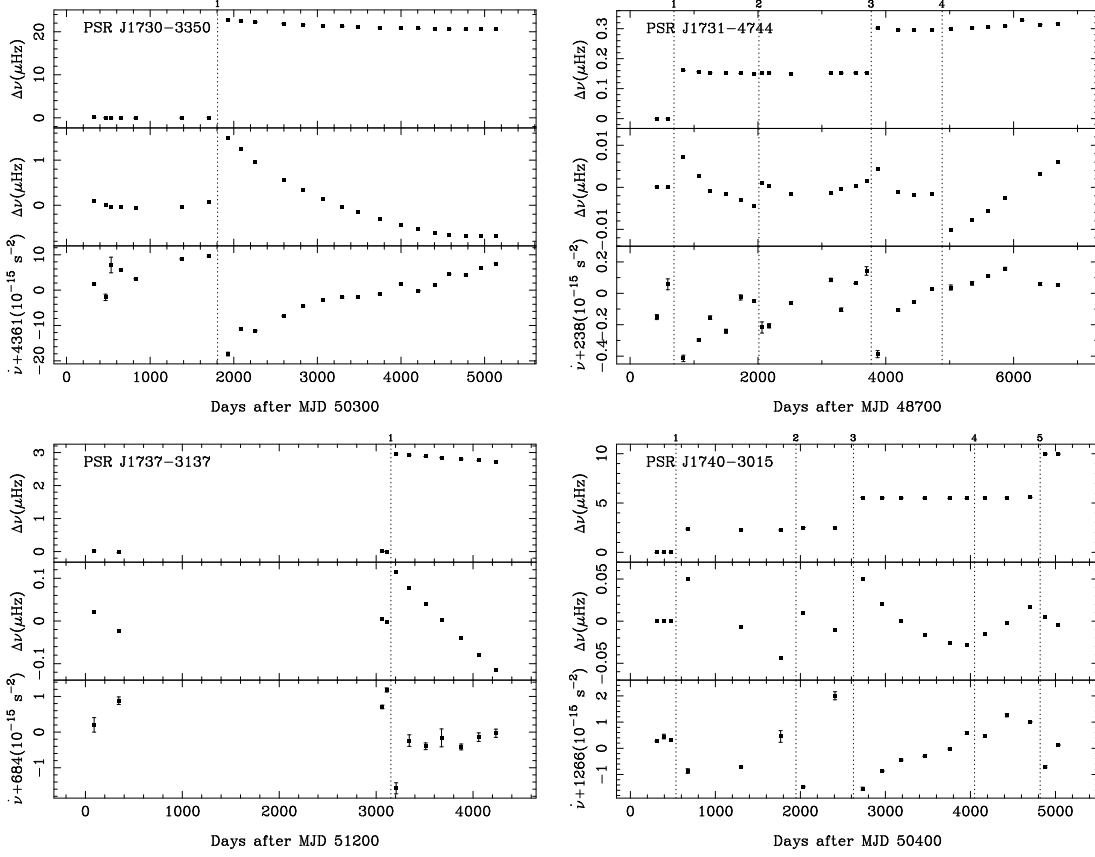


Figure 9. Glitches in PSRs J1730–3350, J1731–4744, J1737–3137 and J1740–3015. See Figure 3 for a description of each sub-plot.

linear recoveries but there may be exponential recoveries as well (Lyne et al. 1996; Wang et al. 2000). In this work, we fit exponential recoveries for glitches 3 and 5. For glitch 3, we obtained $Q \sim 0.025$ and $\tau_d \sim 200$ d and for glitch 5, $Q \sim 0.0065$ and $\tau_d \sim 25$ d.

4.31 PSR J1803–2137 (PSR B1800–21)

PSR J1803–2137 is very similar to PSR J1801–2451 in its timing properties with a characteristic age of 15 kyr. Four glitches have been detected in this pulsar (Shemar & Lyne 1996; Wang et al. 2000; Krawczyk et al. 2003; Yuan et al. 2010a; Espinoza et al. 2011a). Figure 10 shows the two glitches detected in this work. Both of these show clear long-term linear recoveries with a very similar slope (Table A1). Clear exponential recoveries with shorter timescales are also seen. For glitch 1, Wang et al. (2000) fitted a short timescale (~ 18 d) recovery and a ~ 850 d one to the longer-term decay. We found evidence in the phase residuals for two short-term decays with timescales of ~ 12 d and ~ 69 d; further relaxation is dominated by the linear recovery. For glitch 2, Yuan et al. (2010a) fit an exponential decay, obtaining $Q = 0.009(2)$ and $\tau_d = 120(20)$ d. We obtained consistent results as $Q = 0.00630(16)$ and $\tau_d = 133(11)$ d.

4.32 PSR J1809–1917

This pulsar has previously been reported to glitch once (Espinoza et al. 2011a). Figure 10 shows the evolution of

ν and $\dot{\nu}$ for ~ 12 yr. The glitch is large, with $\Delta\nu_g/\nu \sim 1.6 \times 10^{-6}$. Both exponential and linear recoveries can clearly be seen in our observations. Fitting showed that the exponential recovery is characterised by $Q \sim 0.006$ and $\tau_d \sim 125$ d. A linear recovery, presumably from an earlier glitch, is also seen before the glitch. The recovery after the observed glitch is slightly less steep, but both have $\ddot{\nu} \sim 35 \times 10^{-24} \text{ s}^{-3}$.

4.33 PSR J1825–0935 (PSR B1822–09)

So far, eight glitches have been detected for this pulsar; six were identified as “slow” glitches (Zou et al. 2004; Shabanova 2007; Yuan et al. 2010a; Espinoza et al. 2011a). Lyne et al. (2010) have shown that these “slow” glitches probably are a manifestation of “two-state” magnetospheric switching. Figure 11 presents our observations of the evolution of ν and $\dot{\nu}$ for ~ 9 yr. During this period, this pulsar was found to undergo three slow glitches (Zou et al. 2004; Shabanova 2007; Yuan et al. 2010a). Because of insufficient observations, these slow glitches were missed in our data. By using the available data, we were able to identify a “normal” glitch with $\Delta\nu_g/\nu \sim 1.3 \times 10^{-7}$. However, a data gap of ~ 500 d exists shortly after this glitch, making it impossible to study the post-glitch behaviour. This glitch was observed in more detail by the Xinjiang group (Yuan et al. 2010a).

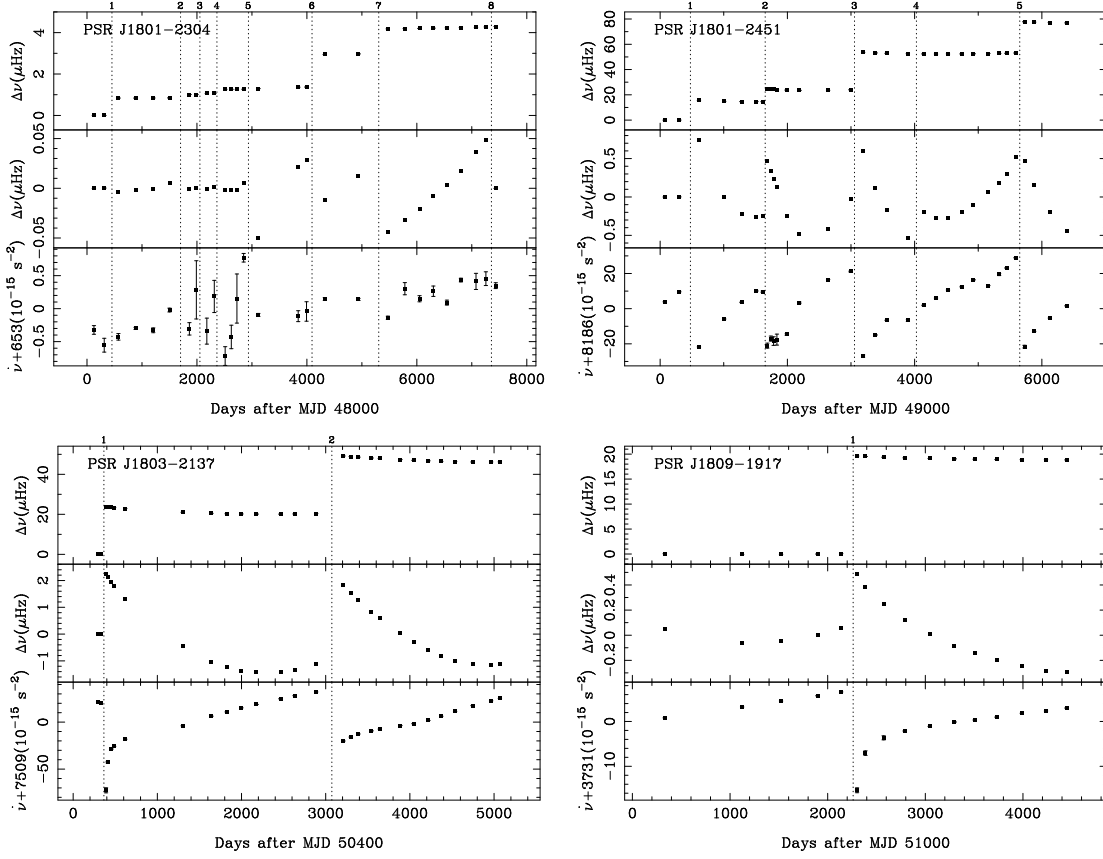


Figure 10. Glitches in PSRs J1801-2304, J1801-2451, J1803-2137 and J1809-1917. See Figure 3 for a description of each sub-plot.

4.34 PSR J1826-1334 (PSR B1823-13)

Five glitch events have been reported for this pulsar (Shemar & Lyne 1996; Yuan et al. 2010a; Espinoza et al. 2011a). Figure 11 presents the evolution of ν and $\dot{\nu}$ for ~ 13 yr. For glitch 1, our last pre-glitch observation was at MJD ~ 53186 , and the first post-glitch observation was at MJD ~ 53279 . Espinoza et al. (2011a) showed that there are actually two small glitches in this interval. One was at MJD ~ 53206 , with $\Delta\nu_g/\nu \sim 0.6 \times 10^{-9}$ and the other was at MJD ~ 53259 , with $\Delta\nu_g/\nu \sim 3 \times 10^{-9}$. The much larger glitch 2 was also observed by both Yuan et al. (2010a) and Espinoza et al. (2011a). We detected an exponential recovery for this glitch, characterised by $Q \sim 0.007$ and $\tau_d \sim 80$ d.

4.35 PSR J1835-1106

Figure 11 shows the evolution of ν and $\dot{\nu}$ for PSR J1835-1106 over about 10 yr. A small glitch with $\Delta\nu_g/\nu \sim 1.6 \times 10^{-8}$ was detected at MJD ~ 52220 . This event was also observed by Zou et al. (2004) and Espinoza et al. (2011a). As shown in Figure 11, the post-glitch frequency residuals exhibit a cubic structure, indicating a measurable $\ddot{\nu}$; fitting showed that this term is $1.58(13) \times 10^{-31} \text{ s}^{-4}$. These significant higher-order frequency derivatives indicate the presence of noise processes in the pulsar rotation. It is possible that this pulsar also has a two-state magnetospheric modulation affecting the value of $\dot{\nu}$ (Lyne et al. 2010).

4.36 PSR J1841-0524

This pulsar has been found to undergo three glitches (Espinoza et al. 2011a). The first two are small, with $\Delta\nu_g/\nu \gtrsim 2 \times 10^{-9}$. The latest one is large, with $\Delta\nu_g/\nu \sim 10^{-6}$. Parkes data have a gap, spanning from MJD ~ 52570 to MJD ~ 53619 . As a result, the MJD ~ 53562 glitch was missed. Figure 11 presents the evolution of ν and $\dot{\nu}$ for the past five years. At least for glitch 2, the post-glitch behaviour exhibits a linear recovery.

5 DISCUSSION

We have searched for glitch events in the timing residuals of 165 pulsars. Out of these, 107 glitches were identified with 46 new discoveries. Most of these new discoveries occur for southern-hemisphere pulsars that cannot be observed by the long-term monitoring programmes carried out in the northern hemisphere. Because of the relatively large gaps between many of our observations, there are 22 known glitches that are undetectable in our data sets. These missed glitches generally have fractional sizes $\Delta\nu_g/\nu$ between 10^{-10} and 10^{-9} . The measurement of $\Delta\nu_g$ is also very dependent on the data sampling as short-term transients can easily be missed or underestimated and in some cases our results differ from those in the literature.

In general, the post-glitch behaviour shows two types of recovery: a short-term exponential recovery (characterised

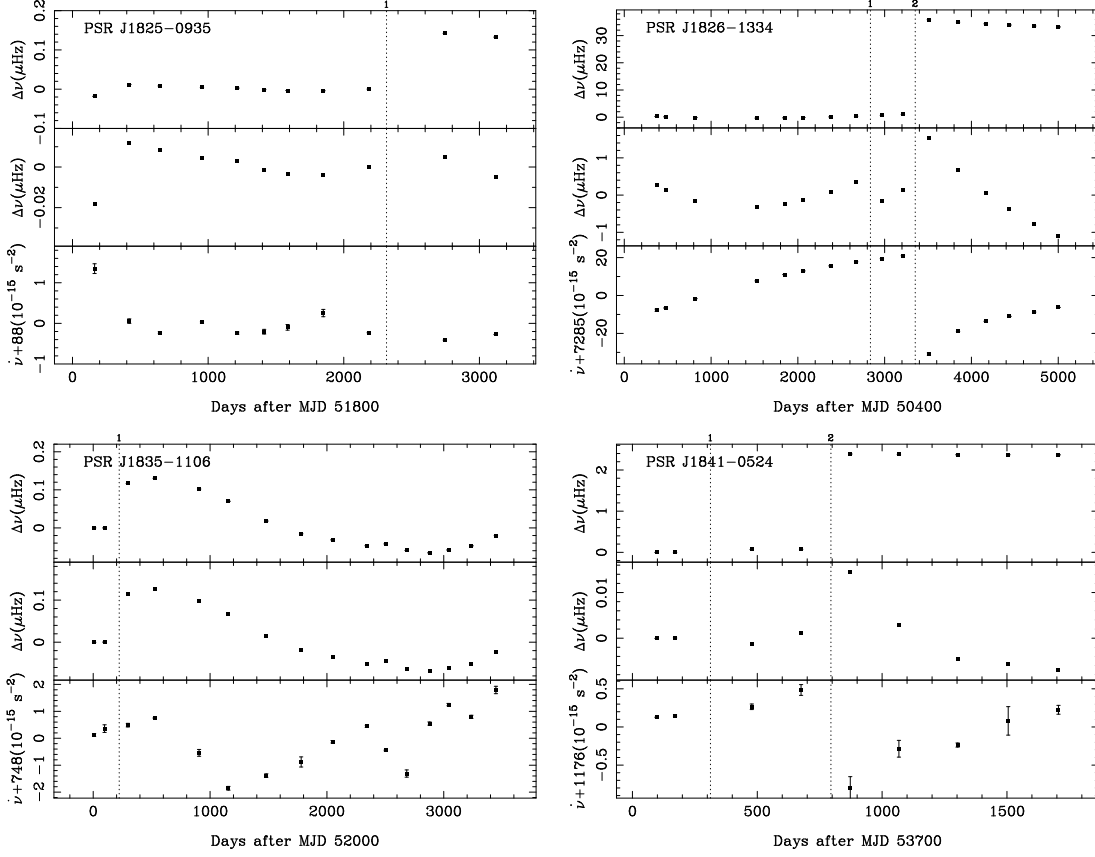


Figure 11. Glitches in PSRs J1825–0935, J1826–1334, J1835–1106 and J1841–0524. See Figure 3 for a description of each sub-plot.

by Q and τ_d) and a longer-term linear recovery in $\dot{\nu}$ (characterised by $\ddot{\nu}$). Both can be identified by inspecting the evolution of $\dot{\nu}$. In most cases, we have insufficient observations to study any exponential recoveries with timescale $\lesssim 20$ d. Most such short-term exponential recoveries will have been missed. However, we found that 27 glitches do show measurable post-glitch exponential recovery with time constants between 12 d and 300 d. For more than 90% of the observed glitches, values of post-glitch $\ddot{\nu}$, indicating a linear recovery in $\dot{\nu}$, were obtained. For many of these, the $\dot{\nu}$ slope was similar before and after the glitch, so the value of $\Delta\ddot{\nu}_p$ was not significant. For 13 glitches, the slope change was larger and a significant value for $\Delta\ddot{\nu}_p$ was obtained.

The discovery of 46 new glitches allows further study on the distribution of glitches and their post-glitch behaviour. The discussion on these two aspects is presented in §5.1 and §5.2 respectively.

5.1 The distribution of glitches

In Figure 12, the upper panel is a histogram of the fractional glitch size $\Delta\nu_g/\nu$. Our results reinforce the bimodal distribution of the observed fractional glitch sizes previously reported by numerous authors (e.g., Wang et al. 2000; Yuan et al. 2010a; Espinoza et al. 2011a). The first peak in this distribution lies around 2×10^{-9} and the second around 10^{-6} . Our observations mainly contribute to the second peak. Because of our rather infrequent sampling, it is very difficult for us to detect glitches with $\Delta\nu_g/\nu \lesssim 10^{-9}$.

As noted by Espinoza et al. (2011a) and others, the left edge of the distribution is strongly limited by observational selection. The actual number of small glitches could be large and the lower peak in Figure 12 may not even exist in the intrinsic distribution. However the dip at $\Delta\nu_g/\nu \sim 10^{-7}$ is clearly real and suggests that there may be two mechanisms that can induce a glitch event. As previously mentioned in §1, it has been proposed that starquakes caused by the cracking of stellar crust may generate small glitches, whereas large glitches may result from the sudden transfer of angular momentum from a crustal superfluid to the rest of the star.

The fractional glitch size is affected both by the size of the glitch and the pulse frequency of the pulsar. In the lower panel of Figure 12, we plot a histogram of the frequency jump $\Delta\nu_g$. As shown in the figure, the distribution of $\Delta\nu_g$ also has a bimodal distribution or at least has a dip between the large and small glitches. It is interesting that the peak for large glitches is much narrower in $\Delta\nu_g$ than it is in $\Delta\nu_g/\nu$, whereas the converse is true for the lower-frequency peak. A large fraction of the peak at the high end comes from just two pulsars, PSR J0537–6910 (Middleditch et al. 2006) and the Vela pulsar. These two pulsars have frequent glitches and most of them have $\Delta\nu_g \sim 20 \mu\text{Hz}$. The pulse frequencies however differ by a factor of about six.

Figure 13 shows the time sequence of glitch fractional sizes for seven pulsars where ten or more glitches were detected. This figure shows that the bimodal distribution of glitch sizes may be seen in individual pulsars as well. For example, most glitches in PSR J0537–6910 and the

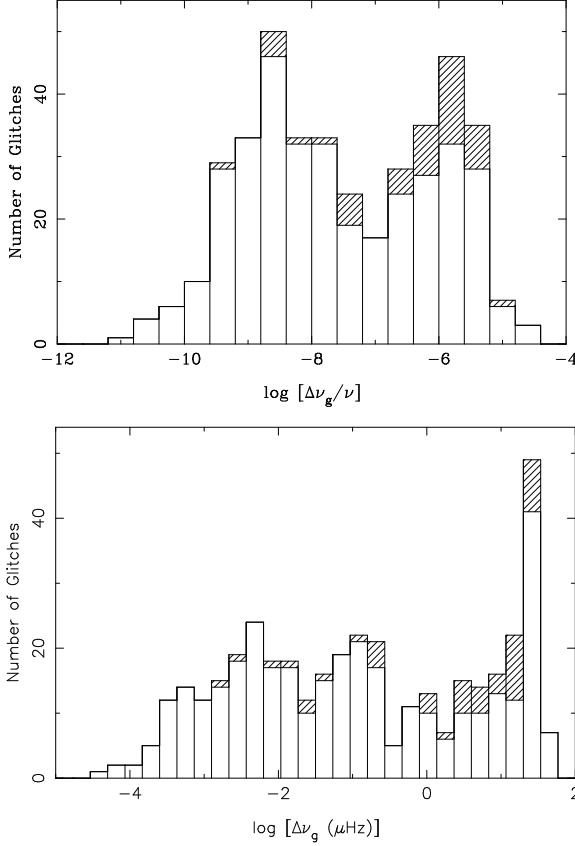


Figure 12. Histograms of the distributions of glitch fractional size $\Delta\nu_g/\nu$ (upper panel) and of glitch size $\Delta\nu_g$ (lower panel). The blank bars show the results from the previous work, while the shaded bars show the new detections from this work added on top of the previous results. For previously reported glitches, we use the ATNF glitch database which includes magnetar glitches.

Vela pulsar (PSR B0833–45) are large and similar in amplitude, but much smaller glitches were occasionally seen. Although not quite so clear, similar behaviour is seen in PSRs J1341–6220, J1740–3015, J0631+1036 (many small glitches and only one large glitch) and J1801–2304. It is evident from Figure 13 that we detected fewer small glitches in PSR J1341–6220 compared to earlier results. This may be because the frequent occurrence of larger glitches obscured some small glitches in our data set which is not as well sampled as the earlier ones.

In Figure 14, we show a set of period–period-derivative ($P-\dot{P}$) diagrams to present six quantities relevant to glitches. For previously published glitches, we refer to the ATNF Pulsar Catalogue glitch table. The six plotted quantities are a) the number of glitches detected in a given pulsar N_g , b) the average number of glitches per year \dot{N}_g , c) the fractional glitch size $\Delta\nu_g/\nu$, d) the glitch size $\Delta\nu_g$, e) the rms glitch fractional size and f) the rms fractional size normalised by the mean value for that pulsar. For sub-plots c) and d), if a pulsar has glitched more than once, then the largest value is plotted. In each $P-\dot{P}$ diagram, the size of the symbols (circle or triangle) is a linear function of the magnitude of the given quantity; we adjusted the slopes and offsets

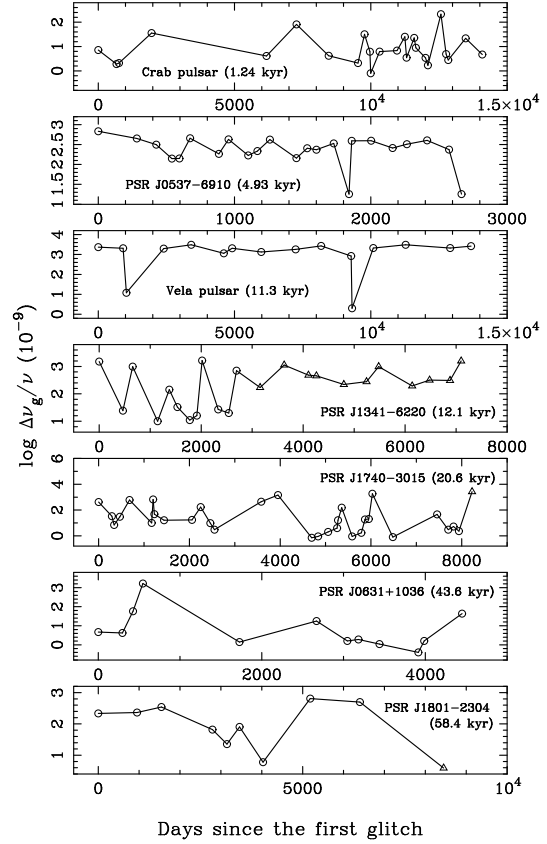


Figure 13. The time series of glitch events for the seven pulsars where ten or more glitches were detected. Data from the ATNF Pulsar Catalogue glitch table are indicated by circles, while those from this work are indicated by triangles. For each pulsar, its characteristic age is shown in parentheses.

for the different functions to give appropriate sizes for the symbols.

Table A3 gives the number of detected glitches N_g , the observation data span and the rate of glitches for known glitching pulsars \dot{N}_g . The uncertainty of the glitch rate was estimated as the square-root of N_g divided by the data span.

We discuss these results in the following subsections.

5.1.1 The number and rate of glitches

Large numbers of glitches were observed in the pulsars with characteristic ages between 10^3 and 10^5 yr; the seven pulsars that have been observed to show ten or more glitches are within this age region. If magnetic-dipole radiation is assumed, then the inferred surface magnetic field for the seven pulsars spans from $\sim 10^{12}$ to $\sim 10^{13}$ G. But there are some young pulsars that have not been observed to glitch, although they also have relatively long data spans. For instance, PSR J1513–5908 has a characteristic age of ~ 1.5 kyr; it is the youngest pulsar in our sample of 165 pulsars. This pulsar has been observed for more than 28 years (Livingstone & Kaspi 2011) with no evidence for any glitch activity. On the other hand, PSR J1119–6127 has a similar characteristic age of ~ 1.6 kyr and three glitches have been observed in its ~ 13 -yr timing data span.

The 23 glitches observed for PSR J0537–6910 oc-

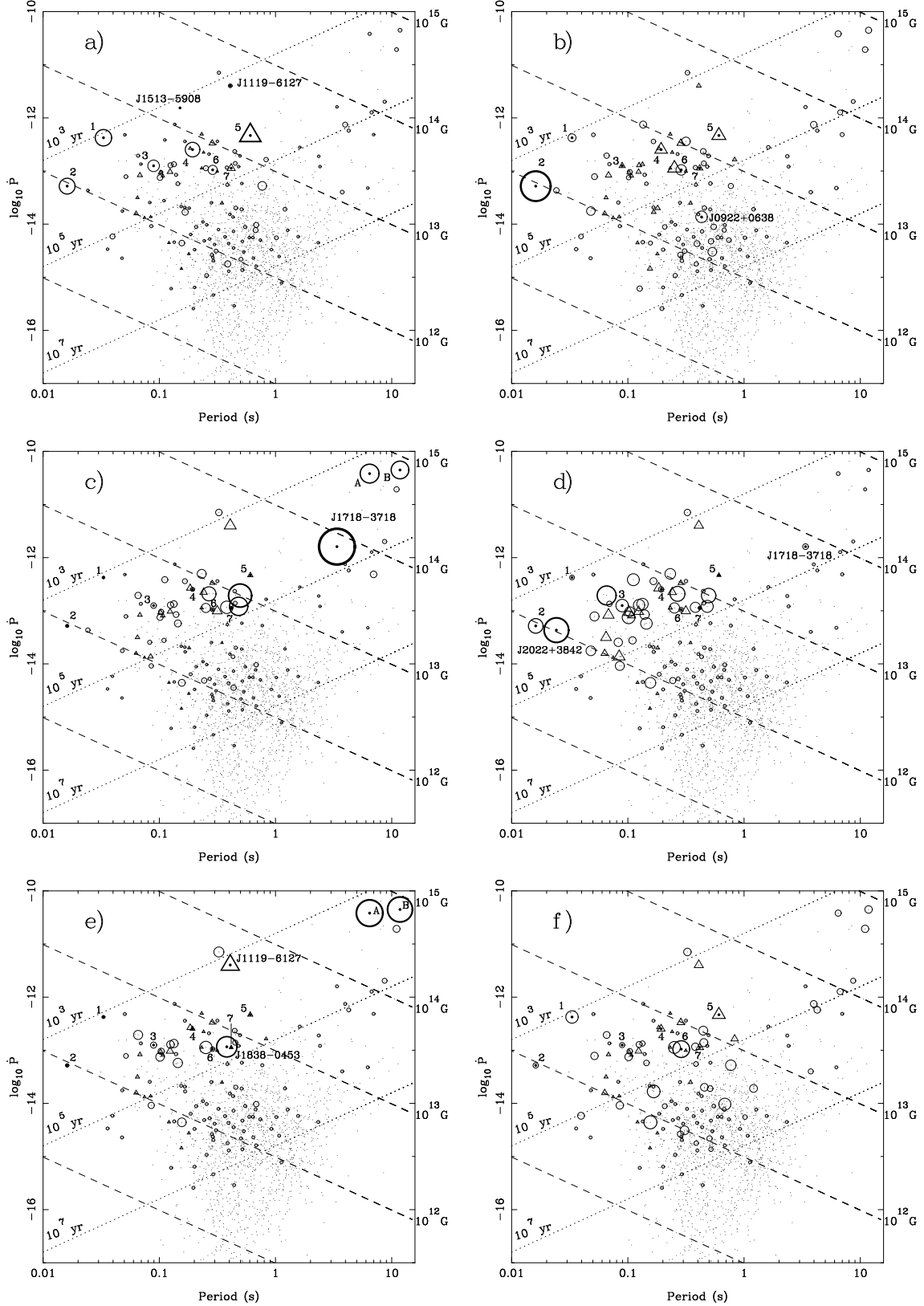


Figure 14. P - \dot{P} diagrams for glitch-related quantities of the a) number of detected glitches; b) average number of glitches per year; c) maximum fractional glitch size; d) maximum glitch size; e) rms fractional glitch size; and f) rms fractional size normalised by the mean. A circle indicates the parameter was obtained from the ATNF Pulsar Catalogue glitch table, whereas a triangle symbol indicates a parameter from this work. In the various plots, the seven pulsars exhibiting ten or more glitches are marked: 1 – PSR B0531+21 (Crab pulsar); 2 – PSR J0537–6910; 3 – PSR B0833–45 (Vela pulsar); 4 – PSR J1341–6220; 5 – PSR J1740–3015; 6 – PSR J0631+1036; 7 – PSR J1801–2304; and two magnetars: A – PSR J1048–5937 (1E 1048.1–5937) and B – PSR J1841–0456 (1E 1841–045).

curred in ~ 7.6 yr, resulting in a large glitch rate of $\sim 3.0 \text{ yr}^{-1}$; this pulsar is the most frequently glitching pulsar known. The second most frequently glitching pulsar is PSR J1740–3015. This pulsar has 32 glitches in ~ 25 yr, giving a glitch rate of $\sim 1.3 \text{ yr}^{-1}$. As shown in sub-plot b) of Figure 14, the positions of these two pulsars on the $P-\dot{P}$ diagram are quite different: the pulse period for PSR J0537–6910 is about a factor of 40 less than that of PSR J1740–3015 and \dot{P} is about an order of magnitude smaller. Hence the two pulsars are both relatively young, with characteristic ages of 5 kyr and 20 kyr respectively. The dipole magnetic field strength of PSR J1740–3015 is more than an order of magnitude stronger than that of PSR J0537–6910. We found that PSRs J0729–1448, J1341–6220 and J0922+0638 also exhibit glitches more than once per year. For PSR J1341–6220, the Parkes observations have detected 25 glitches during ~ 20 yr. PSR J0729–1448 has glitched four times during its data span of ~ 3.3 yr. For PSR J0922+0638, one glitch has been detected in a data span of just one year (Shabanova 2010), so the inferred high glitch rate is very uncertain. On the $P-\dot{P}$ diagram, the characteristic-age lines of 10^3 and 10^5 yr together with the magnetic-field lines of 10^{12} and 10^{13} G define a region where pulsars are observed to exhibit more glitches and large glitch rates.

5.1.2 Glitch sizes

As shown in sub-plot c) in Figure 14, large fractional glitch sizes $\Delta\nu_g/\nu$ are generally observed in young pulsars with long periods (i.e., small ν). The largest known, $\sim 3.3 \times 10^{-5}$, was detected in PSR J1718–3718 which has a pulse period of 3.38 s (Manchester & Hobbs 2011) but a characteristic age of only 34 kyr and an inferred dipole field strength of 7.4×10^{13} G, one of the highest known for radio pulsars. Magnetars detected at X-ray wavelengths are also known to suffer large glitches and have long pulse periods and even higher inferred dipole fields. For example, PSR J1048–5937 (1E 1048.1–5937) and PSR J1841–0456 (1E 1841–045) are both X-ray detected magnetars which have had glitches with $\Delta\nu_g/\nu > 10^{-5}$ (Dib et al. 2008, 2009).

Not surprisingly, the absolute frequency jumps $\Delta\nu_g$ tend to be larger for the shorter-period (larger ν) pulsars since they are not normalised by ν . Sub-plot d) of Figure 14 shows the distribution of $\Delta\nu_g$ values on the $P-\dot{P}$ diagram confirming this expectation. The largest frequency-jump was observed in the 24-ms pulsar J2022+3842; the pulse frequency of this source gained $\sim 78 \mu\text{Hz}$ in its MJD ~ 54675 glitch (Arzoumanian et al. 2011). Sub-plot d) of Figure 14 also shows that the glitch size $\Delta\nu_g$ is also correlated with characteristic age. Pulsars with young ages tend to have larger jumps, but this correlation breaks down for the very young pulsars such as the Crab pulsar (PSR B0531+21) and PSR J1513–5908.

5.1.3 Glitch variability

Sub-plot e) of Figure 14 shows the rms fluctuation in fractional glitch sizes. The magnetars PSR J1048–5937 (1E 1048.1–5937) and PSR J1841–0456 (1E 1841–045) show a wide range of glitch sizes, with $\Delta\nu_g/\nu$ ranging from

$\sim 1.4 \times 10^{-6}$ up to $\sim 1.6 \times 10^{-5}$. Although most of the glitches in the Vela pulsar are large, there have been two small glitches (see Figure 13) and so the rms fluctuation of glitch size is relatively large. After the magnetars, large rms variations are found in the high-magnetic-field radio pulsar J1119–6127 and PSR J1838–0453. There seems a tendency for more variability in glitch size in older pulsars. This is also seen in sub-plot f) where the rms fluctuation has been normalised by the mean value to give an effective “modulation index” for glitch size fluctuations. However, this conclusion is not very certain as only a small number of glitches were detected in PSR J1838–0453 and some other pulsars. Also, the results may be biased by the difficulty in detecting small glitches in noisy pulsars. In sub-plot f) there is more scatter in this plot though with the Crab pulsar being more prominent because of its relatively small mean glitch size.

5.1.4 Implications for neutron-star physics

In the angular-momentum-transfer model, a glitch is understood as a sudden transfer of angular momentum from a more rapidly rotating interior superfluid to the neutron star crust (e.g., Alpar et al. 1981). The angular momentum of a rotating superfluid is carried by an array of vortices; each vortex contains a quantised unit of angular momentum. In principle, if the rotation of a superfluid is slowing down, then the surface density of the vortices will be decreasing, or, in other words, the vortices will migrate away from the rotation axis. However, in the solid crust of a neutron star, the vortices of the neutron superfluid tend to pin onto the nuclear lattice (Alpar 1977; Epstein & Baym 1988). The pinning between the vortices and the crystal lattice will not be broken until the force induced by the differential rotation (or the “Magnus” force) between the superfluid and the crust reaches a critical value, beyond which an avalanche process of unpinning and a substantial transfer of angular momentum could be triggered.

Sub-plots c) and d) of Figure 14 shows that large glitches, either relative or absolute, are mostly confined to the pulsars with characteristic ages smaller than 10^5 yr. The largest fractional glitch sizes are observed in long-period, low- ν pulsars. This suggests that a larger fraction of the excess angular momentum of the superfluid is transferred to the crust in these pulsars. For very young pulsars such as the Crab pulsar, glitch sizes are much smaller and somewhat less frequent. For a very young neutron star, as the result of the internal high temperature, the superfluid vortices could creep against the pinning energy barrier, preventing the formation of pinning zones and the sudden release of pinned vortices (Alpar et al. 1984a). Ruderman et al. (1998) have suggested that, because of tangling of the vortices and magnetic flux tubes, as the neutron star spins down the core flux-tubes are pulled by the vortex lines, moving toward the stellar equator. The moving core flux-tubes lead to a build-up of the shear stress in the stellar crust (Srinivasan et al. 1990). Once the stress grows to exceed the yield strength of the crust, then the consequent cracking of the stellar surface may cause small period jumps in the rotation of the neutron star (Ruderman 2009). This could be the mechanism for the observed small glitches in the Crab and other pulsars such as Vela and PSR J1740–3015. It is also possible that such

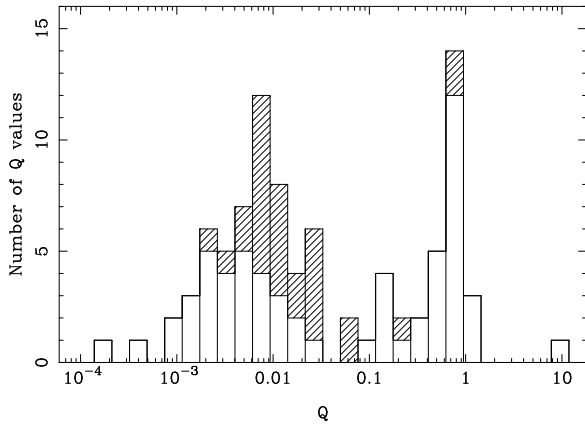


Figure 15. Histogram for the recovery fraction Q of exponential decays. Data for the blank bars are from the literature as given in Table A4, while the shaded bars show values from this work.

processes may trigger the large-scale release of angular momentum needed for glitches with large fractional glitch sizes.

5.2 Glitch recoveries

Pulsars show a variety of behaviours following a glitch. Part of the step change in both ν and $\dot{\nu}$ often recovers exponentially, in some cases with more than one identifiable time constant. Following this exponential recovery, a linear increase in $\dot{\nu}$ (decrease in slow-down rate $|\dot{\nu}|$) is often observed. Normally this continues until the next glitch. Finally, apparently permanent changes in ν , $\dot{\nu}$ and/or $\ddot{\nu}$ are sometimes left after the transient recoveries. We searched for evidence of these different types of recovery in all 107 observed glitches.

5.2.1 Exponential recoveries

In our sample, 27 glitches in 18 pulsars had an identifiable exponential recovery. The observed fractional recovery Q and recovery time constant τ_d for these glitches are given in Table A2. All but two of the exponential recoveries are well modelled by a single exponential term. Two exponential terms were required for glitch 3 in PSR J1119–6127 and glitch 1 in PSR J1803–2137. The largest $Q \sim 0.84$ was detected in glitch 2 in PSR J1119–6127. Table A4 summarises the parameters for the previously reported exponential recoveries. Multiple decays were observed for three pulsars, the Crab pulsar, the Vela pulsar and PSR J2337+6151. However, the strong observational selection against observing short-term recoveries in most pulsars needs to be recognised.⁶

Figure 15 shows the histogram of the fractional exponential recoveries Q . The observed values span a very wide range from the smallest ~ 0.00014 observed in PSR J1841–0425 (Yuan et al. 2010a) to the largest ~ 8.7

recently detected in the young X-ray pulsar J1846–0258 (Livingstone et al. 2010). The histogram is clearly bimodal with a broad peak around 0.01 and another very close to 1.0. This strongly suggests that there are two different mechanisms for the exponential recovery following a glitch.

To further explore the properties of the exponential recoveries, all known values of Q and τ_d are shown in Figure 16 as a function of the fractional glitch size $\Delta\nu_g/\nu$, the pulsar characteristic age and the surface magnetic-dipole field. In sub-plot a), it is striking that glitches with $Q \sim 1$ are found over the whole range of fractional glitch sizes, whereas those with small Q are only found in the larger glitches with $\Delta\nu_g/\nu \gtrsim 10^{-6}$. Because of random period irregularities, it will be difficult or impossible to detect exponential recoveries in many small glitches with $\Delta\nu_g/\nu \lesssim 10^{-8}$. However, such decays should be detectable in most glitches with $\Delta\nu_g/\nu \sim 10^{-7}$. Therefore there appears to be a real absence of exponential recoveries with $Q \sim 0.01$ for glitches with $\Delta\nu_g/\nu \lesssim 3 \times 10^{-7}$. It is also worth noting that, for many glitches, both large and small, no exponential recovery is detected (Table A2), so effectively $Q \sim 0$ in these cases. These results suggest that the real physical distinction between pulsars with large glitches and those with small glitches (cf. Figure 12) is more complex with the glitch recovery parameter also being important.

Unlike Q , the distribution of the time constant τ_d relative to $\Delta\nu_g/\nu$ shown in sub-plot b) is more uniform with decay timescales from a few days to a few hundred days seen in glitches of all sizes.

Sub-plot c) of Figure 16 shows that the large- Q glitch recoveries are observed in both young and old pulsars, whereas the large glitches, which have low Q , are not seen in the very young pulsars. As discussed above, the large glitches primarily occur in pulsars with characteristic ages between 10^4 and 10^5 years. Sub-plot d) gives some support to the suggestion of Yuan et al. (2010a) that there is a positive correlation of τ_d with pulsar characteristic age. There is a clear absence of short-term decays for the older pulsars that cannot be accounted for by observational selection. Sub-plots e) and f) show the dependence of Q and τ_d on surface dipole field strength. Since this is derived from P and \dot{P} , as is the characteristic age, it is not surprising that these plots show basically the same dependences as sub-plots c) and d). However, they do highlight the fact that the magnetars, with $B_s \gtrsim 10^{13}$ G, have high- Q glitch recoveries (Kaspi & Gavril 2003; Dib et al. 2008; Gavril et al. 2011). The largest observed $Q \sim 8.7$, indicating a massive over-recovery, was detected in the young X-ray-detected but spin-powered pulsar PSR J1846–0258, which has an intermediate period, ~ 0.326 s, a very high implied dipole magnetic field, $B_s \sim 5 \times 10^{13}$ G and is located near the centre of the supernova remnant Kes 75 (Livingstone et al. 2010).

5.2.2 Linear recovery

It has been well recognised that the long-term recovery from a glitch is generally dominated by a linear increase in $\dot{\nu}$, that is, a linear decrease in the slow-down rate $|\dot{\nu}|$ or, equivalently, in \dot{P} (Downs 1981; Lyne et al. 1996; Lyne et al. 2000; Wang et al. 2000; Yuan et al. 2010a). This effect is clearly seen in most of the $\dot{\nu}$ plots given in Figures 3 – 11, especially for the larger glitches. The linear trend normally becomes

⁶ Note that we do not consider the 1.2-min recovery observed after the Vela MJD 51559 glitch by Dodson et al. (2002) for two reasons: a) the parameters of the recovery are very uncertain and b) it is unique in that such short timescale recoveries cannot be observed for any other known pulsar.

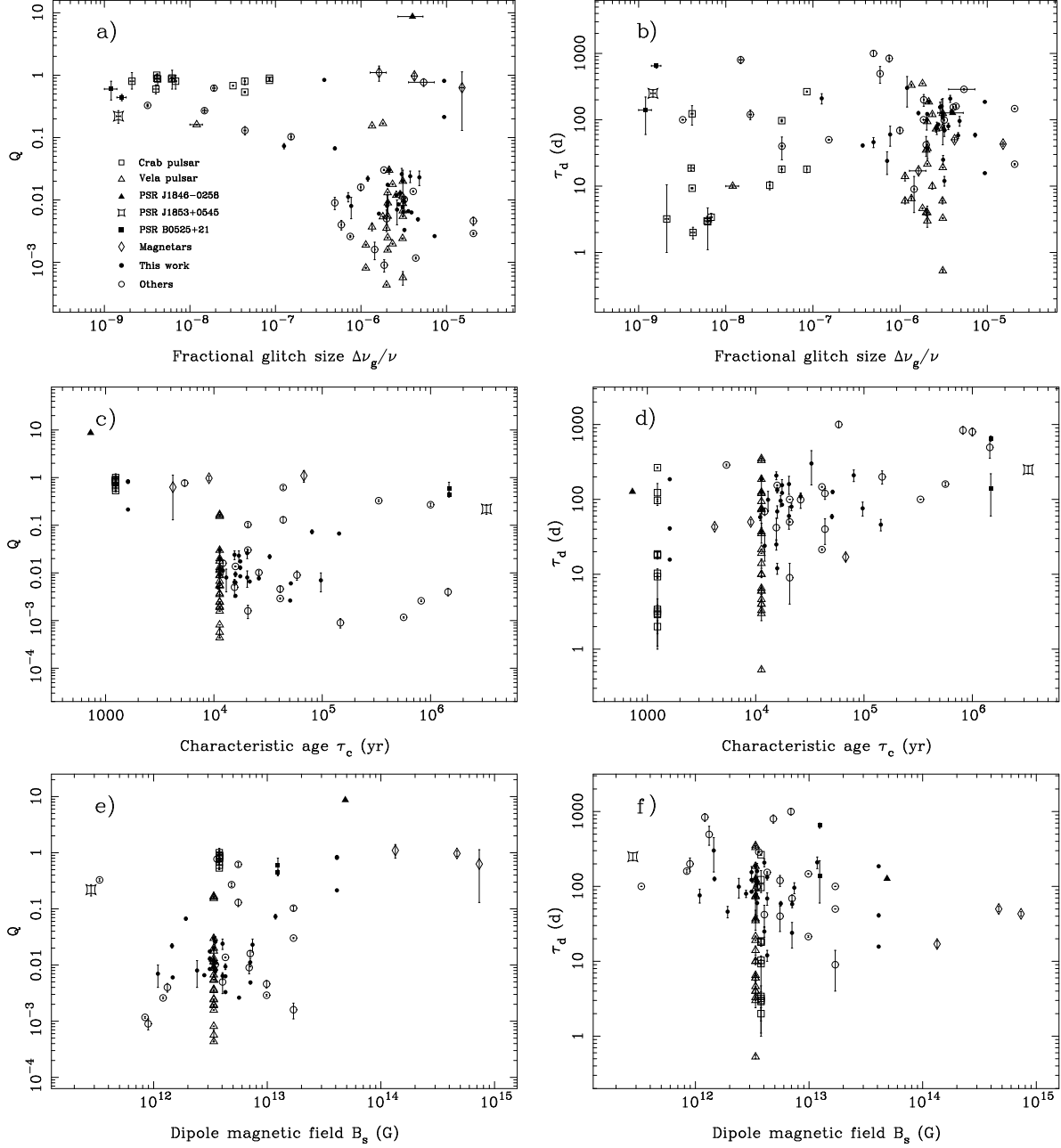


Figure 16. Dependences of the post-glitch exponential recovery parameters Q and τ_d on the observed glitch fractional size, the pulsar characteristic age τ_c and the dipole magnetic field B_s : a) Q versus $\Delta\nu_g/\nu$, b) τ_d versus $\Delta\nu_g/\nu$, c) Q versus τ_c , d) τ_d versus τ_c , e) Q versus B_s and τ_d versus B_s .

evident at the end of the exponential recovery and persists until the next glitch event. In cases where the exponential recovery is absent or has very low Q , e.g., PSR J1301–6305 (Figure 5) the linear recovery begins immediately after the glitch. The rate of increase in $\dot{\nu}$ is quantified by fitting for $\ddot{\nu}$ in the pre-, inter- and post-glitch intervals following the decay of any exponential recovery. Values of $\ddot{\nu}$ obtained in this way are given in Table A1 and are plotted in Figure 17 for 32 pulsars. No significant $\ddot{\nu}$ value was obtained for four glitching pulsars, in most cases because available data spans were too short. Of the 108 $\ddot{\nu}$ values plotted, 11 are negative.

These are for pulsars where timing noise is relatively strong and/or the available data spans are short.

There is no doubt that these linear increases in $\dot{\nu}$ are related to internal neutron-star dynamics and recovery from glitches. Firstly, the value of $\ddot{\nu}$ often changes at the time of a glitch. Clear examples of slope changes at glitches are seen for the Vela pulsar (Figure 3), PSR J1420–6048 (Figure 6) and PSR J1709–4429 (Figure 8). In other cases however, e.g., PSR J1301–6305 (Figure 5) and PSR J1803–2137 (Figure 10), there is little or no slope change at a glitch. Secondly, although a positive value of $\ddot{\nu}$ is expected from normal magnetospheric braking, the observed values are generally

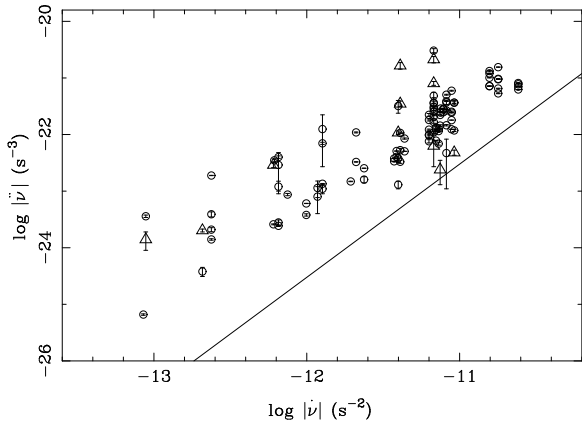


Figure 17. Linear decay rate $\dot{\nu}$ as a function of $|\dot{\nu}|$ for 32 glitching pulsars. The symbols of a circle and triangle indicate positive and negative values, respectively. The solid line gives the $\dot{\nu}_{\text{ext}}$ resulting from external or magnetospheric braking with $n = 3$ and for $\nu = 10$ Hz.

much larger. Pulsar braking is normally described by the braking index n , defined by

$$n = \frac{\dot{\nu}\nu}{\ddot{\nu}^2} \quad (4)$$

where $n = 3$ for magnetic-dipole braking. This relation is shown in Figure 17 assuming $n = 3$ and for a typical young pulsar with $\nu = 10$ Hz. The magnetospheric or external contribution $\dot{\nu}_{\text{ext}}$ is well below the observed values. Observed braking indices attributable to magnetospheric braking are generally less than 3.0 (e.g., Espinoza et al. 2011b) which increases the discrepancy. However, for young long-period pulsars, the discrepancy is less. For example, PSR J1119–6127 has a value of $\dot{\nu}$ for magnetic-dipole braking comparable to the minimum observed values (Table A1) and its braking index is close to 3.0 (Weltevrede et al. 2011). However, there are significant changes in $\dot{\nu}$ at the glitches in this pulsar, with the largest observed value being more than a factor of two higher. So even in this case, it is clear that glitch-related phenomena contribute to the $\dot{\nu}$ value.

Figure 18 shows the change in slope of the linear recoveries at glitches, $\Delta\dot{\nu}$, as a function of slow-down rate $|\dot{\nu}|$ and glitch fractional size. Sometimes $\Delta\dot{\nu}$ is solved for as part of the glitch fit (Table A2), but often the data spans used for this are too short to define $\Delta\dot{\nu}$ well. Therefore, in order to enlarge the sample as much as possible, we took the difference in $\dot{\nu}$ between each pair of the pre- and post-glitch solutions given in Table A1. We found that, out of the available 66 values, 35 are positive (53%) and 31 are negative (47%) in accordance with our expectation that the positive and negative changes would be approximately evenly balanced. Panel a) further illustrates that the changes are comparable in magnitude to the $\dot{\nu}$ values plotted in Figure 17, implying that the amount of additional braking can change dramatically at a glitch. Panel b) shows that the amount of change is not strongly dependent on the glitch size, with both large and small glitches inducing a wide range of slope changes relative to the $\dot{\nu}$ value. Since large glitches usually occur in relatively young pulsars, most of which have a large $|\dot{\nu}|$ (cf. Figure 14, panel d), it is not surprising that the largest values of $\Delta\dot{\nu}$ occur in glitches with large $\Delta\nu_g/\nu$.

5.2.3 Implications for neutron-star physics

Alpar et al. (1984a,b, 1993) have suggested that the observed different types of glitch recoveries are a manifestation of “vortex-capacitive” and “vortex-resistive” regions in the interior superfluid. For the former, the vortices decouple from the normal spin of the crust in a glitch but only share angular momentum at the time of the glitch, whereas for the latter, the vortices drift via a continuous pinning and unpinning, continuously coupling their angular momentum to the crust. At a glitch, the vortices in the resistive zones unpin and then gradually repin until the next glitch, resulting in the observed exponential and linear recoveries in $\dot{\nu}$. The resistive region may contain several sub-layers, some of which may have a linear response and others a non-linear response to the glitch. In this context, a linear response means that the amplitude of the associated exponential recovery toward the steady state is proportional to the perturbation in the angular velocity of a particular sub-layer at the time of a glitch. This occurs when the internal temperature is high compared to the pinning energy and the differential angular velocity between the superfluid layer and the crust is small (Alpar et al. 1993). On the other hand, in outer layers where the temperature is low compared to the pinning energy, the equilibrium lag is large and the response is not linear with the angular-velocity perturbation. Equilibrium is generally not reached before the occurrence of the next glitch and there is an effectively linear increase in $\dot{\nu}$.

Following Alpar et al. (1993), we label the linear-response layers that are responsible for the exponential recoveries, $i = 1, 2, \dots$, with moments of inertia I_i , and the nonlinear response layer, responsible for the linear recovery in $\dot{\nu}$, layer A with moment of inertia I_A . For the exponential recoveries, the decaying part of $\Delta\dot{\nu}$ is

$$\Delta\dot{\nu}_{d,i} = -Q_i \frac{\Delta\nu_g}{\tau_{d,i}} = -\frac{I_i}{I} \frac{\Delta\nu_g}{\tau_{d,i}} \quad (5)$$

where I is the total moment of inertia of the star. For the large glitches, the median observed value of Q is about 0.01 (Figure 16a) showing that the linear-response superfluid layers contain about 1% of the total moment of inertia.

The situation is clearly different for the pulsars for which $Q \sim 1$. In the simplest two-component models with a solid crust and a superfluid interior, where the superfluid is weakly coupled to the crust, $Q \approx I_n/I$, where I_n is the total moment of inertia of the superfluid neutrons (e.g., Baym et al. 1969). So one explanation for the high- Q events is that a large fraction of the total stellar moment of inertia is in the form of superfluid neutrons that are weakly coupled to the crust. The degree of coupling is evidently quite variable, with decay time constants ranging from a few days for the Crab pulsar to tens or hundreds of days for other pulsars. This explanation for high- Q decays can apply regardless of the mechanism for the glitch itself; this may be related to the fact that these decays are observed to follow both large and small glitches. The observed overshoot in the very young pulsar J1846–0258, with an apparent Q of ~ 8.7 (Livingstone et al. 2010), is clearly anomalous with no other similar overshoots being observed. As suggested by Livingstone et al. (2010) it is likely that this behaviour resulted from a glitch-induced change in the external torque.

In the Alpar et al. models, the observed approximately linear recoveries in $\dot{\nu}$ are related to the properties of an outer

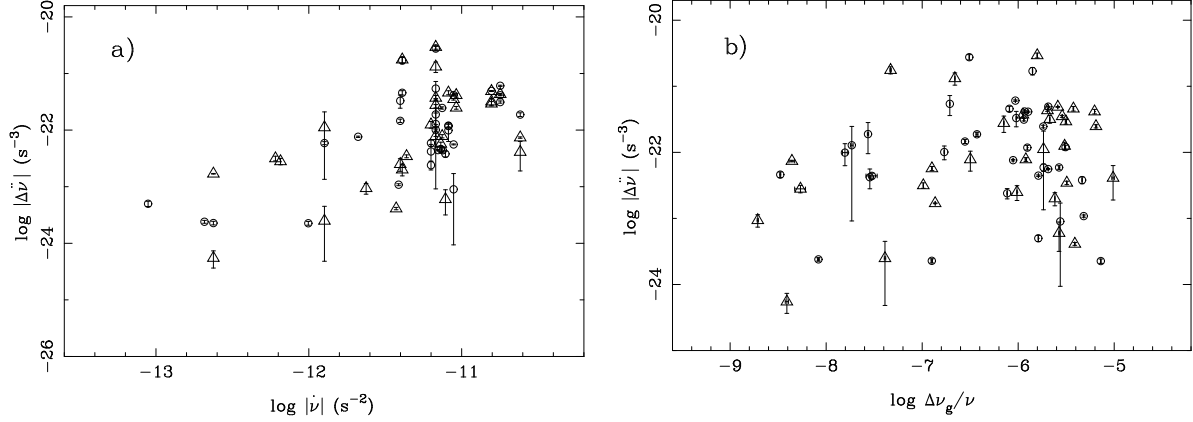


Figure 18. The change in slope of linear $\dot{\nu}$ recoveries at glitches, $\Delta\dot{\nu}$, as a function of a) $|\dot{\nu}|$ and b) glitch fractional size $\Delta\nu_g/\nu$. Circles and triangles indicate the positive and negative values, respectively.

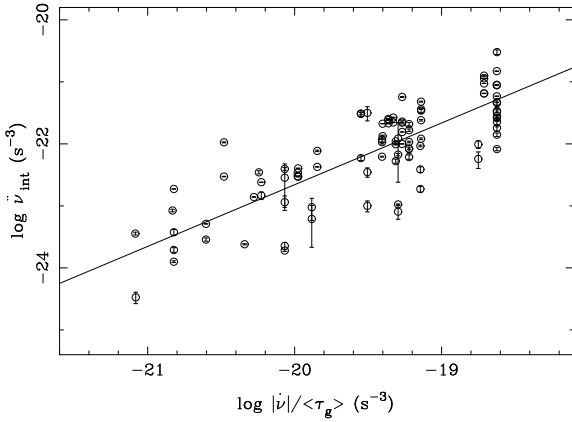


Figure 19. The observed glitch-related $\dot{\nu}_{\text{int}}$ as a function of the ratio of $|\dot{\nu}|$ and the mean interglitch interval $\langle\tau_g\rangle$. The solid line shows a fitted straight line which has a slope very close to 1.0 (see text).

superfluid layer in which the coupling is very weak so that the rotational lag between the crust and the superfluid is very large. For this case, Alpar & Baykal (2006) show that the $\dot{\nu}_{\text{int}}$ related to glitch recovery is given by

$$\dot{\nu}_{\text{int}} = \frac{I_A}{I} \frac{|\dot{\nu}|}{\tau_g} \quad (6)$$

where τ_g is the interglitch interval and I_A is the inertial moment of layer A. Figure 19 shows $\dot{\nu}_{\text{int}} = \dot{\nu}_{\text{obs}} - 3\dot{\nu}^2/\nu$ versus $|\dot{\nu}|/\langle\tau_g\rangle$, where $\langle\tau_g\rangle$ is the mean interglitch interval (Table A3). A correlation is clearly seen, with an unweighted-least-squares fit giving

$$\dot{\nu}_{\text{int}} = 10^{-2.8(1.4)} (|\dot{\nu}|/\langle\tau_g\rangle)^{1.00(7)}. \quad (7)$$

Remarkably, the slope of the fitted line is equal to the expected value of 1.0 based on Equation (6). Furthermore, the proportionality constant, $\sim 10^{-2.8} \approx 0.0016$ is comparable to the median value of $\Delta\dot{\nu}_g/\dot{\nu}$, 0.0034 (Table A2), although this quantity has a large scatter. This is consistent with the non-linear response models where both of these quantities are equal to I_A/I (Alpar et al. 1993; Alpar & Baykal 2006).

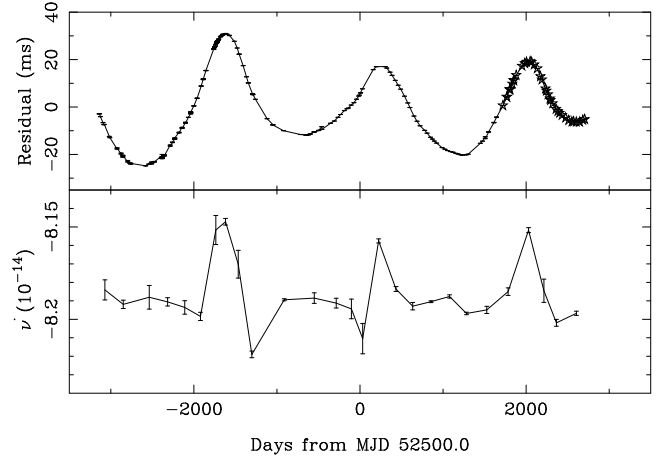


Figure 20. Timing residuals for PSR J1539–5626 after fitting up to $\dot{\nu}$ are shown in the top panel. Points marked with \star are from digital filterbank observations. The bottom panel shows the variations $\dot{\nu}$.

5.3 Slow glitches

So-called “slow glitches” have been observed in a number of pulsars. In these events, $\dot{\nu}$ rises sharply and declines over the next few hundred days roughly to its pre-glitch state. This results in a persistent increase in ν relative to the pre-glitch variation. Slow glitches were first observed in PSR J1825–0935 (PSR B1822–09) (Zou et al. 2004; Shabanova 2007; Yuan et al. 2010a) and have been reported in several other pulsars by Yuan et al. (2010a). Hobbs et al. (2010) suggested that these slow glitches are a manifestation of the discrete states in spin-down rate first seen in PSR B1931+24 (Kramer et al. 2006). Lyne et al. (2010) further showed that the discrete spin-down states were correlated with pulse shape changes, implying that the slow-glitch glitch phenomenon has a different origin to normal glitches for which the pulse shape changes are not expected. Nevertheless they are discrete events which result in a step change in spin frequency, so it is reasonable to label them as “slow glitches”.

Our data for PSR J1825–0935 (Figure 11) do not clearly show the slow glitches since there were insufficient observations at the relevant times. However, for PSR J1539–5626, we see slow-glitch features as shown in Figure 20. The top panel shows the timing residuals for this pulsar showing the quasi-sinusoidal features as observed in many pulsars (Hobbs et al. 2010). The bottom panel shows the episodic increases in $\dot{\nu}$ that characterise the slow-glitch phenomenon. The two states have $\dot{\nu} \sim -8.19 \times 10^{-14} \text{ s}^{-2}$ and $\dot{\nu} \sim -8.15 \times 10^{-14} \text{ s}^{-2}$, a relative variation of just 0.5% in $\dot{\nu}$. Lyne et al. (2010) found values of $\Delta\dot{\nu}/\dot{\nu}$ of between 0.3% and 45% in different pulsars. Furthermore, they found a relationship between the size of the change in $\dot{\nu}$ and the size of the pulse-shape change between the two states. The small percentage change in $\dot{\nu}$ for PSR J1539–5626 therefore suggests that any correlated pulse shape changes will also be small and so far we have been unable to find convincing evidence for the changes in either pulse shape or polarisation properties.

6 CONCLUSION

In this paper, we reported the results of a search for glitch events in the timing residuals of 165 pulsars, covering a total data span of 1911 yr. A total of 107 glitches was detected in 36 pulsars of which 13 were not previously known to glitch and 46 glitches are new discoveries. As constrained by our observational sampling, glitches with $\Delta\nu_g/\nu \lesssim 10^{-9}$ are difficult for us to detect, and 22 events that have previously been reported were missed. Similar difficulties also occur for the detection of post-glitch exponential recoveries with timescales $\lesssim 20$ d. However, our observations do reveal exponential recoveries mostly with timescales of a few tens of days for 27 glitches in 18 pulsars. A linear increase in $\dot{\nu}$ is clearly observed following most glitches. Linear increases, presumably related to a previous unseen glitch, were also seen before the first observed glitch in most pulsars. To quantify the linear recoveries as accurately as possible, the solutions for $\ddot{\nu}$ (see Table A1) were measured after any observed exponential recoveries were essentially complete. Of the 108 $\ddot{\nu}$ measurements obtained, 97 are positive; the 11 negative ones are generally from short data spans and/or for pulsars with strong timing noise.

With the contribution of 46 new glitches, the observed bimodal distribution of the glitch fractional size has been reinforced, implying that there are two different glitch mechanisms, possibly the starquake and the vortex pinning – unpinning theories. Post-glitch exponential recoveries have been observed over a wide range of fractional glitch size and pulsar age. Large recovery fractions Q have been seen in small glitches in both young (e.g. the Crab) and old (e.g. PSR B0525+21) pulsars and also in large glitches in young pulsars (e.g. PSR J1119–6127) and in magnetars. Small values of Q , typically around 0.01, are more commonly observed in large glitches. A bimodal distribution shown in the histogram for Q has also clearly been seen. Moreover, decay timescales τ_d have been observed to show some positive correlation with pulsar age. Figure 17 shows that the inter-glitch $\ddot{\nu}$ has a strong correlation with the slow-down rate $|\dot{\nu}|$ and is generally much larger than the expectation from a magnetic-dipole braking. The excess decay in brak-

ing is clearly related to glitches and is consistent with the predictions of a model based on the properties of a weakly coupled superfluid in the outer layers of the neutron star (Alpar & Baykal 2006).

It is very clear that the true distribution of the glitch fractional size at the low end is not well determined (cf. Figure 12). Glitches with $\Delta\nu_g/\nu \lesssim 10^{-9}$ are at the lower limit of the detectability for most timing programs. The observational sampling, timing accuracy and intrinsic timing noise also hamper the detection of exponential recoveries with very short timescales, leaving an incomplete sample for short time constants. Further studies on these issues require intensive timing observations for the glitching pulsar population supported by simulations to better reveal the true distributions of glitch-related phenomena.

ACKNOWLEDGEMENTS

The Parkes radio telescope is part of the Australia Telescope, which is funded by the Commonwealth of Australia for operation as a National Facility managed by the Commonwealth Scientific and Industrial Research Organisation (CSIRO). MY is funded by the National Basic Research Program of China (2012CB821800) and China Scholarship Council (No. 2009601129). GH is the recipient of an Australian Research Council QEII Fellowship (#DP0878388). VK is funded by NSERC, CIFAR, FQRNT, CRC and is the recipient of the Killam Fellowship and the Lorne Trotter Chair. VR is a recipient of a John Stocker Postgraduate Scholarship from the Science and Industry Endowment Fund. RX and GJ acknowledge the NSFC (10935001, 10973002 and 10833003) and the National Basic Research Program of China (2012CB821800 and 2009CB824800).

REFERENCES

- Alpar M. A., 1977, *ApJ*, 213, 527
- Alpar M. A., Anderson P. W., Pines D., Shaham J., 1981, *ApJ*, 249, L29
- Alpar M. A., Anderson P. W., Pines D., Shaham J., 1984a, *ApJ*, 276, 325
- Alpar M. A., Anderson P. W., Pines D., Shaham J., 1984b, *ApJ*, 278, 791
- Alpar M. A., Baykal A., 2006, *MNRAS*, 372, 489
- Alpar M. A., Chau H. F., Cheng K. S., Pines D., 1993, *ApJ*, 409, 345
- Anderson P. W., Itoh N., 1975, *Nature*, 256, 25
- Arzoumanian Z., Gotthelf E. V., Ransom S. M., Safi-Harb S., Kothes R., Landecker T. L., 2011, *ApJ*, 739, 39
- Baym G., Pethick C., Pines D., Ruderman M., 1969, *Nature*, 224, 872
- Brisken W. F., Carrillo-Barragán M., Kurtz S., Finley J. P., 2006, *ApJ*, 652, 554
- Camilo F., Kaspi V. M., Lyne A. G., Manchester R. N., Bell J. F., D’Amico N., McKay N. P. F., Crawford F., 2000, *ApJ*, 541, 367
- Camilo F., Manchester R. N., Lyne A. G., Gaensler B. M., Possenti A., D’Amico N., Stairs I. H., Faulkner A. J., Kramer M., Lorimer D. R., McLaughlin M. A., Hobbs G., 2004, *ApJ*, 611, L25

- Cognard I., Backer D. C., 2004, *ApJ*, 612, L125
- Coles W., Hobbs G., Champion D. J., Manchester R. N., Verbiest J. P. W., 2011, *MNRAS*, 418, 561
- Cordes J. M., Downs G. S., Krause-Polstorff J., 1988, *ApJ*, 330, 847
- D'Alessandro F., McCulloch P. M., 1997, *MNRAS*, 292, 879
- D'Alessandro F., McCulloch P. M., King E. A., Hamilton P. A., McConnell D., 1993, *MNRAS*, 261, 883
- D'Amico N., Kaspi V. M., Manchester R. N., Camilo F., Lyne A. G., Possenti A., Stairs I. H., Kramer M., Crawford F., Bell J., McKay N. P. F., 2001, *ApJ*, 552, L45
- De Luca A., Mignani R. P., Caraveo P. A., 1999, *A&A*, 354, 1011
- Dib R., Kaspi V. M., Gavriil F. P., 2008, *ApJ*, 673, 1044
- Dib R., Kaspi V. M., Gavriil F. P., 2009, *ApJ*, 702, 614
- Dib R., Kaspi V. M., Gavriil F. P., Woods P. M., 2007, *The Astronomer's Telegram*, 1041, 1
- Dodson R., Buchner S., Reid B., Lewis D., Flanagan C., 2004, *IAU Circ.*, 8370, 4
- Dodson R., Legge D., Reynolds J. E., McCulloch P. M., 2003, *ApJ*, 596, 1137
- Dodson R. G., McCulloch P. M., Lewis D. R., 2002, *ApJ*, 564, L85
- Downs G. S., 1981, *ApJ*, 249, 687
- Edwards R. T., Hobbs G. B., Manchester R. N., 2006, *MNRAS*, 372, 1549
- Epstein R. I., Baym G., 1988, *ApJ*, 328, 680
- Espinoza C. M., Lyne A. G., Kramer M., Manchester R. N., Kaspi V. M., 2011b, *ApJ*, 741, L13
- Espinoza C. M., Lyne A. G., Stappers B. W., Kramer M., 2011a, *MNRAS*, 414, 1679
- Flanagan C., 1996, *IAU Circ.*, 6491, 2
- Flanagan C. S., 1993, *MNRAS*, 260, 643
- Flanagan C. S., Buchner S. J., 2006, *CBET*, 595, 1
- Fomalont E. B., Goss W. M., Manchester R. N., Lyne A. G., 1997, *MNRAS*, 286, 81
- Frail D. A., Kulkarni S. R., Vasisht G., 1993, *Nature*, 365, 136
- Gavriil F. P., Dib R., Kaspi V. M., 2011, *ApJ*, 736, 138
- Hessels J. W. T., Roberts M. S. E., Ransom S. M., Kaspi V. M., Romani R. W., Ng C.-Y., Freire P. C. C., Gaensler B. M., 2004, *ApJ*, 612, 389
- Hobbs G., Coles W., Manchester R., Chen D., 2011, in *Proceedings of the Journées 2010 Systèmes de Référence Spatio-Temporels Developing a pulsar-based timescale*. pp 237–242
- Hobbs G., Faulkner A., Stairs I. H., Camilo F., Manchester R. N., Lyne A. G., Kramer M., D'Amico N., Kaspi V. M., Possenti A., McLaughlin M. A., Lorimer D. R., Burgay M., Joshi B. C., Crawford F., 2004, *MNRAS*, 352, 1439
- Hobbs G., Hollow R., Champion D., Khoo J., et al. 2009, *PASA*, 26, 468
- Hobbs G., Lyne A. G., Kramer M., 2010, *MNRAS*, 402, 1027
- Hobbs G., Lyne A. G., Kramer M., Martin C. E., Jordan C., 2004, *MNRAS*, 353, 1311
- Hobbs G., Miller D., Manchester R. N., Dempsey J., et al. 2011, *PASA*, 28, 202
- Hobbs G. B., Edwards R. T., Manchester R. N., 2006, *MNRAS*, 369, 655
- Hotan A. W., van Straten W., Manchester R. N., 2004, *PASA*, 21, 302
- Jackson M. S., Halpern J. P., Gotthelf E. V., Mattox J. R., 2002, *ApJ*, 578, 935
- Janssen G. H., Stappers B. W., 2006, *A&A*, 457, 611
- Johnston S., Lyne A. G., Manchester R. N., Kniffen D. A., D'Amico N., Lim J., Ashworth M., 1992, *MNRAS*, 255, 401
- Johnston S., Manchester R. N., Lyne A. G., Kaspi V. M., D'Amico N., 1995, *A&A*, 293, 795
- Kaspi V. M., Gavriil F. P., 2003, *ApJ*, 596, L71
- Kaspi V. M., Gavriil F. P., Woods P. M., Jensen J. B., Roberts M. S. E., Chakrabarty D., 2003, *ApJ*, 588, L93
- Kaspi V. M., Lyne A. G., Manchester R. N., Johnston S., D'Amico N., Shemar S. L., 1993, *ApJ*, 409, L57
- Kramer M., Bell J. F., Manchester R. N., Lyne A. G., Camilo F., Stairs I. H., D'Amico N., Kaspi V. M., Hobbs G., Morris D. J., Crawford F., Possenti A., Joshi B. C., McLaughlin M. A., Lorimer D. R., Faulkner A. J., 2003, *MNRAS*, 342, 1299
- Kramer M., Lyne A. G., O'Brien J. T., Jordan C. A., Lorimer D. R., 2006, *Science*, 312, 549
- Kramer M., Stairs I. H., Manchester R. N., McLaughlin M. A., Lyne A. G., Ferdman R. D., Burgay M., Lorimer D. R., Possenti A., D'Amico N., Sarkissian J. M., Hobbs G. B., Reynolds J. E., Freire P. C. C., Camilo F., 2006, *Science*, 314, 97
- Krawczyk A., Lyne A. G., Gil J. A., Joshi B. C., 2003, *MNRAS*, 340, 1087
- Livingstone M. A., Kaspi V. M., 2011, *ApJ*, 742, 31
- Livingstone M. A., Kaspi V. M., Gavriil F. P., 2005, *ApJ*, 633, 1095
- Livingstone M. A., Kaspi V. M., Gavriil F. P., 2010, *ApJ*, 710, 1710
- Livingstone M. A., Kaspi V. M., Gotthelf E. V., Kuiper L., 2006, *ApJ*, 647, 1286
- Livingstone M. A., Ransom S. M., Camilo F., Kaspi V. M., Lyne A. G., Kramer M., Stairs I. H., 2009, *ApJ*, 706, 1163
- Lyne A., Hobbs G., Kramer M., Stairs I., Stappers B., 2010, *Science*, 329, 408
- Lyne A. G., Graham-Smith F., Pritchard R. S., 1992, *Nature*, 359, 706
- Lyne A. G., Kaspi V. M., Bailes M., Manchester R. N., Taylor H., Arzoumanian Z., 1996, *MNRAS*, 281, L14
- Lyne A. G., McLaughlin M. A., Keane E. F., Kramer M., Espinoza C. M., Stappers B. W., Palliyaguru N. T., Miller J., 2009, *MNRAS*, 400, 1439
- Lyne A. G., Pritchard R. S., Graham-Smith F., 1993, *MNRAS*, 265, 1003
- Lyne A. G., Pritchard R. S., Graham-Smith F., Camilo F., 1996, *Nature*, 381, 497
- Lyne A. G., Shemar S. L., Graham-Smith F., 2000, *MNRAS*, 315, 534
- McCulloch P. M., Hamilton P. A., McConnell D., King E. A., 1990, *Nature*, 346, 822
- McCulloch P. M., Klekociuk A. R., Hamilton P. A., Royle G. W. R., 1987, *Aust. J. Phys.*, 40, 725
- Manchester R. N., Hobbs G., 2011, *ApJ*, 736, L31
- Manchester R. N., Hobbs G. B., Bailes M., van Straten W., et al. 2012, *PASA*
- Manchester R. N., Hobbs G. B., Teoh A., Hobbs M., 2005, *AJ*, 129, 1993
- Manchester R. N., Kramer M., Stairs I. H., Burgay M.,

- Camilo F., Hobbs G. B., Lorimer D. R., Lyne A. G., McLaughlin M. A., McPhee C. A., Possenti A., Reynolds J. E., van Straten W., 2010, *ApJ*, 710, 1694
- Manchester R. N., Lyne A. G., Camilo F., Bell J. F., Kaspi V. M., D’Amico N., McKay N. P. F., Crawford F., Stairs I. H., Possenti A., Morris D. J., Sheppard D. C., 2001, *MNRAS*, 328, 17
- Manchester R. N., Newton L. M., Goss W. M., Hamilton P. A., 1978, *MNRAS*, 184, 35P
- Manchester R. N., Taylor J. H., 1974, *ApJ*, 191, L63
- Melatos A., Peralta C., Wyithe J. S. B., 2008, *ApJ*, 672, 1103
- Middleditch J., Marshall F. E., Wang Q. D., Gotthelf E. V., Zhang W., 2006, *ApJ*, 652, 1531
- Morii M., Kawai N., Shibasaki N., 2005, *ApJ*, 622, 544
- Morris D. J., Hobbs G., Lyne A. G., Stairs I. H., Camilo F., Manchester R. N., Possenti A., Bell J. F., Kaspi V. M., Amico N. D., McKay N. P. F., Crawford F., Kramer M., 2002, *MNRAS*, 335, 275
- Newton L. M., Manchester R. N., Cooke D. J., 1981, *MNRAS*, 194, 841
- Pavlov G. G., Kargaltsev O., Briskin W. F., 2008, *ApJ*, 675, 683
- Radhakrishnan V., Manchester R. N., 1969, *Nature*, 222, 228
- Ray P. S., Kerr M., Parent D., Abdo A. A., et al. 2011, *ApJS*, 194, 17
- Reichley P. E., Downs G. S., 1969, *Nature*, 222, 229
- Ruderman M., 1976, *ApJ*, 203, 213
- Ruderman M., 1991, *ApJ*, 382, 587
- Ruderman M., 2009, in Becker W., ed., *Proc. 363rd Her-aeus Seminar on Neutron stars and Pulsars Vol. 357 of Astrophysics and Space Science Library, Pulsar spin, magnetic fields, and glitches*. p. 353
- Ruderman M., Zhu T., Chen K., 1998, *ApJ*, 492, 267
- Sandhu J. S., Bailes M., Manchester R. N., Navarro J., Kulkarni S. R., Anderson S. B., 1997, *ApJ*, 478, L95
- Shabanova T. V., 2005, *MNRAS*, 356, 1435
- Shabanova T. V., 2007, *APSS*, 308, 591
- Shabanova T. V., 2009, *ApJ*, 700, 1009
- Shabanova T. V., 2010, *ApJ*, 721, 251
- Shemar S. L., Lyne A. G., 1996, *MNRAS*, 282, 677
- Smith D. A., Guillemot L., Camilo F., Cognard I., Dumora D., Espinoza C., Freire P. C. C., Gotthelf E. V., et al. 2008, *A&A*, 492, 923
- Srinivasan G., Bhattacharya D., Muslimov A. G., Tsygan A. I., 1990, *Current Sci.*, 59, 31
- Standish E. M., 1998, *JPL Planetary and Lunar Ephemerides, DE405/LE405*, Memo IOM 312.F-98-048. JPL, Pasadena
- Staveley-Smith L., Wilson W. E., Bird T. S., Disney M. J., Ekers R. D., Freeman K. C., Haynes R. F., Sinclair M. W., Vaile R. A., Webster R. L., Wright A. E., 1996, *PASA*, 13, 243
- Thompson D. J., 2008, *Reports on Progress in Physics*, 71, 116901
- Torii K., Gotthelf E. V., Vasisht G., Dotani T., Kinugasa K., 2000, *ApJ*, 534, L71
- Urama J. O., 2002, *MNRAS*, 330, 58
- Wang N., Johnston S., Manchester R. N., 2004, *MNRAS*, 351, 599
- Wang N., Manchester R. N., Pace R., Bailes M., Kaspi V. M., Stappers B. W., Lyne A. G., 2000, *MNRAS*, 317, 843
- Weltevrede P., Johnston S., Espinoza C. M., 2011, *MNRAS*, 411, 1917
- Weltevrede P., Johnston S., Manchester R. N., Bhat R., Burgay M., Champion D., Hobbs G. B., Kızıltan B., Keith M., Possenti A., Reynolds J. E., Watters K., 2010, *PASA*, 27, 64
- Wong T., Backer D. C., Lyne A., 2001, *ApJ*, 548, 447
- Woods P. M., Kaspi V. M., Thompson C., Gavril F. P., Marshall H. L., Chakrabarty D., Flanagan K., Heyl J., Hernquist L., 2004, *ApJ*, 605, 378
- Yardley D. R. B., Coles W. A., Hobbs G. B., Verbiest J. P. W., Manchester R. N., van Straten W., Jenet F. A., Bailes M., Bhat N. D. R., Burke-Spolaor S., Champion D. J., Hotan A. W., Osłowski S., Reynolds J. E., Sarkissian J. M., 2011, *MNRAS*, p. 491
- Yuan J. P., Manchester R. N., Wang N., Zhou X., Liu Z. Y., Gao Z. F., 2010b, *ApJ*, 719, L111
- Yuan J. P., Wang N., Manchester R. N., Liu Z. Y., 2010a, *MNRAS*, 404, 289
- Zeiger B. R., Briskin W. F., Chatterjee S., Goss W. M., 2008, *ApJ*, 674, 271
- Zou W. Z., Wang N., Manchester R. N., Urama J. O., Hobbs G., Liu Z. Y., Yuan J. P., 2008, *MNRAS*, 384, 1063
- Zou W. Z., Wang N., Wang H. X., Manchester R. N., Wu X. J., Zhang J., 2004, *MNRAS*, 354, 811

APPENDIX A: TIMING SOLUTIONS AND GLITCH PARAMETERS

Timing solutions incorporating pre- and post-glitch pulse parameters and glitch parameters, obtained from TEMPO2 fits for the 36 glitching pulsars analysed in this paper are provided here in Tables A1 and A2.

To support the discussion in §5, Table A3 summarises the number of observed glitches, N_g , the observing range and the derived glitching rates \dot{N}_g for the known glitching pulsars. Table A4 gives previously reported exponential-recovery parameters.

ASCII machine-readable versions of the four tables in this Appendix are provided as an on-line supplement.

Table A1. Pre- and post-glitch timing solutions for 36 glitching pulsars.

PSR J	Int.	ν (s ⁻¹)	$\dot{\nu}$ (10 ⁻¹² s ⁻²)	$\ddot{\nu}$ (10 ⁻²⁴ s ⁻³)	Epoch (MJD)	Data range (MJD)	No. of ToAs	Rms res. (ms)	χ^2_r [d.o.f.]
J0729-1448	-1	3.97318845714(15)	-1.7840(4)	-	54263	54218 — 54309	11	0.32	5.23[8]
	1-2	3.9731688132(5)	-1.7824(4)	-	54391	54333 — 54450	13	1.39	34.0[10]
	2-3	3.97314824736(14)	-1.7821(2)	-	54525	54485 — 54565	8	0.21	2.34[5]
	3-4	3.9731315102(3)	-1.7837(4)	-	54634	54597 — 54673	4	0.17	3.41[1]
	4-	3.9730918334(6)	-1.79905(8)	-	55059	54690 — 55429	49	13.2	18000[46]
J0742-2822	-1	5.9964098032(3)	-0.604567(3)	2.59(5)	52188	49364 — 55014	402	32.5	16900000[398]
	1-	5.99624713923(16)	-0.605276(8)	-29(3)	55315	55051 — 55579	79	0.97	26700[75]
J0834-4159	-1	8.256502162607(19)	-0.2918552(9)	-	52347	51299 — 53395	64	1.00	23.5[61]
	1-	8.25645335747(3)	-0.2918531(12)	-	54283	53423 — 55145	56	0.887	27.9[53]
J0835-4510	-1	11.196712768(4)	-15.5997(2)	1326(33)	49985	49608 — 50364	59	14.9	47200[55]
	1-2	11.195158486(3)	-15.58872(12)	1008(26)	51155	50819 — 51493	54	8.25	24500[50]
	2-3	11.1932875878(11)	-15.59077(3)	715(3)	52568	51945 — 53191	73	9.68	21300[69]
	3-4	11.1918782700(4)	-15.61044(5)	1206(6)	53635	53323 — 53948	33	1.37	240[29]
	4-	11.1904829031(5)	-15.587931(19)	719(3)	54687	54202 — 55172	209	4.88	7980[205]
J0905-5127	-1	2.88776598305(12)	-0.20879(7)	-	49425	49364 — 49488	6	0.25	5.64[3]
	1-	2.88776198459(6)	-0.20845(3)	-	49649	49560 — 49739	9	0.26	2.36[6]
	-2	2.88771636557(6)	-0.2071686(11)	-2.02(12)	52195	51526 — 52865	21	0.95	355[17]
	2-	2.88768278363(6)	-0.2073986(12)	0.38(7)	54071	52998 — 55145	65	3.70	2790[61]
J1016-5857	-1	9.3126315989(4)	-6.990896(13)	78(1)	51913	51299 — 52527	97	3.28	1830[93]
	1-2	9.3115113267(6)	-6.994765(11)	122.4(5)	53791	52571 — 55011	134	15.3	27700[130]
	2-	9.3106478766(6)	-7.00431(5)	133(18)	55250	55072 — 55429	19	0.78	64.8[15]
J1048-5832	-1	8.0873027360(12)	-6.27372(4)	76(5)	48418	47910 — 48928	60	10.6	52500[56]
	1-2	8.08699243910(13)	-6.27060(14)	88(9)	48991	48957 — 49025	9	0.09	3.85[6]
	2-3	8.0863750399(8)	-6.27954(3)	98(3)	50172	49559 — 50786	61	7.22	148000[57]
	3-4	8.0854473241(13)	-6.26780(3)	122(3)	51894	51093 — 52696	61	16.4	1000000[57]
	4-5	8.0847483076(11)	-6.27386(5)	181(7)	53212	52771 — 53653	35	6.29	96600[31]
	5-6	8.0842772583(18)	-6.26424(9)	223(12)	54082	53680 — 54486	34	7.37	393000[30]
	6-	8.0838894263(12)	-6.28529(6)	98(12)	54843	54505 — 55183	34	4.42	214000[30]
J1052-5954	-1	5.5372526159(4)	-0.61341(11)	-	54352	54220 — 54485	12	1.25	8.34[9]
	1-	5.53721546844(16)	-0.617277(7)	35(2)	55096	54733 — 55461	27	0.98	3.37[23]
J1105-6107	-1	15.8248209436(12)	-3.95900(6)	-108(8)	49995	49589 — 50402	41	2.54	2590[37]
	1-2	15.8245012491(16)	-3.96232(4)	38(6)	50942	50434 — 51451	108	6.19	17400[104]
	2-3	15.823737653(2)	-3.96361(4)	13(2)	53217	51744 — 54690	99	28.0	661000[95]
	3-4	15.8231268298(20)	-3.96587(13)	-11(30)	55002	54733 — 55272	38	3.38	13200[34]
	4-	15.8230116650(6)	-3.96652(9)	319(81)	55382	55304 — 55461	11	0.13	35.9[7]
J1112-6103	-1	15.3936495872(5)	-7.45479(4)	-24(11)	51055	50850 — 51261	50	0.67	6.61[46]
	1-2	15.3927981288(7)	-7.471152(13)	222(1)	52417	51529 — 53307	58	5.26	904[54]
	2-	15.3913344780(9)	-7.46853(4)	144(5)	54712	54220 — 55206	42	3.21	344[38]
J1119-6127	-1	2.45326884390(8)	-24.211160(7)	700(2)	51121	50852 — 51392	57	1.08	7.46[53]
	1-2	2.4507184171(3)	-24.142246(5)	626.2(4)	52342	51405 — 53279	149	21.04	3800[145]
	2-3	2.447638860(2)	-24.0540(1)	814(14)	53821	53423 — 54220	33	19.5	3230[29]
	3-	2.444874218(3)	-23.95777(11)	773(17)	55154	54733 — 55576	56	64.8	11000[52]
J1301-6305	-1	5.4190840865(3)	-7.82942(1)	248(2)	51420	50941 — 51901	62	3.61	17.1[58]
	1-2	5.4182027029(12)	-7.84022(4)	286(4)	52758	52145 — 53371	40	17.3	434[36]
	2-	5.417207268(1)	-7.833490(18)	276(2)	54249	53395 — 55104	64	20.2	580[60]
J1341-6220	-1	5.1729360602(5)	-6.76765(6)	253(38)	49651	49540 — 49763	10	0.47	6.36[6]
	1-2	5.1728273829(3)	-6.76580(19)	-	49837	49787 — 49888	6	0.30	11.3[3]
	2-3	5.1727579534(9)	-6.7529(14)	-	49956	49920 — 49992	7	0.65	8.79[4]
	3-4	5.17263893435(17)	-6.77137(3)	167(9)	50174	50026 — 50322	16	0.36	4.75[12]
	4-5	5.1724951732(7)	-6.76951(12)	356(93)	50420	50341 — 50501	13	0.42	9.74[9]
	5-6	5.1723882419(4)	-6.76865(7)	484(74)	50603	50537 — 50670	17	0.31	8.02[13]
	6-7	5.1721912539(7)	-6.76959(5)	207(20)	50946	50760 — 51133	30	1.29	158[26]
	7-8	5.1719833589(3)	-6.76796(4)	308(13)	51303	51155 — 51451	8	0.41	10.9[4]
	8-9	5.1716336852(6)	-6.76774(8)	-63(36)	51911	51782 — 52041	16	0.93	68.5[12]
	9-10	5.1714729568(9)	-6.7725(9)	-	52190	52145 — 52235	4	0.48	57.6[1]
	10-11	5.171283363(4)	-6.7866(3)	-803(63)	52518	52266 — 52771	17	11.8	11700[13]
	11-12	5.170994398(12)	-6.7534(8)	-2120(269)	53013	52804 — 53222	15	32.0	188000[11]
	12-13	5.1708006160(7)	-6.7484(3)	-	53347	53241 — 53455	9	2.01	640[6]
	13-14	5.170541851(19)	-6.7618(8)	-177(181)	53799	53488 — 54112	19	71.7	26.4[11]
	14-15	5.1702517491(3)	-6.76414(4)	365(14)	54297	54144 — 54451	15	0.58	189[11]
	15-16	5.1700342469(7)	-6.76214(7)	287(22)	54672	54486 — 54860	15	1.71	189[11]
	16-17	5.169858206(3)	-6.7592(4)	3044(251)	54976	54881 — 55072	10	1.90	362[6]
	17-	5.16968689489(14)	-6.764590(16)	109(5)	55282	55104 — 55461	20	0.45	13.5[16]
J1412-6145	-1	3.17232313958(4)	-0.9928240(13)	3.80(17)	51353	50850 — 51858	45	0.79	2.59[41]
	1-	3.17212789172(5)	-0.9969084(6)	6.06(3)	53887	52314 — 55461	101	4.73	110[97]
J1413-6141	-1	3.5012521433(5)	-4.08114(8)	-	51055	50850 — 51261	26	7.20	36.7[23]
	1-2	3.5011397601(19)	-4.0842(8)	-	51374	51294 — 51454	9	5.52	21.8[6]
	2-3	3.50105387384(14)	-4.08410(5)	-	51627	51472 — 51782	24	0.90	3.02[21]
	3-4	3.5009433012(4)	-4.08332(7)	-350(40)	51941	51844 — 52039	16	0.79	3.21[12]
	4-5	3.5007434868(4)	-4.084389(14)	107(3)	52515	52145 — 52886	27	3.05	60.9[23]
	5-6	3.5005683237(18)	-4.0871(3)	-1648(218)	53012	52925 — 53101	6	1.61	35.9[2]
	6-7	3.5003276299(11)	-4.08149(4)	53(4)	53708	53150 — 54268	36	17.5	1470[32]
	7-	3.4999222810(7)	-4.077751(19)	33(2)	54882	54303 — 55461	54	14.0	630[50]
J1420-6048	-1	14.6675125451(3)	-17.83946(3)	651(7)	51311	51100 — 51523	26	0.37	15.5[22]
	1-2	14.666147261(2)	-17.83559(11)	964(12)	52207	51678 — 52737	80	13.9	17000[76]
	2-3	14.6644360883(7)	-17.85639(4)	533(6)	53336	52957 — 53716	58	2.51	618[54]
	3-4	14.6631475381(9)	-17.85577(3)	945(5)	54183	53734 — 54633	38	2.20	599[34]
	4-5	14.6618531329(16)	-17.84922(8)	1552(14)	55031	54672 — 55391	46	4.95	2.91[42]
	5-	14.6612348736(20)	-17.90(12)	-	55445	55429 — 55461	5	0.15	4.40[2]

Table A1. — *continued*

PSR J	Int.	ν (s ⁻¹)	$\dot{\nu}$ (10 ⁻¹² s ⁻²)	$\ddot{\nu}$ (10 ⁻²⁴ s ⁻³)	Epoch (MJD)	Data range (MJD)	No. of ToAs	Rms res. (ms)	χ^2_r [d.o.f]
J1452–6036	–1	6.451956870952(9)	–0.060343(1)	-	54635	54220 — 55051	35	0.16	52.2[32]
	1–	6.451953766111(19)	–0.060447(5)	-	55266	55072 — 55461	17	0.12	33.4[14]
J1453–6413	–1	5.571461007545(8)	–0.08520253(5)	0.0659(19)	52608	50669 — 54548	117	0.29	643[113]
	1–	5.571444247574(7)	–0.0852032(9)	-	54885	54566 — 55206	28	0.09	237[25]
J1531–5610	–1	11.87624700867(4)	–1.938066(6)	-	51448	51215 — 51680	31	0.15	4.98[28]
	1–	11.8758384521(3)	–1.946724(4)	14.85(15)	54060	52659 — 55461	99	5.11	6700[95]
J1614–5048	–1	4.31760554(1)	–9.1754(2)	366(13)	48848	47910 — 49784	100	447	2740000[96]
	1–2	4.316214218(3)	–9.22347(7)	118(5)	50635	49819 — 51451	171	95.5	632000[167]
		4.314824505(11)	–9.1601(3)	366(32)	52385	51782 — 52989	43	159	3800000[39]
	2–	4.313373849(7)	–9.17841(7)	–48(5)	54248	53036 — 55461	100	282	4330000[96]
J1646–4346	–1	4.3173283630(18)	–2.095392(11)	32.8(3)	50857	47913 — 53803	258	294	1080000[254]
	1–	4.3166537681(7)	–2.091929(20)	109(2)	54610	53949 — 55273	47	13.1	718[43]
J1702–4310	–1	4.15729055112(16)	–3.864815(4)	40.25(14)	52498	51223 — 53774	76	7.49	1100[72]
	1–	4.15649409771(9)	–3.868451(3)	51.1(4)	54941	54421 — 55461	36	1.15	10.1[32]
J1709–4429	–1	9.76127199222(13)	–8.863764(4)	123.9(8)	48327	47910 — 48746	46	0.56	487[42]
	1–2	9.7597767546(8)	–8.853391(18)	179.7(7)	50305	49160 — 51451	168	17.5	385000[164]
	2–3	9.758422208(3)	–8.8516(1)	595(11)	52091	51524 — 52659	36	17.1	1280000[32]
	3–4	9.7570513620(17)	–8.85369(4)	244(4)	53919	53150 — 54689	60	18.7	1120000[56]
	4–	9.7560834373(5)	–8.86295(3)	253(7)	55219	54932 — 55507	19	1.21	3890[15]
J1718–3825	–1	13.39192401122(9)	–2.3679369(7)	25.38(3)	52890	50878 — 54903	146	2.85	1500[142]
	1–	13.39144806554(9)	–2.362796(5)	16(2)	55219	54931 — 55507	18	0.14	7.09[14]
J1730–3350	–1	7.170087711(1)	–4.35574(2)	85(2)	51303	50539 — 52069	69	11.5	35900[65]
	1–	7.1690354505(5)	–4.361361(6)	50.5(3)	54155	52805 — 55507	90	14.2	36200[86]
J1731–4744	–1	1.20511216181(5)	–0.2382630(12)	18.89(12)	48773	48184 — 49363	21	0.41	8.58[17]
	1–2	1.20508590674(6)	–0.2376701(20)	2.09(17)	50059	49415 — 50703	47	3.18	6330[43]
	2–3	1.20505448010(3)	–0.2375479(7)	1.40(4)	51590	50722 — 52458	60	1.53	2230[56]
	3–4	1.20502077952(3)	–0.2375618(16)	3.9(4)	53239	52925 — 53554	24	0.50	108[20]
	4–	1.204993924876(15)	–0.2374356(6)	-	54548	53589 — 55507	64	1.96	23500[61]
J1737–3137	–1	2.21990926991(9)	–0.68317(5)	-	54286	54221 — 54351	10	0.33	0.75[7]
	1–	2.21987416781(9)	–0.684329(8)	-	54930	54353 — 55507	49	8.16	141[46]
J1740–3015	–1	1.648184042812(13)	–1.265524(4)	-	50798	50669 — 50927	42	0.26	82.3[39]
	1–2	1.64809155129(19)	–1.266547(13)	-	51665	50987 — 52344	27	19.8	399000[24]
	2–3	1.6479812921(9)	–1.26564(5)	125(98)	52675	52361 — 52989	19	13.0	179000[15]
	3–4	1.64786917225(7)	–1.266266(2)	13.49(18)	53728	53036 — 54420	48	2.16	26600[44]
	4–5	1.64774895802(16)	–1.264817(7)	11(2)	54828	54450 — 55206	37	3.65	134000[33]
	5–	1.64769409872(4)	–1.266147(5)	70(3)	55370	55234 — 55507	17	0.24	625[13]
J1801–2304	–1	2.4051703923(3)	–0.65365(4)	-	48176	47911 — 48442	16	3.19	23.0[13]
	1–2	2.40512164856(9)	–0.653541(3)	2.8(3)	49054	48465 — 49643	61	3.26	21.5[57]
	2–3	2.40507528156(11)	–0.65348(5)	-	49878	49730 — 50026	11	0.93	5.07[8]
	3–4	2.4050548970(3)	–0.65345(4)	29(19)	50240	50117 — 50363	25	1.19	7.83[21]
	4–5	2.40502945211(8)	–0.653426(7)	40(2)	50694	50462 — 50927	83	1.32	8.79[79]
	5–6	2.4049822461(6)	–0.65254(3)	12(3)	51531	51021 — 52041	20	7.93	464[16]
	6–7	2.40491876991(6)	–0.653179(5)	-	52684	52145 — 53223	17	2.22	45.8[14]
	7–8	2.40482774696(6)	–0.653049(1)	2.44(7)	54318	53307 — 55330	73	3.72	37.5[69]
	8–	2.40476474326(9)	–0.65292(5)	-	55435	55364 — 55507	5	0.22	0.24[2]
J1801–2451	–1	8.0071549008(15)	–8.17840(11)	369(32)	49171	48957 — 49386	17	2.71	1020[13]
	1–2	8.006538717(1)	–8.19043(3)	387(3)	50064	49482 — 50646	81	8.59	8550[77]
	2–3	8.005640187(4)	–8.18049(8)	505(9)	51348	50656 — 52041	97	41.5	234000[93]
	3–4	8.004687982(3)	–8.19041(14)	47(36)	52737	52484 — 52990	19	4.77	4330[15]
	4–5	8.0039126298(19)	–8.17244(5)	146(4)	53834	53036 — 54633	58	26.5	73400[54]
	5–	8.0029848506(6)	–8.19035(3)	266(7)	55182	54857 — 55507	35	2.16	343[31]
J1803–2137	–1	7.48329875057(11)	–7.48842(10)	-	50709	50669 — 50750	16	0.12	9.17[13]
	1–2	7.4820940765(8)	–7.4904029(17)	244(2)	52602	51782 — 53423	58	11.8	101000[54]
	2–	7.4807378694(16)	–7.50335(4)	288(4)	54739	53949 — 55530	58	25.4	192000[54]
J1809–1917	–1	12.08488375958(18)	–3.727797(2)	37.74(12)	52012	50782 — 53242	57	1.99	365[53]
	1–	12.08405907802(11)	–3.7299474(3)	33.63(16)	54632	53734 — 55530	62	1.04	62.6[58]
J1825–0935	–1	1.3003898596(5)	–0.088534(7)	–1.4(5)	52978	51844 — 54112	69	46.3	578000[65]
	1–	1.30037753992(5)	–0.0888195(16)	3.60(18)	54608	54144 — 55073	16	0.32	485[12]
J1826–1334	–1	9.8548791982(16)	–7.277563(15)	126(1)	51967	50749 — 53187	86	24.9	180000[82]
	1–2	9.85391251222(15)	–7.264712(11)	69(4)	53506	53279 — 53734	17	0.21	23.4[13]
	2–	9.8531185307(7)	–7.296496(18)	115(2)	54821	54112 — 55530	62	7.17	7620[58]
J1835–1106	–1	6.02730411248(17)	–0.74791(6)	-	52068	51945 — 52191	9	0.47	395[6]
	1–	6.0271868732(8)	–0.74881(1)	8.7(4)	53882	52234 — 55530	96	39.5	1210000[92]
J1841–0524	–1	2.243267777344(15)	–1.175696(4)	-	53813	53619 — 54008	8	0.19	0.09[5]
	1–2	2.24322183389(19)	–1.175543(14)	8(4)	54266	54048 — 54485	18	1.34	2.06[14]
	2–	2.24314896191(9)	–1.175947(3)	11.4(37)	55006	54506 — 55507	37	1.96	4.40[33]

Table A2. Observed glitch parameters.

PSR J	Gl. No.	Gl. Epoch (MJD)	New? (N/P)	$\Delta\nu_{\text{g}}/\nu$ (10^{-9})	$\Delta\dot{\nu}_{\text{g}}/\dot{\nu}$ (10^{-3})	$\Delta\dot{\nu}_{\text{p}}$ (10^{-15} s^{-2})	$\Delta\dot{\nu}_{\text{p}}$ (10^{-24} s^{-3})	Q	τ_{d} (d)	No. of ToAs	Data span (MJD)	Rms res. (ms)	χ^2_{r} [d.o.f]
J0729–1448	1	54316.8(3)*	P	21.2(7)	-	-	-	-	-	21	54220 – 54380	0.42	6.25[16]
	2	54479.5(9)*	P	15.4(7)	-	-	-	-	-	15	54351 – 54565	0.55	11.4[10]
	3	54589.8(9)*	P	13.0(9)	-	-	-	-	-	12	54485 – 54673	0.44	10.8[7]
	4	54681(9)	P	6651.6(8)	-	-	-	-	-	15	54597 – 54763	0.58	16.0[9]
J0742–2822	1	55020.66(9)*	P	102.73(11)	2.1(5)	-1.3(3)	-	-	-	90	54772 – 55309	0.60	8820[83]
J0834–4159	1	53415(2)*	N	1.85(4)	0.26(4)	-0.07(1)	-	-	-	25	52822 – 54144	0.30	2.43[19]
J0835–4510	1	50369.394 ¹	P	2133(10)	7.7(4)	-76(3)	-	0.030(4)	186(12)	159	50214 – 50669	0.17	11.3[150]
	2	51559.3190(5) ²	P	3140(46)	8(4)	-57(11)	-	0.02(1)	125(83)	58	51093 – 51900	4.04	4600[49]
	3	53193.09 ³	P	2059(6)	11(2)	-104.1(8)	304(23)	0.009(3)	37(11)	78	52666 – 53803	0.99	245[68]
	4	53959.93 ⁴	P	2585(3)	8.1(5)	-72(2)	-	0.0119(6)	73(8)	103	53523 – 54390	0.73	124[94]
J0905–5127	1	49552(2)*	N	13.6(4)	-1.8(9)	0.38(18)	-	-	-	11	49364 – 49644	0.23	4.89[5]
	2	52931(67)	N	8.31(16)(53)	1.2(1)	-0.258(20)	-	-	-	16	52463 – 53367	0.55	165[10]
J1016–5857	1	52549(22)	N	1622.6(3)(51)	3.69(5)	-25.8(3)(4)	69(7)	-	-	97	51941 – 53244	1.89	717[89]
	2	55041(30)	N	1912.4(3)	4.4(3)	-31(2)	-	-	-	13	54858 – 55236	0.24	7.14[6]
J1048–5832	1	48946.9(2)*	P	17.95(19)	-	-	-	-	-	17	48814 – 49025	0.17	17.5[11]
	2	49034(9)	P	2995(26)	-	-	-	0.026(6)(7)	160(43)	28	48957 – 49236	0.39	84.3[20]
	3	50791.485(5) ⁵	P	768(3)	3.7(8)	-13.5(1)	-	0.008(3)	60(20)	43	50703 – 50939	0.12	67[35]
	4	52733(37)	N	1838.4(5)(90)	3.7(3)	-23(2)	-	-	-	33	52312 – 53151	2.72	25200[26]
	5	53673.0(8)*	N	28.5(4)	0.19(14)	-1.2(9)	-	-	-	23	53349 – 53959	0.88	2002[16]
	6	54495(10)	P	3042.56(14)(340)	5.6(1)	-35.2(7)	-	-	-	32	54303 – 54690	0.28	1050[25]
J1052–5954	1	54495(10)	P	495(3)(7)	86(14)(19)	-6.4(5)	-	0.067(4)(13)	46(8)	32	54220 – 54787	1.05	4.26[24]
J1105–6107	1	50417(16)	P	279.20(7)(36)	1.07(20)	-4.2(8)	-	-	-	38	50267 – 50576	0.086	5.02[31]
	2	51598(147)	N	971.7(2)(5)	0.13(9)	-0.5(4)	-	-	-	32	50986 – 52004	0.36	49.5[25]
	3	54711(21)	P	29.5(3)(15)	3.4(6)	-13(3)	-	-	-	26	54504 – 54903	0.40	169[19]
	4	55288(16)	N	954.42(7)	-	-	-	-	-	21	55145 – 55461	0.13	40.2[15]
J1112–6103	1	51395(134)	N	1825(2)(25)	4.66(11)(38)	-34.8(8)(29)	242(20)	-	-	81	50850 – 52397	1.04	21.3[73]
	2	53337(30)	N	1202(20)(21)	7(2)	-35(3)	-	0.022(2)	302(146)	44	52661 – 54008	1.37	78.0[35]
J1119–6127	1	51399(3)*	P	4.4(3)	0.036(5)	-0.86(10)	-	-	-	29	51258 – 51557	0.72	4.81[23]
	2	53293(13)	P	372(9)(80)	8.9(4)(23)	2(2)	-	0.84(3)(28)	41(2)	31	53148 – 53427	0.23	0.77[22]
	3	54244(24)	P	9400(300)(5900)	580(14)(440)	24.9(9)	-	0.81(4)(81) 0.214(7)(136)	15.7(3) 186(3)	65	53651 – 54820	3.31	50.4[54]
J1301–6305	1	51923(23)	N	4630(2)(17)	8.6(4)(11)	-42.9(3)	-	0.0049(3)(11)	58(6)	59	51370 – 52507	1.39	2.97[50]
	2	53383(12)	N	2664(2)(6)	3.92(11)	-30.7(8)	-	-	-	17	53185 – 53523	1.63	5.94[11]
J1341–6220	1	49775(12)	P	12.2(3)	-	-	-	-	-	14	49589 – 49888	0.30	5.91[8]
	2	49904(16)	P	14(1)	-	-	-	-	-	13	49787 – 49992	0.28	5.91[7]
	3	50008(16)	P	1634(1)(5)	2.87(17)	-19(2)	-	-	-	16	49920 – 50190	0.49	6.17[10]
	4	50332(10)	P	27.3(4)	0.06(6)	-0.4(4)	-	-	-	14	50213 – 50434	0.35	5.96[8]
	5	50532.1(8)*	P	18.5(6)	0.18(8)	-1.2(5)	-	-	-	22	50399 – 50621	0.40	12.4[16]
	6	50683(13)	P	709(2)(4)	-	-	-	0.0112(19)(49)	24(9)	43	50576 – 50799	0.22	4.49[35]
	7	51144(11)	N	170(1)	-	-	-	-	-	8	50987 – 51241	0.51	30.1[2]
	8	51617(165)	N	1121.5(7)(8)	-	-	-	-	-	14	51241 – 51901	0.35	8.77[8]
	9	52093(53)	N	480(4)	-	-	-	-	-	9	52001 – 52235	1.06	161[4]
	10	52250(16)	N	454.5(7)	-	-	-	-	-	9	52145 – 52360	0.33	19.0[3]
	11	52788(17)	N	219.2(4)(150)	-8.3(3)	57(2)	-	-	-	9	52659 – 52886	0.05	0.80[2]
	12	53232(10)	N	277(3)	-	-	-	-	-	8	53101 – 53307	0.77	488[2]
	13	53471(17)	N	985(6)	-	-	-	-	-	8	53371 – 53553	1.65	541.9[2]
	14	54128(16)	N	194.0(4)(84)	4.97(12)	-33.5(8)	-	-	-	15	54008 – 54306	0.18	4.11[8]
	15	54468(18)	P	317.2(4)(18)	0.90(4)	-6.1(3)	-	-	-	11	54335 – 54597	0.27	6.67[5]
	16	54871(11)	P	309.6(6)	-	-	-	-	-	11	54763 – 54975	0.42	16.5[5]
	17	55088(16)	N	1579(2)	-	-	-	-	-	8	54975 – 55183	0.57	67.5[2]
J1412–6145	1	51868(10)	N	7253.0(7)(31)	17.5(8)(19)	-5.67(3)	-	0.00263(8)(38)	59(4)	33	51370 – 52348	0.58	1.94[25]
J1413–6141	1	51290(3)*	N	39(4)	-	-	-	-	-	19	51146 – 51405	4.26	15.9[14]
	2	51463(9)	N	970(2)	-	-	-	-	-	30	51370 – 51556	1.53	7.33[25]
	3	51796.3(4)*	N	59.7(4)	-0.33(3)	1.35(12)	-	-	-	39	51472 – 52004	0.94	3.66[3]
	4	52092(53)	N	811(2)	0.28(20)(58)	-1.1(8)(24)	491(42)	-	-	27	51844 – 52426	0.69	3.15[19]
	5	52899.4(3)*	N	46.9(8)	-	-	-	-	-	11	52771 – 53036	0.64	4.47[6]
	6	53125(24)	N	1410(5)	-	-	-	-	-	8	52990 – 53279	2.87	222[2]
	7	54286(18)	N	2409.8(7)(11)	0.4(4)	-2(2)	-	-	-	18	54112 – 54421	0.71	2.64[11]
J1420–6048	1	51600(77)	N	1146.2(6)(300)	3.83(8)(14)	-68(2)(24)	281(62)	-	-	24	51333 – 51901	0.17	2.98[16]
	2	52754(16)	N	2019(10)(13)	6.6(8)(9)	-90(6)	-269(152)	0.008(4)	99(29)	47	52526 – 53105	0.16	2.83[37]
	3	53725(9)	N	1270(3)(4)	3.9(3)	-70(5)	371(234)	-	-	32	53488 – 54144	1.68	179[24]
	4	54653(20)	P	934.5(4)(97)	4.84(6)(8)	-86(1)(2)	633(50)	-	-	41	54335 – 55011	0.62	48.0[33]
	5	55410(19)	N	1346.00(18)	-	-	-	-	-	11	55304 – 55461	0.12	2.35[6]

Table A2. — *continued*

PSR J	Gl. No.	Gl. Epoch (MJD)	New? (N/P)	$\Delta\nu_g/\nu$ (10^{-9})	$\Delta\dot{\nu}_g/\dot{\nu}$ (10^{-3})	$\Delta\dot{\nu}_p$ (10^{-15} s^{-2})	$\Delta\dot{\nu}_p$ (10^{-24} s^{-3})	Q	τ_d (d)	No. of ToAs	Data span (MJD)	Rms res. (ms)	χ_r^2 [d.o.f]
J1452–6036	1	55055.22(4)*	N	28.95(20)	2.37(20)	−0.143(12)	-	-	-	20	54820 – 55304	0.054	8.18[14]
J1453–6413	1	54552(4)*	N	0.299(18)	0.55(11)	−0.047(9)	-	-	-	27	54335 – 54794	0.054	78.3[21]
J1531–5610	1	51731(51)	N	2637(2)(11)	25(4)(10)	−15.1(8)	-	0.007(3)(4)	76(16)	29	51453 – 52042	0.20	11.3[21]
J1614–5048	1	49803(16)	P	6456.7(8)(257)	9.3(3)	−85(2)	-	-	-	20	49589 – 49985	1.44	57.8[13]
	2	53013(24)	N	6242.4(6)(370)	9.14(4)	−83.8(4)	-	-	-	12	52886 – 53150	0.40	27.0[6]
J1646–4346	1	53876(73)	N	885(3)(5)	1.5(3)(4)	−3.1(8)	-	-	-	16	53524 – 54112	2.09	32.6[10]
J1702–4310	1	53943(169)	N	4810(27)(104)	17(4)(13)	−13.3(4)(6)	30(6)	0.023(6)(20)	96(16)	73	52883 – 54932	0.92	16.3[63]
J1709–4429	1	48779(33)	P	2050.6(4)(99)	5.86(8)(87)	−18.72(11)(22)	70(2)	0.01748(8)(404)	122(3)	106	47910 – 50026	0.50	336[96]
	2	51488(37)	N	1166.73(17)(1680)	6.22(3)(17)	−55.0(3)(15)	470(8)	-	-	30	50987 – 51901	0.23	150[22]
	3	52716(57)	N	2872(7)(26)	8.0(7)(12)	−44(2)(20)	−248(18)(20)	0.0129(12)(42)	155(29)(32)	67	51946 – 53734	2.10	22900[57]
	4	54711(22)	P	2743.9(4)(96)	8.41(8)(78)	−43.27(11)	-	0.00849(7)(187)	85(2)	49	54221 – 55104	0.14	49.2[40]
J1718–3825	1	54911(2)*	N	1.94(3)	−0.12(4)	0.28(9)	-	-	-	32	54451 – 55391	0.15	10.0[25]
J1730–3350	1	52107(38)	P	3208(6)(15)	11(2)(3)	−20(1)	-	0.0102(9)(34)	99(23)	30	51844 – 52458	0.60	127[22]
J1731–4744	1	49386.72(12)*	P	136.37(20)	1.25(11)	−0.30(3)	-	-	-	40	49044 – 50026	1.03	125[33]
	2	50715.8(9)*	P	3.90(15)	0.46(14)	−0.11(4)	-	-	-	20	50588 – 50819	0.16	62.1[14]
	3	52472.65(10)*	P	126(2)	2.7(5)	−0.041(19)	-	0.073(7)	210(37)	49	51782 – 53243	0.84	142[41]
	4	53582(6)*	N	2.69(12)	0.2(2)	−0.06(6)	-	-	-	23	53223 – 53949	0.36	51.4[16]
J1737–3137	1	54352.334(8)*	P	1342.2(3)	3.01(15)	−2.0(1)	-	-	-	26	54221 – 54505	0.66	1.65[20]
J1740–3015	1	50936.803(4) ⁵	P	1440.7(3)	0.97(3)	−1.23(4)	-	-	-	34	50750 – 51155	0.46	241[28]
	2	52348.1(8)*	P	151(2)	5.4(7)	−6.8(8)	-	-	-	23	52002 – 52659	4.78	26800[16]
	3	53023.5190(4) ⁶	P	1835(2)	4.69(18)	−5.9(3)	-	-	-	14	52805 – 53223	2.66	10200[8]
	4	54449(1)*	P	41.0(7)	0.19(8)	−0.24(10)	-	-	-	27	54267 – 54634	0.95	9940[21]
	5	55220(14)	N	2664.50(15)(120)	1.35(3)	−1.71(3)	-	-	-	19	55052 – 55364	0.23	546[13]
J1801–2304	1	48453.68(6)*	P	348.3(3)	−0.14(4)	0.09(3)	-	-	-	53	47911 – 48896	2.07	8.10[47]
	2	49702.1(4)*	P	63.4(4)	0.3(1)	−0.20(6)	-	-	-	19	49364 – 50026	1.01	3.72[13]
	3	50054(2)*	P	22.5(5)	−0.06(11)	0.04(7)	-	-	-	36	49730 – 50363	1.25	7.43[30]
	4	50363.414(4) ⁷	P	80.2(4)	0.61(13)	−0.40(9)	-	-	-	58	50191 – 50647	0.98	5.17[52]
	5	50936(9)*	P	5.4(7)	-	-	-	-	-	47	50696 – 51211	1.64	12.7[41]
	6	52093(53)	P	649.1(3)(4)	−0.1(1)	0.09(7)	-	-	-	25	51783 – 52823	0.94	7.90[18]
	7	53306.98(1) ⁶	P	493.29(10)	0.19(5)	−0.12(3)	-	-	-	61	52145 – 54380	2.41	28.8[54]
	8	55356(3)*	N	3.9(3)	-	-	-	-	-	12	55145 – 55507	0.48	0.64[7]
J1801–2451	1	49475.95(3) ⁶	P	1989(1)	3.95(18)	−32(2)	-	-	-	20	49160 – 49643	0.62	50.3[13]
	2	50651.44(3) ⁶	P	1245.27(12)	3.37(7)	−27.5(6)	-	-	-	80	50462 – 50799	0.39	20.9[73]
	3	52054.74(7) ⁶	P	3757(26)	8(2)	−25(5)	-	0.024(5)	208(25)	25	51879 – 52427	0.27	16.3[16]
	4	53032(4)*	P	15.7(9)	−1.0(5)	8(4)	-	-	-	20	52805 – 53243	1.45	529[13]
	5	54653(19)	P	3113(3)(15)	15(2)(6)	−49(2)	-	0.0064(9)(35)	25(4)	20	54451 – 54860	0.25	5.92[11]
J1803–2137	1	50765(15)	P	3220(4)(22)	37.36(18)(2012)	−51.8(5)	-	0.0094(11)(65) 0.00330(17)(64)	12(2) 69(13)	54	50669 – 51451	0.16	12.2[43]
	2	53473(50)	P	3889(2)(30)	8.96(18)(69)	−50.97(20)	-	0.00630(16)(196)	133(11)	46	52804 – 54145	0.67	325[37]
J1809–1917	1	53261(18)	P	1620.8(3)(19)	5.84(17)(41)	−10.90(7)	3.5(8)	0.00602(9)(77)	126(7)	100	51783 – 54690	0.49	22.6[90]
J1825–0935	1	54115.5(3)*	P	126.4(3)	-	-	-	-	-	23	53949 – 55073	0.38	471[17]
J1826–1334	1	53236(2)*	P	3.33(4)	0.054(18)	−0.39(13)	-	-	-	31	52805 – 53619	0.18	15.8[24]
	2	53752(18)	P	3575(2)(9)	11.1(6)(11)	−47.5(6)	-	0.0066(3)(13)	80(9)	20	53423 – 54048	0.06	1.80[11]
J1835–1106	1	52222.1(7)*	P	18.33(12)	1.0(5)	−0.7(4)	-	-	-	20	51945 – 52505	0.33	202[13]
J1841–0524	1	54011.3(5)*	P	30.89(17)	−0.131(18)	0.15(2)	-	-	-	26	53619 – 54485	1.11	1.86[20]
	2	54495(10)	P	1032.5(4)(6)	1.00(7)	−1.18(8)	-	-	-	27	54269 – 54762	1.13	1.49[21]

* Glitch epoch determined by phase fit in this work. References are given for glitch epochs adopted from previously published work. Other values are determined from our data sets. References: 1 – Flanagan (1996); 2 – Dodson et al. (2002); 3 – Dodson et al. (2004); 4 – Flanagan & Buchner (2006); 5 – Urama (2002); 6 – Espinoza et al. (2011a); 7 – Krawczyk et al. (2003).

Table A3. Number of observed glitches and their mean rate for known glitching pulsars.

PSR J	Name	Data span (MJD)	N_g	\dot{N}_g (yr^{-1})	References
J0007+7303	J0007+7303	54682 — 55222	1	0.7(7)	Ray et al. (2011)
J0146+6145	4U 0142+61	49613 — 54239	2	0.16(12)	Morii et al. (2005); Gavril et al. (2011)
J0147+5922	B0144+59	52486 — 54831	1	0.1(2)	Yuan et al. (2010a)
J0157+6212	B0154+61	46866 — 50496	1	0.1(1)	Krawczyk et al. (2003)
J0205+6449	J0205+6449	52327 — 54669	2	0.3(3)	Livingstone et al. (2009)
J0358+5413	B0355+54	41808 — 54946	6	0.17(7)	Espinoza et al. (2011a)
J0406+6138	B0402+61	52469 — 54830	1	0.2(2)	Yuan et al. (2010a)
J0502+4654	B0458+46	46238 — 54946	1	0.04(5)	Espinoza et al. (2011a)
J0528+2200	B0525+21	45010 — 54947	3	0.11(7)	Espinoza et al. (2011a)
J0534+2200	B0531+21	40491 — 54947	24	0.61(13)	Espinoza et al. (2011a)
J0537+6910	J0537+6910	51197 — 53968	23	3.0(7)	Middleditch et al. (2006)
J0540+6919	B0540+09	50150 — 52935	1	0.13(14)	Livingstone et al. (2005)
J0601+0527	B0559+05	44815 — 54948	1	0.04(4)	Espinoza et al. (2011a)
J0631+1036	J0631+1036	49994 — 54942	12	0.9(3)	Espinoza et al. (2011a)
J0633+1746	J0633+1746	41725 — 51673	1	0.04(4)	Jackson et al. (2002)
J0659+1414	B0656+14	43955 — 54949	2	0.07(5)	Espinoza et al. (2011a)
J0729+1836	B0727+18	43584 — 54949	2	0.06(5)	Espinoza et al. (2011a)
J0729+1448	J0729+1448	54218 — 55429	4	1.2(6)	this work
J0742+2822	B0740+28	44838 — 55579	7	0.24(9)	Espinoza et al. (2011a), this work
J0758+1528	B0756+15	47133 — 54939	1	0.05(5)	Espinoza et al. (2011a)
J0834+4159	J0834+4159	51299 — 55145	1	0.09(10)	this work
J0835+4510	B0833+45	40276 — 55172	16	0.4(1)	Cordes et al. (1988), this work
J0905+5127	J0905+5127	49363 — 55145	2	0.13(9)	this work
J0922+0638	B0919+06	54892 — 55254	1	1(1)	Shabanova (2010)
J1016+5857	J1016+5857	51299 — 55429	2	0.18(13)	this work
J1048+5832	B1046+58	47910 — 55183	6	0.30(13)	this work
J1048+5937	1E 1048.1+5937	52386 — 54202	2	0.4(3)	Dib et al. (2009)
J1052+5954	J1052+5954	54220 — 55460	1	0.3(3)	this work
J1105+6107	J1105+6107	49589 — 55461	4	0.25(13)	this work
J1112+6103	J1112+6103	50850 — 55207	2	0.17(12)	this work
J1119+6127	J1119+6127	50852 — 55576	3	0.23(14)	this work
J1123+6259	J1123+6259	49316 — 51155	1	0.2(2)	Wang et al. (2000)
J1124+5916	J1124+5916	54682 — 55415	1	0.5(5)	Ray et al. (2011)
J1141+3322	J1141+3322	49420 — 54940	1	0.07(7)	Espinoza et al. (2011a)
J1141+6545	J1141+6545	53834 — 54785	1	0.4(4)	Manchester et al. (2010)
J1301+6305	J1301+6305	50941 — 55104	2	0.18(13)	this work
J1302+6350	B1259+63	47900 — 52900	1	0.07(8)	Wang et al. (2004)
J1328+4357	B1325+43	43566 — 44098	1	0.7(7)	Newton et al. (1981)
J1341+6220	B1338+62	47915 — 55461	23	1.1(3)	Wang et al. (2000), this work
J1357+6429	J1357+6429	51458 — 53104	1	0.2(3)	Camilo et al. (2004)
J1412+6145	J1412+6145	50850 — 55461	1	0.08(8)	this work
J1413+6141	J1413+6141	50850 — 55461	7	0.6(2)	this work
J1420+6048	J1420+6048	51100 — 55461	5	0.42(19)	this work
J1452+6036	J1452+6036	54220 — 55461	1	0.3(3)	this work
J1453+6413	J1453+6413	50669 — 55205	1	0.08(8)	this work
J1509+5531	B1508+55	40500 — 42000	1	0.2(3)	Manchester & Taylor (1974)
J1531+5610	J1531+5610	51215 — 55461	1	0.09(9)	this work
J1532+2745	B1530+27	45109 — 54946	1	0.04(4)	Espinoza et al. (2011a)
J1614+5048	B1610+50	47910 — 55461	2	0.10(7)	this work
J1617+5055	J1617+5055	47590 — 51434	1	0.1(1)	Torii et al. (2000)
J1644+4559	B1641+45	42563 — 47888	3	0.20(12)	Manchester et al. (1978); Flanagan (1993)
J1645+0317	B1642+03	40000 — 54000	7	0.18(7)	Shabanova (2009)
J1646+4346	B1643+43	47913 — 55273	1	0.05(5)	this work
J1702+4310	J1702+4310	51223 — 55461	1	0.09(9)	this work
J1705+1906	B1702+19	43587 — 54935	1	0.03(4)	Espinoza et al. (2011a)
J1705+3423	J1705+3423	49086 — 54936	3	0.19(11)	Espinoza et al. (2011a)
J1708+4009	1RXS J1708+4009	50826 — 54015	3	0.34(20)	Dib et al. (2008)
J1709+4429	B1706+44	47910 — 55507	4	0.19(10)	this work
J1718+3718	J1718+3718	51383 — 55649	1	0.09(9)	Manchester & Hobbs (2011)
J1718+3825	J1718+3825	50878 — 55507	1	0.08(8)	this work
J1720+1633	B1717+16	46718 — 54945	1	0.04(5)	Espinoza et al. (2011a)
J1721+3532	B1718+35	47907 — 54934	1	0.05(6)	Espinoza et al. (2011a)
J1730+3350	B1727+33	47880 — 54946	2	0.10(8)	Espinoza et al. (2011a)
J1731+4744	B1727+47	48184 — 55507	4	0.2(1)	this work
J1739+2903	B1736+29	46270 — 54947	1	0.04(5)	Espinoza et al. (2011a)

Table A3. — *continued*

PSR J	Name	Data span (MJD)	N_g	\dot{N}_g (yr^{-1})	References
J1740–3015	B1737–30	46270 — 55507	32	1.3(3)	Espinoza et al. (2011a), this work
J1737–3137	J1737–3137	50759 — 54925	3	0.26(16)	Espinoza et al. (2011a)
J1743–3150	B1740–31	47880 — 54926	1	0.05(6)	Espinoza et al. (2011a)
J1751–3323	J1751–3323	52496 — 54714	2	0.3(3)	Yuan et al. (2010a)
J1801–2451	B1757–24	48957 — 55507	5	0.28(13)	this work
J1801–0357	B1758–03	46719 — 54935	1	0.04(5)	Espinoza et al. (2011a)
J1801–2304	B1758–23	46694 — 55507	10	0.41(14)	Espinoza et al. (2011a), this work
J1803–2137	B1800–21	46270 — 55530	5	0.20(9)	Espinoza et al. (2011a), this work
J1806–2125	J1806–2125	50802 — 54940	1	0.09(9)	Espinoza et al. (2011a)
J1809–1917	J1809–1917	50821 — 54939	1	0.09(9)	Espinoza et al. (2011a)
J1809–2004	J1809–2004	51510 — 54945	1	0.11(11)	Espinoza et al. (2011a)
J1812–1718	B1809–173	46271 — 54936	3	0.13(8)	Espinoza et al. (2011a)
J1813–1246	J1813–1246	54682 — 55226	1	0.7(7)	Ray et al. (2011)
J1814–1744	J1814–1744	50833 — 54945	5	0.44(20)	Espinoza et al. (2011a)
J1818–1422	B1815–14	51512 — 54831	1	0.11(11)	Yuan et al. (2010a)
J1819–1458	J1819–1458	51031 — 54938	1	0.1(1)	Lyne et al. (2009)
J1824–1118	B1821–11	46612 — 54936	1	0.04(5)	Espinoza et al. (2011a)
J1824–2452	B1821–24	47800 — 52800	1	0.07(8)	Cognard & Backer (2004)
J1825–0935	B1822–09	45008 — 54948	8	0.29(11)	Espinoza et al. (2011a)
J1826–1334	B1823–13	46302 — 54944	5	0.2(1)	Espinoza et al. (2011a)
J1833–0827	B1830–08	46449 — 54944	2	0.08(6)	Espinoza et al. (2011a)
J1830–1135	J1830–1135	51816 — 54945	1	0.12(12)	Espinoza et al. (2011a)
J1834–0731	J1834–0731	51833 — 54945	1	0.12(12)	Espinoza et al. (2011a)
J1835–1106	J1835–1106	49071 — 54940	1	0.06(7)	Espinoza et al. (2011a)
J1837–0559	J1837–0559	51153 — 54945	1	0.1(1)	Espinoza et al. (2011a)
J1838–0453	J1838–0453	51251 — 54948	2	0.20(14)	Espinoza et al. (2011a)
J1841–0425	B1838–04	46270 — 54936	1	0.04(5)	Espinoza et al. (2011a)
J1844–0538	B1841–05	46270 — 54936	1	0.04(5)	Espinoza et al. (2011a)
J1841–0456	1E 1841–045	51224 — 53970	3	0.4(3)	Dib et al. (2008)
J1841–0524	J1841–0524	51816 — 54939	3	0.4(2)	Espinoza et al. (2011a)
J1845–0316	J1845–0316	51609 — 54942	2	0.22(16)	Espinoza et al. (2011a)
J1846–0258	J1846–0258	51574 — 54800	2	0.23(16)	Livingstone et al. (2006, 2010)
J1847–0130	J1847–0130	52135 — 54942	2	0.26(19)	Espinoza et al. (2011a)
J1851–0029	J1851–0029	53817 — 54948	1	0.3(4)	Espinoza et al. (2011a)
J1853+0545	J1853+0545	52493 — 54830	1	0.16(16)	Yuan et al. (2010a)
J1856+0113	B1853+01	47577 — 54948	1	0.05(5)	Espinoza et al. (2011a)
J1901+0156	B1859+01	46724 — 54936	1	0.04(5)	Espinoza et al. (2011a)
J1901+0716	B1859+07	46564 — 54938	1	0.04(5)	Espinoza et al. (2011a)
J1902+0615	B1900+06	44817 — 54938	5	0.18(8)	Espinoza et al. (2011a)
J1909+0007	B1907+00	44818 — 54936	3	0.11(7)	Espinoza et al. (2011a)
J1909+1102	B1907+10	52470 — 54821	2	0.3(3)	Yuan et al. (2010a)
J1910–0309	B1907–03	44817 — 54938	3	0.11(7)	Espinoza et al. (2011a)
J1910+0358	B1907+03	47389 — 54936	1	0.05(5)	Espinoza et al. (2011a)
J1913+0446	J1913+0446	51832 — 54939	1	0.12(12)	Espinoza et al. (2011a)
J1913+0832	J1913+0832	51643 — 54939	1	0.11(11)	Espinoza et al. (2011a)
J1913+1011	J1913+1011	51465 — 54935	1	0.11(11)	Espinoza et al. (2011a)
J1915+1009	B1913+10	45279 — 54948	1	0.04(4)	Espinoza et al. (2011a)
J1915+1606	B1913+16	46671 — 54929	1	0.04(5)	Espinoza et al. (2011a)
J1919+0021	B1917+00	46001 — 54948	1	0.04(4)	Espinoza et al. (2011a)
J1926+0431	B1923+04	44819 — 54948	1	0.04(4)	Espinoza et al. (2011a)
J1932+2220	B1930+22	44816 — 54947	3	0.11(7)	Espinoza et al. (2011a)
J1937+2544	B1935+25	46786 — 54937	1	0.04(5)	Espinoza et al. (2011a)
J1952+3252	B1951+32	47029 — 54945	5	0.23(11)	Espinoza et al. (2011a)
J1955+5059	B1953+50	43960 — 54938	2	0.07(5)	Espinoza et al. (2011a)
J1957+2831	J1957+2831	50239 — 54938	3	0.23(14)	Espinoza et al. (2011a)
J2021+3651	J2021+3651	52305 — 54948	2	0.28(20)	Hessels et al. (2004); Espinoza et al. (2011a)
J2022+3842	J2022+3842	54400 — 55500	1	0.3(4)	Arzoumanian et al. (2011)
J2116+1414	B2113+14	44329 — 54934	1	0.03(4)	Espinoza et al. (2011a)
J2225+6535	B2224+65	42000 — 54831	5	0.14(7)	Shemar & Lyne (1996); Yuan et al. (2010a)
J2229+6114	J2229+6114	51977 — 54946	3	0.4(3)	Espinoza et al. (2011a)
J2257+5909	B2255+58	44817 — 54935	1	0.04(4)	Espinoza et al. (2011a)
J2301+5852	1E 2259+586	50356 — 52575	1	0.16(17)	Kaspi et al. (2003)
J2337+6151	B2334+61	52486 — 55045	1	0.14(15)	Yuan et al. (2010b)

